TÉCNICO LISBOA

Methodology to aid in the decision-making of retrofit solutions in the residential sector using calibrated building energy simulation models

Luís Maria Soveral Padeira Bívar de Azevedo

Thesis to obtain the Master of Science degree in

Mechanical Engineering

Supervisor: Prof. Carlos Augusto Santos Silva

Examination Committee

Chairperson: Prof. Edgar Caetano Fernandes
Supervisor: Prof. Carlos Augusto Santos Silva
Members of the Committee: Prof. Maria da Glória de Almeida Gomes
Prof. Susana Margarida da Silva Vieira

June 2018

AGRADECIMENTOS

Queria agradecer ao meu orientador, o Professor Carlos Silva, pela sua disponibilidade, apoio e otimismo durante todo o desenvolvimento desta dissertação.

Em segundo lugar, gostaria de agradecer ao Ricardo Gomes por toda a sua constante disponibilidade, acompanhamento e conhecimento transmitido em inúmeros assuntos durante todas as etapas que fizeram parte deste trabalho.

Por último, gostaria de agradecer à minha família por toda a motivação que me deu, não apenas na realização desta dissertação, mas também para durante todo o meu percurso académico.

RESUMO

Este trabalho envolve numa primeira fase, a calibração de um modelo de simulação energética de edifícios de uma fração autónoma de habitação Portuguesa, localizada em Lisboa, em que são conhecidas as más condições de conforto térmico. Após os parâmetros em que há incerteza terem sido calibrados através de uma otimização mono-objectivo com o algoritmo genético, as previsões de temperatura do ar interior poderão ser realizadas com um maior grau de exatidão, o que contribui para uma maior confiança ao estimar o conforto térmico da casa.

Numa segunda etapa, é realizada uma análise de medidas de melhoria, utilizando uma rede neuronal artificial como modelo substituto do *EnergyPlus®* (programa de simulação energética de edifícios utilizado neste trabalho) para otimizar o modelo calibrado da casa, recorrendo-se para tal a um algoritmo genético multiobjectivo. Serão tidos em conta vários objetivos, como o custo de investimento, o custo energético e ainda o conforto térmico. É também realizada uma análise que procurará identificar possíveis diferenças das soluções ótimas entre o modelo calibrado e dois outros modelos da mesma casa com diferente grau de incerteza nos parâmetros que os definem.

Os processos de otimização multiobjectivo aplicados ao modelo calibrado conseguiram identificar uma vasta gama de soluções ótimas, garantindo condições aceitáveis de conforto térmico durante todo o ano. Concluiu-se ainda que estas soluções podem variar consideravelmente consoante o grau de exatidão do modelo, facto este que poderá afetar a tomada de decisão da solução.

Palavras-chave: calibração de modelos de simulação energética de edifícios, conforto térmico, medidas de melhoria, análise de sensibilidade, algoritmo genético, rede neuronal artificial

ABSTRACT

This work involves firstly, the calibration of the Building Energy Simulation model of one Portuguese residential household, located in Lisbon, which is known by the occupants as having poor thermal conditions (i.e. thermal comfort). After the uncertain parameters of the model are calibrated with a single-objective optimization using the genetic algorithm, more accurate predictions of the indoor air temperature can be performed, increasing the confidence on the thermal comfort.

In a second phase, a retrofit analysis is performed by using an artificial neural network as a *surrogate model* to replace the *EnergyPlus®* (building energy simulation program used in this dissertation) and to optimize the calibrated model of the household using a multi-objective genetic algorithm. Several objectives will be considered in this optimization, such as the investment cost, the energy cost and also the thermal comfort. Another analysis is also performed, which intends to find possible differences on the optimal retrofit solutions between the calibrated model and two other models with different uncertainty on their parameters.

The multi-objective optimizations performed on the calibrated model succeeded to identify a wide range of optimal retrofit solutions that guarantee the minimum thermal comfort conditions during the whole year. It was concluded that these solutions can vary considerably, depending on the accuracy of the model, which may affect the decision-making process to identify the optimal solution.

Keywords: calibration of BES models, thermal comfort, retrofit measures, sensitivity analysis, genetic algorithm, artificial neural network

INDEX

List of Tables

List of Figures

List of Acronyms

ANN	Artificial Neural Network
ASHRAE	American Society of Heating, Refrigeration and Air Conditioning Engineers
BES	Building Energy Simulation
cv(RMSE)	Coefficient of Variation of the Root Mean Square Error
CFD	Computational Fluid Dynamics
CFL	Compact Fluorescent Lamp
DHW	Domestic Hot Water
DM	Decision-Maker
ECM	Energy Conservation Measures
GA	Genetic Algorithm
HVAC	Heating, Ventilation and Air Conditioning
LED	Light-Emitting Diode
LHS	Latin Hypercube Sampling
MLP	Multi-Layer Perceptron
MBE	Mean Bias Error
MSE	Mean Square Error
MOO	Multi-Objective Optimization
NMBE	Normalized Mean Bias Error
NSGA-II	Non-Dominated Sorted Genetic Algorithm-II
OAT	One At a Time
PMV	Predicted Mean Vote
PPD	Percentage of People Dissatisfied
PSO	Particle Swarm Optimization
RGCA	Real-Coded Genetic Algorithm
SCOP	Seasonal Coefficient of Performance

SEER	Seasonal Energy Efficiency Ratio
TB	Thermal break

Notation

α_J	Weight of the J zone
c [€/kWh]	Unitary energy cost
C_E [€/$year$]	Annual energy cost
C [$J/kg.K$]	Specific heat
C_{PF}	Conversion factor primary/final energy
d	Data point
Δ	Increment
ΔT_{DHW} [°C]	Hot water temperature variation
E [kW]	Final energy
EE	Elementary-effect
η_{wh}	Efficiency of hot water equipment
f	Fraction of heat
f_{eh}	Efficiency of the shower system
F_{obj}	Objective function(s)
F_X	Cumulative distribution function
$g_\perp$	Solar factor
I [€]	Investment cost
I_{cl} [clo]	Clothing insulation
K	Number of variables
k [$W/m.K$]	Conductivity
L [W/m^2]	Thermal body load
M [W]	Metabolic activity
M_{DHW} [L]	Average volume of hot water daily consumption
n	Size of the data
n_d [$days$]	Number of days with consumed hot water

N	Number of periods
$N_{occupants}$	Number of occupants
ω	Discretized grid for each variable
Ω	Domain of uncertainty
μ	Sample mean
μ^*	Mean of the absolute value of the elementary-effects
p	Number of discretized levels
p_c	Crossover probability
p_m	Mutation probability
$P\ [W]$	Power
$Q_C\ [kWh/year]$	Cooling load
$Q_{DHW}\ [kWh/year]$	Useful energy for DHW
$Q_H\ [kWh/year]$	Heating load
$Q_{res}\ [W/m^2]$	Heat lost through respiration
$Q_{sk}\ [W/m^2]$	Heat lost through skin and clothes
r	Number of trajectories
$R\ [m^2.K/W]$	Thermal resistance
$RH\ [\%]$	Relative humidity
$\rho\ [Kg/m^3]$	Density
ρ_s	Reflectivity of the shading device
σ	Sample standard deviation
$t\ [m]$	Thickness
$t_a\ [°C]$	Air temperature
$t_o\ [°C]$	Operative temperature
$t_{out}\ [°C]$	Mean monthly outdoor air temperature
$\bar{t}_r\ [°C]$	Mean radiant temperature
$T\ [°C]$	Thermostat temperature

τ_s	Transmissivity of the shading device
$U\ [W/m^2.K]$	Overall heat transfer coefficient
$u_a\ [m/s]$	Air speed
$\dot{V}\ [h^{-1}]$	Air infiltration rate
$V\ [m^3]$	Zone Volume
$W\ [W/m^2]$	Mechanical work done by muscles
x	Input variable
X	Vector with the input variables
y	output variable
Y	Vector with output variables
Z	Number of zones to estimate the thermal comfort

Subscripts

$adapt80\%$	80% acceptability criterion, adaptive model
avg	average
C	cooling
$equip$	electric equipment
e	electricity
ext	exterior wall
g	glazed surface
H	heating
int	interior wall
$light$	lighting equipment
$occupied_J$	Occupied J thermal zone
pre	Pre-occupation
Q_1	Main bedroom

Q_2	Secondary bedroom
S	Living-room
sb	stand-by
$static0.7$	0.7 acceptability criterion, PMV model
$valid$	validation
w	window
DHW	Domestic hot water

Superscripts

c	Convective
cs	Cooling season
hs	Heating season
(l)	Lower bound
m	Measured
pen	Penalty
r	Radiant
s	Simulated
(u)	Upper bound
v	Visible
$*$	Base point of the trajectory

1 INTRODUCTION

Buildings represent approximately 40% of the final energy consumption in the European Union, so there is an urgent need to adopt efficient measures in the building stock. In 2010, the European Commission has published an updated version of the Energy Performance of Buildings Directive (European Directive 2010/31/EU, 2010), which emphasizes the need for "Energy Efficient Retrofitting" of existing buildings. In general, Energy Conservation Measures (ECM) focus on the implementation of retrofit measures in a building, aiming at reducing the energy demand, while guaranteeing the thermal comfort conditions of the occupants.

Typically, building retrofit projects focus especially in decreasing the energy consumption and so, most of the calibration studies and methodologies (ASHRAE, Guideline 14-2002) suggest using only energy consumption data to reduce the model's errors, instead of using indoor environmental parameters such as the air temperature. Not only can this latter succeed to estimate more accurately the thermal comfort conditions on the non-retrofitted buildings but also to increase the confidence on the predictions of the energy consumption reduction due to ECM applied to the buildings.

Moreover, the calibration of the simulation models is considered mostly for large buildings, frequently offices or services buildings, since the effort needed to calibrate residential simulation models is too high and does not compensate when analysing simple retrofit measures, especially due to budget reasons. Usually, the retrofit projects or energy audits of residential buildings is made with the help of simple static calculations, which can over-simplify the model and lead to more inaccurate results than if dynamic building energy simulation was used. To estimate the optimal retrofit solutions in residential buildings, a calibrated Building Energy Simulation (BES) model may be fundamental to identify more reliably the retrofit solutions, which might compensate the effort involved.

To identify these solutions, some efficient techniques like the genetic algorithms (GAs) had good results in the past studies, more specifically the multi-objective GAs such as the NSGA - II (Deb, 2011). The main disadvantage of implementing a multi-objective optimization using directly the BES programs, is the high computational effort involved. Some studies (Magnier & Haghighat, 2010) overcame this problem with success by using surrogate models such as the Artificial Neural Networks (ANNs) which induce very small errors on the solutions and have negligible computational effort.

1.1 Objectives and methodology overview

This work focuses on developing a methodology to aid in the decision-making of retrofit solutions for the residential sector using calibrated building energy simulation models. This methodology is developed and tested using as case study, a Portuguese household with poor thermal comfort conditions.

The first step of this work is the *model calibration* and aims at obtaining a model with the lowest possible error, using the BES program: *EnergyPlus*. This step includes three phases: defining a *baseline model* using high

level information about the house, followed by a *detailed model*, using detailed data, and finally developing a *calibrated model* using air temperature measured data.

The second step of this work is the *retrofit analysis* and consists of implementing a multi-objective optimization (MOO) approach to determine the best set of solutions that minimize several objectives while guaranteeing minimum thermal comfort conditions (given by the Predicted Mean Vote, PMV). Two different optimization scenarios are studied in this work: The first consists of minimizing the investment cost and simultaneously, the annual energy cost and the second scenario searches for the optimal measures that maximize the thermal comfort and minimize the annual energy cost.

As a final analysis, the two models of the household that were created before the calibration (*baseline* and *detailed* models) are compared in terms of optimal solutions: one model having only general information, in which its parameters are highly uncertain, and another one generated with the information collected in walkthroughs to the household, therefore with less uncertainty. The comparison between the three models intends to find if models with different uncertainty have significant differences between their optimal solutions, and how these differences may influence the decision-making process.

Two different types of optimization using the Genetic Algorithm (GA) are used in this work: the first aims at calibrating the model until a minimum overall error has been found (which is a single-objective optimization) and the other is a multi-objective GA, which intends to search for the combination of retrofit measured that represent the *trade-off* between several objectives (*Pareto solutions*), considering the scenarios previously referred. Some tools are also used to help these two types of optimizations: the first is sensitivity analysis and its objective is to reduce the number of variables of the single-objective error minimization, as it is a common practice in the calibration of BES models. The second tool has the objective of reducing the high computational effort of optimizing a BES model with several objectives, which would require an infeasible number of simulations of the BES program. For this, it is used an Artificial Neural Network (ANN) to approximate the outputs of the *EnergyPlus* in the multi-objective optimization.

The methodology of this work, is presented in the flowchart of the Figure 1.

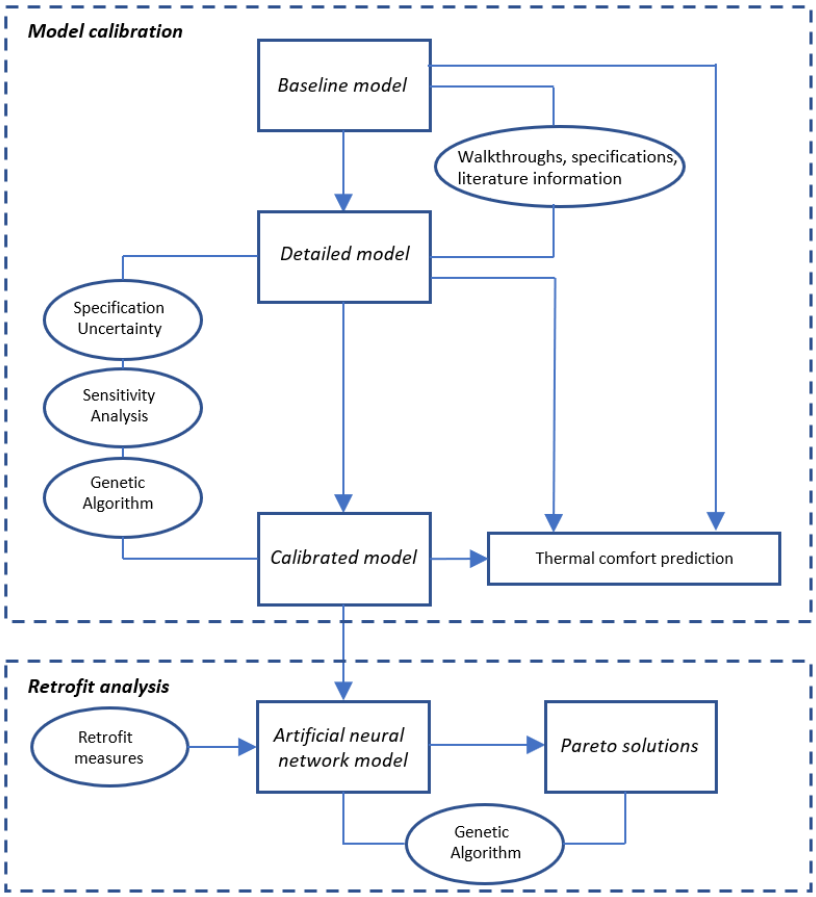

Figure 1: Methodology of this work

1.2 Structure of the dissertation

This work is divided in the following chapters:

- The second chapter details the state of art of BES models, focusing on the uncertainty that these models have and the methods adopted to deal with this uncertainty;
- The third chapter includes the methods that were used in this work to calibrate the BES model;
- The fourth chapter describes the methods that were used to evaluate the thermal comfort of the household;
- The fifth chapter describes the methods that were used to identify the optimal combination of retrofit measures;
- The sixth chapter includes the description of the case-study, more specifically, the parameters used in the construction of the BES models and the methodology adopted for the calibration of the model and subsequent retrofit analysis;
- The seventh chapter presents the results of the methodology applied to the case-study and their discussion;

2 BUILDING ENERGY SIMULATION MODELS: STATE OF ART

This chapter presents a brief introduction of Building Energy Simulation (BES) and the problems related to its inaccuracy, followed by the types of uncertainty sources in BES models and their quantification. Then, it introduces the topic of the calibration of BES models, which conversely to an uncertainty analysis, aims to deterministically adjust the uncertain parameters within their ranges of uncertainty.

2.1 Building Energy Simulation models

According to (ASHRAE, 2009), there are two types of modelling approaches for predicting energy consumption and/or thermal comfort conditions in buildings. The first one is the forward approach, which consists of models with a known set of equations or physical laws that represent the actual phenomena. This is the reason why these types of models are also called *law-driven* models. These models give a deterministic output (i.e. hourly energy consumption, temperature profiles, humidity and so on) that depend on the detailed description of the building and external factors as the inputs of the model, such as the weather, infiltration, geometry, location, materials, equipment, HVAC systems and operating schedules of the building. This type of simulation is usually carried on with computer programs, such as *DOE-2*, *EnergyPlus*, *BLAST* and *TRNSYS*. These BES programs all have in common the fact that after the inputs are specified, they calculate a prediction of the space loads using room mass and heat balances, usually to maintain a certain degree of comfort. Finally, they predict the primary and secondary equipment energy requirements.

The other modelling type is a data-driven approach. With this type of methods, it is only necessary to know the input and output variables, which are previously measured. The objective of this type of modelling is to determine a mathematical formulation of the system (ASHRAE, 2009) using the actual data of the building so that future data can be accurately predicted. These models are less flexible than forward models because it is not possible to adjust the parameters of the model to change its behaviour.

2.2 Uncertainty in Building Energy Simulation models

Most studies address to the uncertainty of BES using forward approaches based on the computer programs discussed before. The uncertainty of a model, often neglected by several studies of BES, is the inability to represent accurately the reality due to lack of information on the variables of the model, simplification of important and complex processes and by the algorithm of the model itself. Several studies using BES programs have shown significant discrepancies between the output of the models and the actual measured data, up to an error of $100\ \%$ (Coakley, Raftery, & Keane, 2014).

This inaccuracy of the models is a major problem of BES models, since it decreases the confidence in the model, particularly when evaluating the implementation of possible energy conservation measures, where accuracy should play a key role for estimating the actual energy savings or the improvement in the comfort of a

building. When creating a BES model, there are numerous uncertainty sources that are addressed differently in several studies on this topic.

2.3 Sources of uncertainty

As stated before, several authors address differently to the specification of the uncertainty sources. One important study on the uncertainty of BES models (De Wit, 2001) states that globally there are four sources of uncertainty. Firstly, there is the *specification uncertainty*, referring to the incomplete or inaccurate specification of the whole system's inputs. This is usually due to the lack of knowledge on the building's properties and the simplifications or the assumptions that are made, which generate the specification errors.

Secondly, there is the *modelling uncertainty*, which is due to several assumptions and simplifications of complex physical processes. Examples of modelling errors are the selection of the thermal zones of the buildings, or the approach to model the infiltration and ventilation. This latter is a complex physical process which is usually simplified in BES (more accurate ventilation and infiltration modelling is achieved with detailed flow simulation, usually based on CFD programs).

Thirdly, we have the *numerical* uncertainty, which is related to the BES program itself, due to assumptions, algorithms and time steps used by the program (De Wit, 2001).

The last uncertainty source and probably the most difficult to quantify is due to the non-deterministic nature of external processes to the buildings such as the occupation, lighting and other equipment usage or the outdoor climate conditions.

Another relevant study under the topic of uncertainty (Macdonald, 2002) classifies the various sources of uncertainty in a more detailed manner, by answering some uncertainty related questions, such as: how well does the model represent reality; what values should be used in the absence of measured data; to what extent do the assumptions made regarding future weather, occupancy and operation factors affect the predictions; what uncertainties are associated with the choice of algorithms for the various heat and mass transfer processes; and what will be the effect of changing one aspect of the design. All these questions generate a specific source of error in the model that is related, respectively to: the *Model realism,* the *Input parameters,* the *Stochastic processes,* the *Simulation program capabilities* and the *Design variations.*

To study quantitatively all these sources of uncertainty, it is a current practice to describe mathematically the uncertainty with probability distributions, which express the "degree of belief" on the uncertain factors used in the model. Ideally, if observations of the uncertain factors are available, the probability distribution should be quantitatively obtained with the frequency of observations (if a large sample of observations exist). However, this data is usually not available, so other assumptions for the probability distributions that correctly estimate the uncertainty sources, must be considered.

Some studies deal with this issue of the unavailability of observed data and adopt a methodology to assign probability distributions to the uncertain sources of the model. Chong, Xu, & Lam (2015) suggest that after

choosing the uncertain parameters of the model (which can be related to any of sources referred before), ideally the probability distribution of a given uncertain parameter should be chosen from a finite set of distributions according to the fit to the observed data (in this study, the *goodness-of-fit* is given by the maximum likelihood estimator). This study acknowledges the difficulty to gather data for all the uncertain parameters and suggests that if observed data for specific parameters is not available, the probability distribution is chosen using subjective assessment of information in drawings and/or specifications. However, in the cases where none of this information is available, the probability distribution is assigned according to the information in standards, literature and case studies (Chong, Xu, & Lam, 2015).

Another study that performed uncertainty analysis of a BES model (Rodríguez, Andrés, Muñoz, López, & Zhang, 2013) suggests that the most suitable probability distributions for the parameters are the discrete distributions, uniform or triangular, or normal distribution, according to a subjective assessment on the "degree of uncertainty" of the parameters. If there is large uncertainty on a specific variable, it will follow a uniform distribution and conversely, if the variable has a small uncertainty associated, it will follow a normal distribution. In the middle of both distributions, the triangular distribution is used to express higher uncertainty than the normal distribution but lower than with the uniform distribution.

2.3.1 Specification uncertainty

The overall uncertainty of a specific parameter of a BES model is the result of both systematic and random errors. Systematic errors exist in a model due to an incorrect use of the data for a certain parameter or because it is incomplete or wrongly defined (Macdonald, 2002). An example of these errors comes from the fact that usually models, in an early design stage, have lack of information about the exact properties of the envelope materials. Wrong assumptions made on these properties, e.g. thickness or conductivity, can result in large systematic errors, even if the material type is correctly defined. This type of errors can be removed from the model with a better definition of its properties. Conversely, random errors do not depend on the accuracy in the definition of the model's properties. These are errors which are not attributed to a particular cause and are defined as the measurement error in all the measured properties of the model.

When modelling the overall uncertainty of the parameters of BES models, (Macdonald, 2002) suggests using for continuous variables, the uniform, normal, log-normal and triangular distributions.

The simplest of the distributions is the uniform probability distribution (Figure 2, c)) and it ensures that every value of a specific parameter, within a lower and upper bound, has the same probability. This means that all the values inside the range of variation of the parameter are equally probable. This distribution suits the parameters that are poorly defined and highly uncertain, as for example the internal gains of a building.

The normal probability distribution (Figure 2, b)) of a sample of values for a given parameter is defined with the average and standard deviation, i.e. $N \sim (\mu, \sigma)$. It is the most appropriate distribution for physical data (Macdonald, 2002). Since it is an unbounded distribution, it is a current practice to truncate this distribution so that the variables assume realistic values. This is usually done by setting the lower and upper bound equal to

$\pm a.\sigma$, so that when $a = 1$, there is a probability of approximately 68% that the values of the distribution are within the lower and upper bound (symmetrically to the average); if $a = 2$, the same probability is approximately 95% and so on.

The triangular distribution (Figure 2, a)) is, unlike the normal, a bounded distribution usually used as an intermediate step between the uniform and normal distributions (Macdonald, 2002). It is bounded by the least likely values that linearly evolve towards the most likely value (i.e. the mode or average in symmetric triangular distributions), so it is fully defined with the minimum (a), the maximum (b) and the mode (m), i.e. $Tri{\sim}(a, b, m)$.

The log-normal distribution (Figure 2, d)) is always positive and an unbounded distribution. It is the normal distribution of the logarithm of the variable and, like the normal distribution, it is defined with the average and standard deviation, i.e. $LogN{\sim}(\mu, \sigma)$.

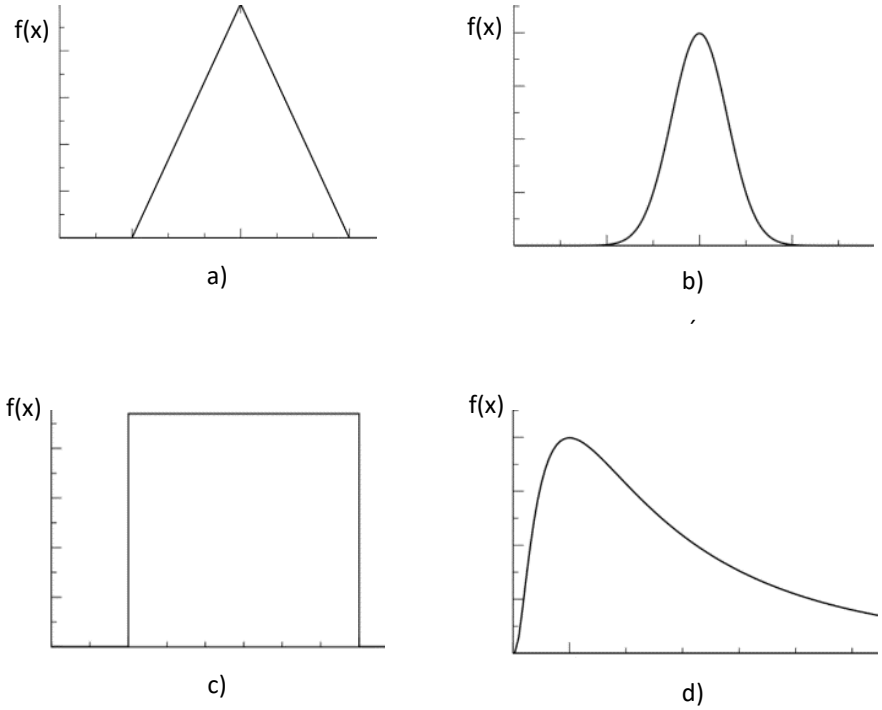

Figure 2: Probability density of: a) Triangular distribution; b) Normal distribution; c) Uniform distribution; d) Log-normal distribution

Regarding the thermal properties of the building's envelope, in an early stage of the design of the model (i.e. when there is no information on the actual materials), (Macdonald, 2002) suggests to describe the variability of the properties (conductivity (k), density (ρ) and specific heat capacity (C)) with values for the average and standard deviation that cover all the possible materials and usage levels within a certain material type.

The Internal gains of a building refer to the total heat generated by the occupants (metabolic activity), by electric or gas equipment and by the lighting equipment. When introduced in the simulation, all these heat sources have uncertainty related to the specification (in this section, the internal gains refer only to the parameters that define the heat generation, and not their operating schedules, as for example to the power and fraction of sensible heat).

The metabolic activity (M) is the total heat generated by the occupants and is usually defined as the heat generated per unit area, expressed in met (1 $met = 58.1 W/m^2$). The accuracy level of the metabolic activity depends on the way it is estimated. ASHRAE (2009) states that there are three ways of knowing M. The first and most accurate method consists of measuring the rate of respiratory oxygen consumption and carbon dioxide production and then obtaining M through empirical correlations. The second method, much less accurate, consists of measuring the occupants' heart rate, relating it to the oxygen consumption and finally applying the same empirical correlations as in the first method. One last, non-intrusive, method is based on tabled information in function of the occupant's type of activity being performed. According to (ASHRAE, 2009), for well-defined activities having $M < 1.5\, met$, the tabled information is sufficiently accurate, but for $M > 3\, met$, where activities are poorly defined, the uncertainty is $\pm 50\%$ of the tabled information.

The total heat gain generated by the occupants is divided in latent (i.e. evaporative) and sensible heat gain. This last one is partially lost by convection and by long-wave radiation to the environment. These fractions of convective, radiative and latent heat gains are usually assumed as in steady-state during the whole BES. This represents a specification uncertainty that assumes a uniform distribution for a single person, triangular distribution for a small group of occupants and normal distribution for large groups (Macdonald, 2002).

2.3.2 Scenario uncertainty

The scenario uncertainty is related to the parameters that are external to the building, such as the outdoor climate conditions and the usage schedules (the most commons are occupation, lighting, equipment, shading and thermostat). All these uncertain parameters are much more unpredictable than the other referred uncertainty sources and represent all the *Stochastic processes* (Macdonald, 2002) that happen in a building (sources of natural variability).

The outdoor climate is a highly influential and unpredictable factor in BES that is considered in most of the studies with a weather file containing information about the outdoor climate conditions averaged through the last years. This information is usually the solar radiation, wind speed and direction, dry-bulb temperature and relative humidity from a specific region and might be considerably different than the actual weather conditions (Bae, 2016), which may lead to inaccurate predictions of the model. Since a weather file has a lot of climate information, i.e. a lot of uncertain weather-related variables, a complete quantification of the uncertainty of these parameters would be a very complex challenge, so some studies assume the weather file as the uncertain parameter and a discrete probability distribution for its uncertainty (Rodríguez, Andrés, Muñoz, López, & Zhang, 2013).

Another great source of natural variability is the occupation, from which usually depend other usage schedules such as lighting, equipment, shading and the thermostat. This factor is more predictable in non-residential buildings (for example, in office buildings) because usually these have rigid schedules and are only active during specific periods. A study made on the calibration of three office buildings (Reddy, Maor, & Panjapornpon) used schedules with three degrees of freedom (A, B and C) to represent the variability of occupation in these buildings (Figure 3).

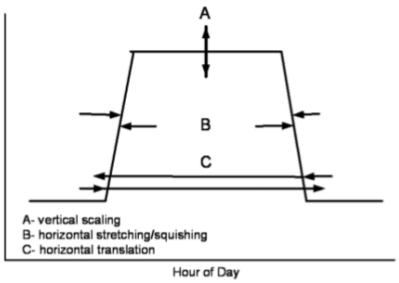

Figure 3: Variability of the occupation schedules, taken from (Reddy, Maor, & Panjapornpon)

Conversely, in residential BES models it is more difficult to know exactly the periods when the occupants are at home or what is their exact behaviour pattern because these are affected by many factors, such as the lifestyle, socio-demographic and environmental factors. A study made on optimization of BES models under *scenario uncertainty* (Bae, 2016) quantified the uncertainty of the internal loads' schedules in a house, by assigning each type of internal load (occupation and lighting in each division) a normal distribution.

2.4 Uncertainty Analysis

Considering that all the sources of uncertainty referred before are quantified with probability distributions (usually truncated to avoid unphysical results), a statistical approach is usually used to study the effects that these errors have on the outcomes of the model. Knowing the outputs of a model along with their probability (frequency) can influence decision-making processes when there is uncertainty present in the model. This is known as an uncertainty analysis based on *Monte Carlo* simulation, which consists of finding the outputs of the model for a sample of solutions randomly chosen (each parameter randomly chosen from its probability distribution) from the whole population of possible solutions.

An uncertainty analysis is known as a non-deterministic approach and it can be used to perform single or multi-objective optimizations with uncertainty present in the model. Bae (2016) suggests an intermediate step between the quantification of the parameter's uncertainty and the decision-making process. This step consists of performing an iterative optimization, by randomly choosing a set of samples from the "uncertainty domain", optimize them and find the probability distributions of the optimal retrofit solutions.

Conversely, another method that deals with the uncertainty of a model consists of reducing its error by properly tuning the uncertain parameters. This is called model calibration and contrarily to an uncertainty analysis, it is a deterministic approach because the output of the method is not a probability distribution but instead, one or more calibrated solutions with less uncertainty than the initial model.

2.5 Calibration of Building Energy Simulation models

The calibration of a model consists of tuning its uncertain parameters to represent the reality in the most accurate way so that the model is validated by the *goodness-of-fit* between the output of the BES program and the corresponding measured data.

This issue is commonly addressed as an approximation of the inverse of the model because it encompasses tuning the inputs so that the model's output fits as closely as possible the measured data, as it is shown in Figure 4, where X is the vector of uncertain parameters, Y^s is the output of the model and $e(Y^s, Y^m)$ is the error between the model's output and the measured data (Y^m). In other words, calibrating a model is as similar as searching for its inverse function, where the input for the calibration is the measured data and one is interested in finding the set of parameters in which the output is approximately the same as the observable data. Since this kind of models have lots of discontinuities, non-linearities and cannot be treated as analytical functions, it is impossible to calculate their inverse function and so, models are considered calibrated if there is a small error between the simulated and the measured data. This will give a higher level of accuracy and confidence on future analysis/predictions of the model.

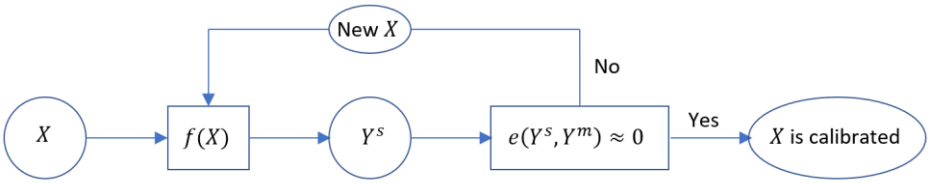

Figure 4: Flowchart showing the procedure of calibration

According to (Coakley, Raftery, & Keane, 2014), apparently successful calibrations might not be able to ensure accurate results of retrofit measures. Most of the BES models are defined with many input variables and therefore many degrees-of-freedom (high order systems) exist in calibration. This is the reason why calibration is commonly referred as an indeterminate problem, i.e. several non-unique solutions might exist.

This problem is also known as the equifinality and is usually minimized with the reduction of the degrees of freedom of the model by fixing the non-influential parameters and calibrating only the most important ones. Sensitivity analysis is used for this factor-fixing, more specifically screening techniques (Bertagnolio, 2012). Other studies, such as (Reddy, Maor, & Panjapornpon, 2011) increase the robustness of calibration not only by performing sensitivity analysis to fix the non-influential parameters, but also by considering as calibrated several solutions with small errors instead of only one. This method also allows to quantify the uncertainty of the calibrated solution.

2.5.1 Error indicators

Calibration of building energy models consists of the minimization of statistical error indicators between measured and simulated data, usually the Mean Bias Error (MBE) and/or the coefficient of variation of the Root Mean Square Error ($cv(RMSE)$). The first one (equation (1)), is basically the average of the sum off all errors and

indicates the overall *bias* of the model (Coakley, Raftery, & Keane, 2014). A positive MBE indicates an overall under-estimation of the data predicted by the BES program and a negative MBE indicates an over-estimation of the same data. The problem of this error estimator is that the over-estimations cancel the under-estimations (*cancelation effect*) and so, another measure of the error is usually required.

The coefficient of variation of the root mean square error ($cv(RMSE)$, calculated through equation (2)), solves the *cancelation effect* because it turns all the residuals into positive values. This is analogous to the standard deviation of the simulated values to the measured data, which is then normalized by the mean of the measured data.

$$MBE = \frac{\sum_{i=1}^{n}(d_i^m - d_i^s)}{n} \quad (1)$$

$$cv(RMSE) = \frac{\sqrt{(\sum_{i=1}^{n}(d_i^m - d_i^s)^2/n)}}{(\sum_{i=1}^{n} d_i^m)/n} \quad (2)$$

In both estimators, d_i^m and d_i^s are respectively, the measured and simulated data value at the i period, n is the number of periods in which the data is being compared, usually on a monthly or hourly basis (i.e. measured and simulated values with a time step of one month or one hour, respectively).

Comparing monthly to hourly basis, the validation criteria through the first one must be much tighter than the second. This is because measuring the error month to month represents a much cruder measure, ignoring every hourly oscillation between measured and simulated values and only considering monthly fluctuations. Some works on this topic calibrate models using only the $cv(RMSE)$, as for example in (Roberti, Oberegger, & Gasparella, 2015) or with a multi-objective approach, where both the errors are minimized simultaneously.

2.5.2 Multi-objective error calibration

When a model is calibrated using multi-objective optimization (MOO) it makes sense to compare the *bias* of the model to the $cv(RMSE)$. This is done by normalizing the MBE with the average of the measured data, originating the measure $NMBE$ (equation (3))

$$NMBE = \frac{\sum_{i=1}^{n}(d_i^m - d_i^s)}{\sum_{i=1}^{n} d_i^m} \quad (3)$$

Some multi-objective approaches minimize several errors by scalarizing all the indicators into a single error indicator and then minimize that value, which is known as the overall *goodness-of-fit* indicator (Reddy, Maor, & Panjapornpon, 2011). Other studies (Lara, et al., 2017) calibrate models using a MOO without scalarizing the errors, but instead, assuming that the $cv(RMSE)$ and the $NMBE$ are conflicting objectives and the objective is to find the set of *non-dominant* solutions (*Pareto optimal* solutions). This study considers as calibrated the best solutions (with acceptable errors, according to the standard) that are located among the *non-dominant* solutions, in the *Pareto* front.

2.5.3 Standard validation criteria

Regarding the validation of a model, one is considered sufficiently accurate when satisfying the standard criteria. Globally, three different entities (ASHRAE, IPMVP and FEMP) recommend different criteria. All these criteria are used for calibrations with consumed energy, with hourly or monthly data, as presented in Table 1. Currently, the criteria used in almost every calibration is the one established by the (ASHRAE, Guideline 14-2002), which intends to provide guidelines for the modellers to accurately predict the energy savings in future retrofit measures.

Table 1: Standard Criteria to validate BES models, adapted from (Coakley, Raftery, & Keane, 2014)

	Monthly Calibration			Hourly Calibration		
	*ASHRAE**	*IPMVP*[2]*	*FEMP*[3]*	*ASHRAE**	*IPMVP*[2]*	*FEMP*[3]*
$NMBE$ (%)	± 5	± 20	± 5	± 10	± 5	± 10
$cv(RMSE)$ (%)	15	-	15	30	20	30

* ASHRAE, American Society of Heating, Refrigerating and Air-Conditioning Engineers

*[2] IPMVP, International Performance Measurements and Verification Protocol

*[3] FEMP, U.S. Department of Energy: Federal Energy Management Program

According to (ASHRAE, 2009) one of the major difficulties that could prevent achieving a calibrated solution of a BES model is the choice of the calibration methods. Regarding the types of calibration approaches found in the literature, (Coakley, Raftery, & Keane, 2014) distinguish between manual and automated calibration techniques. Manual calibration is the procedure of manually changing specific inputs of the model with an iterative and pragmatic intervention from the modeller. Conversely, automated calibration are all the methods that employ algorithms to automatically find the calibrated solution(s), with mathematical and/or statistical techniques.

2.5.4 Calibration approaches

A work developed by (Reddy, Maor, & Panjapornpon, 2011) suggests a methodology to estimate, in the most accurate way, the energy conservation measures in BES, using observable data of gas and electricity consumption. This work suggests a pre-calibration task, which consists of gathering all the possible error-free information about the properties of the building, systems, usage patterns and climate data. This pre-calibration stage involves collecting baseline information from drawings, audits, *walkthrough* site visits and involves also creating a detailed model with the base-case influential input values along with their expected ranges of variation (lower and upper bounds). In this early design stage, the influential variables and their bounds are identified with heuristic knowledge and modelling experience.

After manually generating the detailed BES model, which depends purely on the knowledge of the modeller himself, (Reddy, Maor, & Panjapornpon, 2011) suggest calibrating the model, by performing two types of search in the "domain of uncertainty". One method is the *blind coarse grid* approach, which consist of finding local optima and performing sensitivity analysis at the same time. This method is called a blind search because,

as it is a *Monte Carlo* approach, a sample of solutions is randomly chosen from the domain and it is used to calculate both *goodness-of-fit* (without any searching algorithm) and sensitivity measures.

The other method is the *refined guided search*. Instead of implementing pure random walks in the domain, the *guided search* tries to find the global optimum error (*goodness-of-fit*) using manual or automated techniques, which can be traditional gradient-based methods, or non-gradient techniques, such as *genetic algorithms* or *simulated annealing*. The methodology proposed in this work (Reddy, Maor, & Panjapornpon, 2011) suggests to start searching from the local optima found in the first calibration stage and then minimize the error by tuning the influential parameters (found by sensitivity analysis), using one of the referred methods.

Finally, to solve the problem of the indeterminacy of calibration (i.e. several solutions with high *goodness-of-fit*), (Reddy, Maor, & Panjapornpon, 2011) propose several plausible solutions, identified in both calibration stages, rather than a single vector of parameters expressing the global optimum fit to the observable data.

2.5.5 Calibration data

Most of the studies calibrate BES models using measured and simulated energy consumption (i.e. using gas and/or electricity bills or measured data), since their major concern is on applying energy conservation measures and estimate accurately what the actual energy savings will be. These studies usually leave on a secondary plan other objectives, such as the thermal comfort, which depends strongly on the indoor temperature, indoor relative humidity and outdoor climate conditions. However, a literature review could identify some studies that use observable data regarding some of these parameters, to obtain calibrated solutions.

One example is a study that calibrated one historic building with indoor air and surface temperatures (Roberti, Oberegger, & Gasparella, 2015). This work considered the calibration to be fundamental not only to save energy and investment cost of the retrofit measures, but also stated that non-calibrated models may lead to thermal discomfort in buildings. This work consists of the calibration of the envelope properties of the building (thermal properties of the opaque materials and glazed surfaces) and the renewable air rate. For this, it was used the root mean square error ($RMSE$) to compare the simulated and measured temperatures in several areas of the building. Both simulated and measured temperature for each hour were then averaged to a single value of temperature (using the weighted average, where the weight of each zone is proportional to its area). The proposed methodology consists of firstly, performing a sensitivity analysis, in particular the elementary-effects method, to know what the most influential parameters to the error are (thus, reducing the order of the problem). Then, the error is minimized in a seasonal basis (during the cooling period), using Particle Swarm Optimization, (PSO). Finally, another set of data, more specifically, surface and indoor air temperatures during the heating period were used to validate all the calibration.

3 METHODS FOR THE MODEL CALIBRATION

3.1 Sensitivity Analysis

A sensitivity analysis has the main purpose of finding which of the parameters of a model (which can be analytical or a black-box model) are the most influential and/or quantify the effects of their variation on the output of a model.

In BES, the sensitivity analysis is used in several applications, such as building design, building retrofit, BES model calibration among others (Tian, 2013). BES programs use complex models with lots of discontinuities and in general cannot be described analytically so, a black-box approach is usually used, i.e. the analysis occurs externally to the model, which is considered as a black-box (even if it is a physical model), only by studying its outputs when specific inputs are applied.

Overall, two types of sensitivity analysis exist, although the classification may vary from one author to another: the local and the global sensitivity methods. The local sensitivity methods focus their analysis around only one point of the domain and the sensitivity measures derive from the variation of the parameters of that base case, one parameter at a time (OAT). Since these methods only explore the domain around one point, they ignore every interaction effect and so their use is very limited.

The global sensitivity methods aim at quantifying the influence of the model's parameters over the whole domain. In BES models, the most used global sensitivity methods are the regression-based methods, the variance-based methods and the screening-based methods.

Since BES models are treated as black-box models, all the global methods referred in the last paragraph require a sample of representative points to explore the domain. Rather than the use a simple random sampling, different methods can be used, such as the Latin hypercube sampling (LHS), the FAST (Fourier amplitude sensitivity test) sampling method or the Sobol sequence (Nguyen & Reiter, 2015).

Regarding the calibration of a BES model, sensitivity analysis is usually used to reduce the order of the calibration system, i.e. the number of uncertain parameters to be calibrated. To perform this analysis, a global sensitivity method is usually used to screen the most influence uncertain parameters inside the boundaries and including the probability distributions of the parameters. One example of this type of approach is the elementary-effects method or Morris method (Morris, 1991).

3.1.1 Elementary-Effects method

The elementary-effects method, or Morris method, was introduced by (Morris, 1991) and is a screening technique that belongs to the category of the global sensitivity methods. This method is usually used for computationally expensive models, such as in BES, since other sensitivity techniques would need numerous simulations and would be infeasible (Sohier, Farges, & Piet-Lahanier, 2014). This method is also used when there

is no interest in knowing quantitatively the sensitivity of each variable but instead, a qualitative measure to rank the uncertain variables in terms of influence.

Once the most influential inputs have been screened, the other non-influential variables can remain constant without affecting considerably the output of the model. This method allows to reduce the order of the calibration problem $g(X)$, as shown in the example of equation (4) where the order of a model with K initial variables can be reduced by removing from the function, i non-influential variables $(x_1, \dots, x_i)$, which become constant after the other $K - i$ variables are screened.

$$g(x_1, x_2, x_3, \dots, x_k) \approx g(x_{i+1}, \dots, x_K) \quad (4)$$

Although this is a OAT technique - i.e. it changes the value of one variable at a time, while keeping the others constant - the elementary-effects method overcomes its main limitation of being *local*, since it involves a sample of solutions on the entire domain, instead of only the solutions around one base solution, as the local OAT methods do.

3.1.1.1 Elementary-Effect

Consider a function $y = g(x_1, \dots, x_K)$ that could be any analytical function or a *black-box model* with K uncertain parameters, defined by the vector $X = (x_1, \dots, x_K),\ X \in \Omega$, where Ω is the domain, also known as the K dimensional hyperspace, in which each variable has been discretized in a p *level* grid (i.e. each variable can have p equally spaced values).

An elementary-effect approximates the partial derivative of the function $g(X)$ around one point X_0, as it shown in equation (5). The elementary-effect of the i variable (EE_i) is calculated simply as the slope of the line that passes through the point X_0 and the point X_0', where X_0' corresponds to increasing or decreasing X_0 by a finite quantity of Δ in its i variable (equations (6) and (7)).

$$EE_i(X_0) \approx \left.\frac{\partial y}{\partial x_i}\right|_{X_0} \quad (5)$$

$$EE_i(X_0) = \frac{y(X_0) - y(X_0')}{\Delta} \quad (6)$$

$$EE_i(X_0) = \frac{y(x_1^0, x_2^0, \dots, x_i^0 + \Delta, \dots, x_K^0) - y(x_1^0, x_2^0, \dots, x_i^0, \dots, x_K^0)}{\Delta} \quad (7)$$

Morris initially proposed the calculation of r elementary-effects for each variable $x_i,\ i = 1, \dots, K$, by filling the hyperspace with a sample of points $r.K$ points. Because each point needs a second one for an elementary-effect to be calculated, these base points are randomly increased or decreased in a specific direction and EE_i is calculated from that. After all the $r.K$ elementary-effects are calculated, each sample of r elementary--effects is treated as a representative sample of the whole population of independent elementary-effects of the i variable. This method requires $2.r.K$ evaluations of $g(X)$, which can be computationally expensive for some models.

To solve this problem, (Morris, 1991) suggested a more economical design, where the same point could be used to calculate two elementary effects. This new method involves using r trajectories, instead of r

elementary-effects per parameter, each trajectory with K elementary-effects, calculated with $K+1$ points. Using the "trajectories approach", the number of simulations is reduced to $r.(K+1)$, which has a lower computational cost than the previous method. Another approach, with the same "economy" as the trajectories, involves the calculation of "radial-points" (Sohier, Farges, & Piet-Lahanier, 2014), where a central point is used to calculate K elementary-effects.

As an example, Figure 5 represents two trajectories (a) and two radial-points (b) exploring on the $K=3$ domain – where each trajectory/radial-point has three elementary-effects ($K=3$) and 4 points. This gives a total of 8 evaluations of $g(X)$, using either (a) or (b) (i.e. $r.(K+1)=2.(3+1)$).

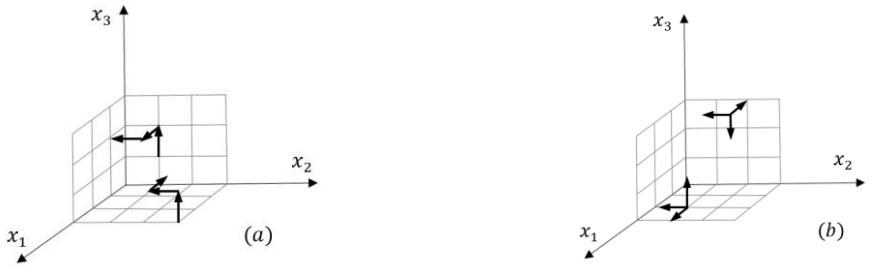

Figure 5: Two trajectories in the K=3 hyperspace (a) and Two radial points in the K=3 hyperspace (b)

3.1.1.2 Sensitivity measures

Independently of the method used to generate the elementary-effects, for each variable it is always withdrawn a sample of independent elementary-effects, which represents the whole population. Each sample has a probability distribution function F_i, that is described by its mean (μ_i, given by equation (8)) and variance (σ_i^2, given by equation (10)), so $F_i \sim (\mu_i,\ \sigma_i^2)$. Since there are K variables, there are also K samples, and therefore K means and variances. (Morris, 1991) suggests that each parameter i has two sensitivity measures: μ_i (the mean) and σ_i^2(the variance).

The sample mean (μ_i) measures the overall influence of the variable on the output and the variance (σ_i^2) gives information about the non-linear and/or interaction behaviour of the variable. For example, when a variable has a high variance, it means that the effect on the output of changing that variable depends largely on the values of the other variables (interaction effects) and/or on the values of the changed input (non-linear effects) because the elementary-effects for that variable are all very different. Smaller values of the variance mean that the elementary-effects are similar to the mean and therefore the variable has small non-linear and/or interaction behaviour. If the variance is small enough, the variable has an approximately linear behaviour.

An alternative to the variance is the standard deviation (σ_i), which is the square root of the sample variance and it is usually preferred, in order to be comparable to the mean in terms of order of magnitude.

Usually, the quantity Δ is constant for all elementary-effects and because there are models that have non-monotonic behaviour, two elementary-effects of the same order of magnitude but one positive and the other negative can cancel each other effects when they are accounted in terms of μ_i. This could be a problem because large elementary-effects associated to a variable i should be an indicator of large impact of that variable

on the output. As the *cancelation effect* decreases the value of μ_i, an influential variable becomes then non-influential.

An alternative to overcome this problem is to calculate the sample mean of the absolute value of the elementary-effects. The procedure is the same, but instead of considering the sample of the elementary-effects (F_i), it is considered the sample of their absolute values, i.e. G_i (Saltelli, et al., 2008). The mean of this sample, defined as μ_i^* (equation (9)) solves the cancelation problem. In most of the studies, this is the only sensitivity measure considered to rank the variables, as an overall sensitivity measure. Usually, to study the "overall monotony" of a model, both means from the two distributions are plotted against each other.

$$\mu_i = \frac{1}{r}\sum_{j=1}^{r} EE_i^j \qquad (8)$$

$$\mu_i^* = \frac{1}{r}\sum_{j=1}^{r} |EE|_i^j \qquad (9)$$

$$\sigma_i^2 = \frac{1}{r-1}\sum_{j=1}^{r} (EE_i^j - \mu_i)^2 \qquad (10)$$

In Figure 6, it is presented an example of a sensitivity analysis using the elementary-effects method for a model with 20 variables and one output (i.e. $y = g(x_1, x_2, \dots, x_{20})$). The objective of this problem is to qualitatively study the model, more specifically the most important variables (screened variables), the non-influential parameters, the variables with non-linear behaviour and the monotony of the model in respect to all the variables.

According to (Saltelli, et al., 2008), after calculating the elementary-effects using r trajectories to explore the 20-dimensional domain, a plot of the overall sensitivity measure (μ_i^*) against the standard deviation of G_i (σ_i, instead of the variance, to be comparable to the mean), such that $G_i \sim (\mu_i^*, \sigma_i)$, will help identify the several areas where the parameters have different behaviour, according to their relative importance and non-linear/interaction effects. In Figure 6 we can distinguish four main areas:

- The lower left area (Figure 6, 1)) has a low standard deviation and a low mean. These variables have no significant effect on the output and the objective function won't change considerably if those variables change value, independently of variations in other parameters (if they change, the output of the model varies almost linearly in respect to these variables);
- The upper left area (Figure 6, 2)) has a low mean and a high standard deviation. The variables in this zone have also no significant effect on the output due to their low mean values. However, their variation is non-linear and/or have interaction effects;
- The lower right area (Figure 6, 3)) has parameters with low standard deviation and high mean. In this zone, all the parameters have strong linear (i.e. additive) effect on the output, due to their low σ (low non-linear effects);

- The upper right area (Figure 6, 4)) has both high mean and standard deviation, which means that the parameters in this area are equally influential as the ones in the area 3), but the effect of their variation is now strongly linked to other variables and/or to non-linear variations;

For a screening analysis only, one should focus on areas 3) and 4), i.e. variables with high μ_i^*, because their effects on the output are very strong compared to all other variables, which means that the parameters in the areas 1) and 2) can remain approximately constant in future simulations without changing the output significantly.

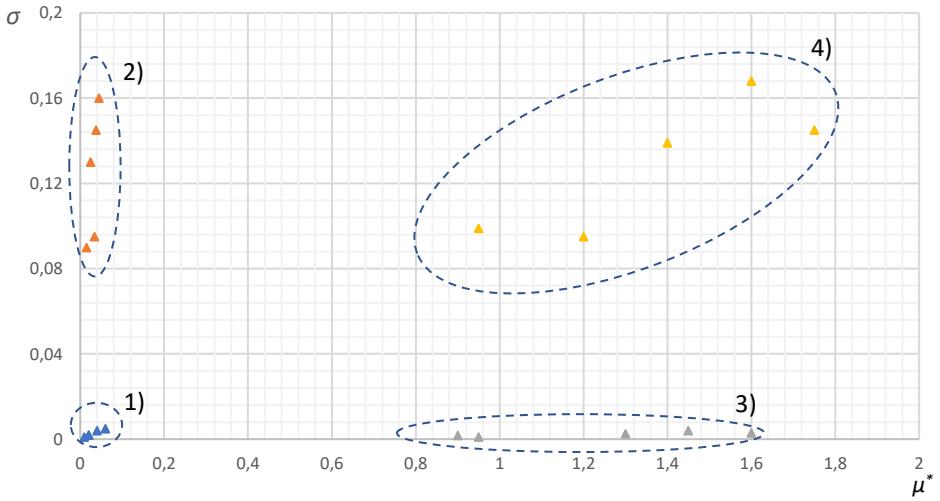

Figure 6: Plot of the two most sensitivity measures to qualitatively study the model

To analyse the monotony of the function in respect to all the 20 variables and see what are the parameters whose elementary-effects suffer from the cancelation effect, the absolute mean is plotted against the mean: if they are equal (i.e. $\mu^* = \mu$), the effect is inexistent. From the chart in Figure 7, we can distinguish from the points in the line i.e. the function is monotonic in respect to these variables, and the points above the line (i.e. $\mu^* > \mu$) that have non-monotonic behaviour.

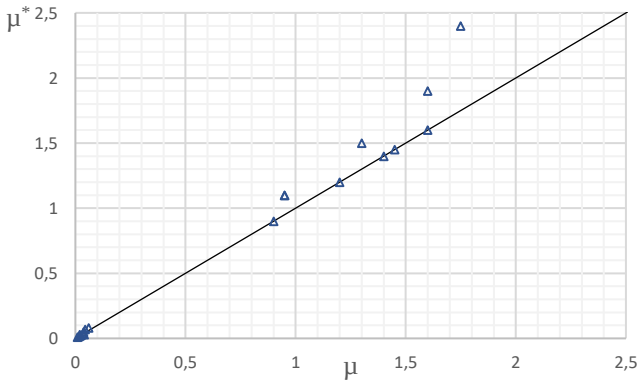

Figure 7: Plot of μ and μ^* to study the monotony of the model

Regarding the discretization of the domain, each parameter is firstly discretized in a grid with p levels, such that $x_i \in \omega$, $\omega = \{0, \frac{1}{p-1}, \frac{2}{p-1}, \dots, 1\}$. To build each trajectory, according to (Saltelli, et al., 2008), the procedure consists of: in first place to create a *base point* $X^* = (x_1^*, x_2^*, \dots, x_K^*)$, randomly selected from Ω, with the following conditions:

- The first trajectory point $X^1 = (x_1^1, x_2^1, \dots, x_K^1)$ is obtained by simply adding or subtracting Δ to one or more of the components of X^*, with the condition that the resulting point is still in the domain (Saltelli, et al., 2008);
- Once $X^1 \in \Omega$, the procedure is the same for all the other K points of the trajectory, i.e. $X^{m+1} = X^m \pm e_i.\Delta$; $(m, i) = 1 \dots K$, with the condition that each order i of the changed variable is only changed once in a trajectory and Δ is randomly added or subtracted to the previous point; e_i is a vector with K zeros, except in its i entry;

The choice of the value Δ is important for a good performance of this method. Δ can take integer values from the smallest division of the grid ($\frac{1}{p-1}$) to the maximum ($1 - \frac{1}{p-1}$). According to (Saltelli, et al., 2008), if p is even, then $\Delta = \frac{p}{2(p-1)}$. This choice for Δ allows all the p levels to have equal probability of being selected.

Since all the levels are equally spaced and the calculation of the output of the model does not account for the probability distribution of the parameters (if not uniformly distributed), usually the levels represent the quantiles of the distribution of each parameter and are mapped to real quantities, by calculating the inverse of the cumulative probability distribution function in the quantiles of each variable. As it is shown in the example of Figure 8 (taken from (Saltelli, et al., 2008)), 5 equally spaced levels (q_1, q_2, q_3, q_4 and q_5) are mapped with the inverse of the cumulative normal distribution. In this way, the sensitivity of each parameter accounts for its probability distribution (usually used for sensitivity analysis of parameters with uncertainty).

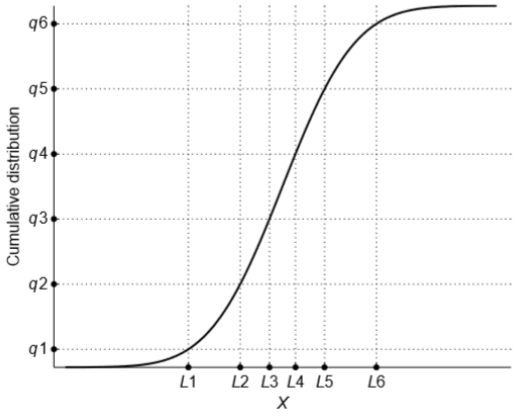

Figure 8: Mapping five equally spaced levels (q) to the space of the probability distribution of the parameter

One major drawback of this method, as in all the non-deterministic methods, is the problem of the non-representativity of the sensitivity factors, because it is based on the randomness of the trajectories and trusts in its dispersion over the domain. To try to solve this problem, some improvements of the initial method by (Morris, 1991) have been proposed.

One example of a method to solve the representativeness problems of the trajectories, as suggested by (Sohier, Farges, & Piet-Lahanier, 2014), is to sample the base points of the trajectories (X^*) using the *Latin hypercube sampling* (LHS). This sampling method is as an improvement of the random sampling because it tries to cover uniformly the hyperspace by allowing all levels of each parameter to be selected.

The basic property of the LHS is that for every point $X = (x_1, x_2 \dots, x_K)$, such that its variables $\{x_1, x_2, \dots, x_K\}$ belong respectively to the levels $\{q_1, q_2, \dots, q_K\}$, no other point can have the same variables in any of the levels of the first. This property creates the condition that the number of levels (p) must be equal to the number of sampled points (r). For example, in Figure 9 a), 4 points are chosen using random sampling. This sample of points is far from being uniformly distributed, contrarily to Figure 9 b) in which the points were sampled with the LHS and at least one level of each variable has been explored.

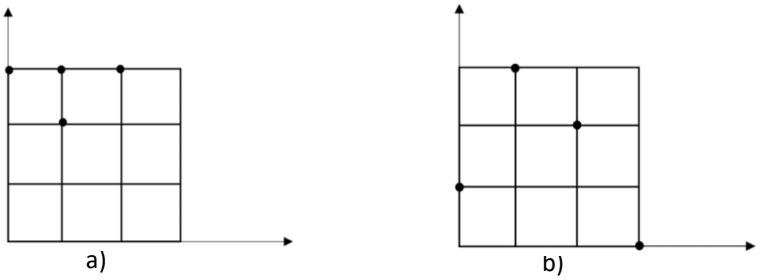

Figure 9: a) Example of random sampling and b) Example of a Latin Hypercube Sampling

3.2 Optimization using Genetic Algorithms

The genetic algorithms (GAs) are an example of a biologically inspired tool to optimize engineering problems. The GAs are included in the random optimization methods (Goldberg, 1989) and are usually used to search for the global optimum in high-dimensional problems, where the enumerative or calculus-based methods fail due to high computational effort or the inability to calculate the gradient of the objective function.

These optimization methods simulate the biological evolution of a generation of a population of solutions based on their natural selection, also known as the *survival of the fittest* (*Darwinian Theory*). In computer systems, the ability to survive is given by the value of the objective function: individuals with higher fitness (lower value of the objective function) will have higher probability of being chosen to reproduce the individuals of the next generation. This *selection* operator, along with *crossover* and *mutation* makes the genetic algorithm, which allows the individuals to evolve through the generations (or iterations) under these survival rules.

In terms of analogy between biology and the genetic algorithm, we can distinguish between *genes*, *chromosomes* and the *fitness*: the *gene* is a block that encodes a parameter of the candidate solution (Mitchell, 1999); one *chromosome* is a set of *genes* which describe one candidate solution for a given problem (sometimes called an individual); the *fitness* of an organism is the ability to survive through the generations and reproduce (Mitchell, 1999) and is represented by the value of the objective function of the problem.

Firstly, as in any other optimization technique, the objective or cost function and the input variables must be chosen. The GA will choose a set of the fittest individuals of each generation using the *selection* operator and will modify the values of these variables using the *crossover* and the *mutation* operators and evaluate the objective function. The variables may be unbounded, taking any possible value, or limited by their *lower bounds* and/or *upper bounds*. The problem may be subjected to equality and/or inequality constraints which are handled

differently, depending on the constraint handling method (Deb, 2000). Furthermore, some variables may only have integer values (integer constrained variables).

After generating the initial population of *chromosomes* or before any evaluation of the fitness function in between generations, the principles of genetics are applied to a set of candidates defined in the *selection* process, whose intent is to evolve from one generation to another. Moreover, there may exist a small fraction of highly fit candidates in each generation who get copied, unchanged, to the next generation. This is known as the *elitism* or *elite solutions* (Haupt & Haupt, 2004). The process goes on for several iterations until a stopping criterion is achieved, which means that a promising optimal solution has been found.

3.2.1 Chromosome representation

The way the solutions are encoded in chromosomes is a very important process of the GA, as it influences the way the *crossover* and the *mutation* operators are implemented, which are key for the success of the algorithm. Two types of GA exist based on the encoding: the binary GA and the real-coded GA (RCGA).

3.2.1.1 Binary GA

The simplest and original genetic algorithm works in a binary alphabet (this is known as the binary GA (Haupt & Haupt, 2004)), so it's necessary to decode all the input variables before evaluating the fitness function (Figure 10). The initial population can be randomly generated or partially introduced in the first generation before encoded in bits.

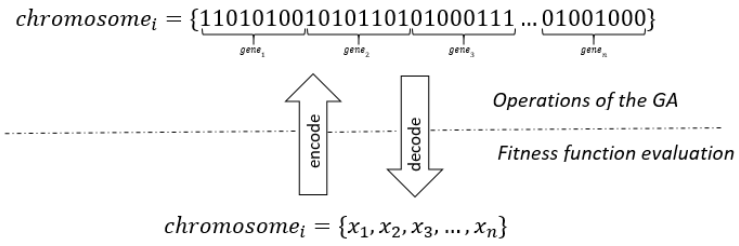

Figure 10: Example of encoding and decoding a chromosome

3.2.1.2 Real-Coded Genetic Algorithm (RGCA)

Although used in many problems, binary GAs have some downsides related to the accuracy of the variables and to the convergence of the solutions (Haupt & Haupt, 2004). There is always a discretization error associated to encoding a gene and the accuracy of the "real variable" is related to the size of the *gene* (number of bits). Therefore, for a higher precision of the results, more bits are needed to compose a *gene*, which may slow down the process of convergence.

To overcome this limitation, real-coded genetic algorithms or RCGAs (Deep, Singh, Kansal, & Mohan, 2009) are used. The way these GAs work is very similar to the binary GA. The major difference is that they do not work with bits but with floating-point (continuous) variables. In this case, the *chromosome* has the real or integer values of the input variables instead of "ones and zeros" encoding each *gene*. After applying the classical genetic operators, the fitness function is directly evaluated without the need for a decoding.

3.2.2 Selection

This operator simulates the *survival of the fittest,* i.e. the candidate solutions with a lower value of the cost function will have higher probability of being selected for the *crossover* operation. The *selection* is carried on by choosing one pair of parent *chromosomes*, usually with a *roulette-wheel sampling* or *tournament selection,* to generate two or more offspring *chromosomes*. Both *selection* methods are used for the binary GA and RGCA.

The *Roulette-wheel sampling* is analogous to a physical biased roulette, where each slot on the wheel has an area proportional to the fitness of the *chromosome* (Goldberg, 1989). The probability of reproducing is proportional to the fitness of the *chromosome* and the parents are selected in pairs, based on this probability. As an example, Figure 11 shows four *chromosomes* disposed in a *roullete-wheel*, with four slots with different areas. The *chromosome* 2 has the highest fitness, so it has the slot with the largest area and highest probability of being selected for reproduction.

The other most used selection operator is the *Tournament selection*, which is carried on by randomly choosing a set of chromosomes from the population and assign the parent function to the one with the lowest cost. This process repeats until all the parents needed to reproduce are selected (Haupt & Haupt, 2004).

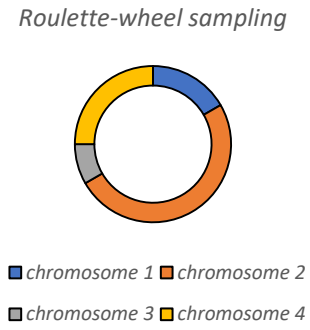

Figure 11: Example of a biased roulette-wheel with four candidate chromosomes

3.2.3 Crossover

After selecting the pairs that will generate the offspring's *chromosomes*, an operation known as *crossover* is performed for each mating pair of *chromosomes*, with a probability of occurrence of p_c (*crossover probability* or *crossover rate*). This operation consists of "trading" genetic information between the two parents to originate their offspring in such a way that part of the offspring's genes comes from one parent and the other part comes from the other parent. This exchange of genes allows that highly fit candidate solutions may produce also fit solutions while searching in other potential promising locations of the domain.

The simplest type of *crossover* for the binary GA, consists of exchanging parts of the parents' *chromosomes* until a randomly chosen crossover point, as presented in the following example (Figure 12), where the crossover point is between the sixth and seventh bit of each parent and the each originated offspring is composed of *genes* from both parents. An example of a variation of this method allows not only one but multiple crossover points to be chosen in a *chromosome*.

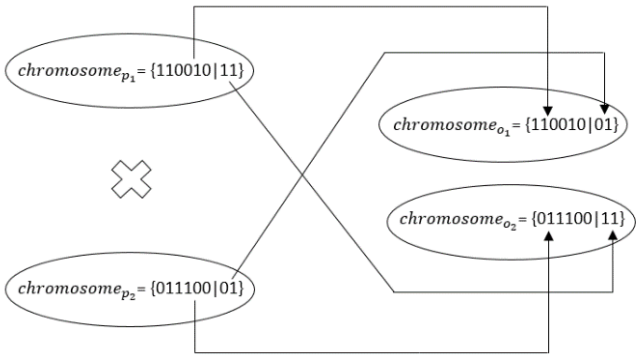

Figure 12: Example of a crossover in the binary GA

In the RCGA, the *crossover* operation is usually different. When the "binary crossover" is applied, it allows to exchange genes between parents and new information is generated (if crossover point(s) divide a *gene* in parts then new information related to that *gene* is generated). If this crossover technique is performed on the real-valued *chromosomes*, although new individuals are created, no new inputs are introduced, so there is a need for a new crossover technique.

One example of a crossover technique for the RCGA is the *arithmetic crossover* and it is simply the linear combination of both parents, as it is presented in equation (11), adapted from (Haupt & Haupt, 2004).

$$\begin{cases} x_i^{o_1} = \beta x_i^{p_1} + (1-\beta)x_i^{p_2} \\ x_i^{o_2} = \beta x_i^{p_2} + (1-\beta)x_i^{p_1} \end{cases} \quad (11)$$

In the first equation, i is the order of the offspring's variable ($x_i^{o_1}$) that is obtained from the combination of the i-order variable which comes from one parent ($x_i^{p_1}$) and the same order's variable coming from the other parent ($x_i^{p_2}$). The weight β is a random number uniformly distributed between $[0,1]$ that weights the contributions of both parents. Identically to the previous binary crossover, this operation usually generates two offspring, one of them simply by applying the first equation and the other by exchanging the weights (β and $(1-\beta)$) from p_1 to p_2 (second equation, in (11)).

Also like in the binary, a crossover point is randomly chosen, and the linear combination is calculated for all the variables from the beginning (or the end) of the *chromosome*, to the crossover point.

3.2.4 Mutation

The *mutation* is the final operation of a generation and it allows the algorithm to escape the local minima and search new areas for a global minimum. If mutation didn't exist, solutions would prematurely converge to a local optimum (Haupt & Haupt, 2004), which is not the objective. In the binary GA, this is simply the process of flipping a bit (0 to 1 or 1 to 0) in a randomly chosen point of the chromosome (as in the example of Figure 13) with a probability of p_m, *mutation probability* or *mutation rate,* which is usually much smaller than p_c.

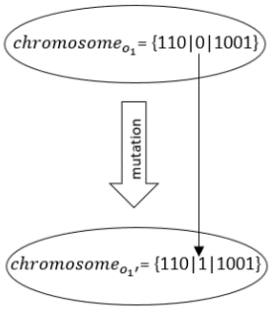

Figure 13: Example of a mutation in the binary GA

In the real-coded GA, *mutation* occurs also in some variables with a rate of p_m ($p_m \ll p_c$). The variables are then mutated by simply exchanging their values by a uniformly distributed one (*uniform mutation*), or by linearly combining them with values chosen from a certain distribution.

3.2.5 Stopping criteria

After the *crossover* and *mutation* operations, the algorithm goes on again through all these processes of *selection, crossover* and *mutation* until acceptable solutions are reached, as it is summarized in the flowchart of Figure 14. The stopping criteria are usually the number of generations, time spent on the optimization, lack of improvement in the best or average cost of the iteration along a specific number of generations, or a certain limit value of the fitness function.

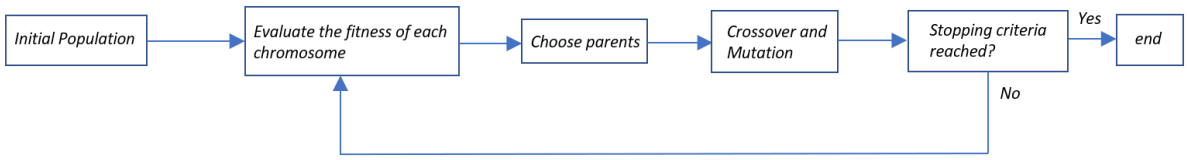

Figure 14: Flowchart of a genetic algorithm

4 METHODS FOR THERMAL COMFORT EVALUATION

According to the (ASHRAE Standard 55-2010), thermal comfort is the condition of mind that expresses satisfaction with the thermal environment, which may be influenced by many physical, psychological or physiological factors and therefore vary from one individual to another. Despite this inherent variability of the conditions for achieving thermal comfort, there are specific indoor conditions determined by laboratory or field studies and supported by statistical data that guarantee a large fraction of a population to feel comfortable within a certain range of indoor environmental conditions.

Usually, the acceptable conditions for thermal comfort of the whole body are determined by one of two types of models: analytical or adaptive models. Analytical models are usually called heat balance models and assume that individuals experience a certain level of comfort, interacting passively with the environment. These models are based on the heat balance between the individual and the environment. The adaptive models suggest a possible adaptation of the individual to the thermal conditions, which may be psychological, physiological or physical adaptation, such as changing clothes, increasing/decreasing the activity level or opening/closing windows. In conclusion, the adaptive approach accepts that people interact actively with their environment to optimize their conditions of comfort.

Apart from the whole body thermal comfort, there is also thermal discomfort in localized parts of the body, also called local discomfort. This type of discomfort may be caused by draughts, vertical air temperature difference, warm and/or cold floors and radiant asymmetry (ASHRAE, 2009).

4.1 Predicted Mean Vote model

One of the most well-known and accepted analytical models is the Predicted Mean Vote (PMV) model developed by (Fanger, 1970). In numerous experiments, (Fanger, 1970) used a seven-point sensation scale that goes from -3 (cold sensation) to $+3$ (hot sensation), to relate several variables to the mean response of a large group of people.

Although this thermal comfort model is more accurate to buildings with high occupancy rates and with forced ventilation, it is also often used to evaluate thermal comfort on residential buildings, where the concentration of people is smaller than in the non-residential sector (e.g. schools and offices).

The PMV index is obtained through the heat balance between the individual and the environment and is a function of the metabolic activity (M) and of the thermal body load (L) given by equation (12), where this last one is the accumulation of heat in the body. As explained in equation (13), L is related to M, to the mechanical work done by muscles (W), to the total heat lost through the skin and clothes (Q_{sk}) and to the total heat lost by respiration (Q_{res}).

$$PMV = [0{,}303e^{-0{,}036M} + 0{,}028]L \qquad (12)$$

$$L = (M - W) - (Q_{sk} + Q_{res}) \quad (W/m^2) \qquad (13)$$

Theoretically, using this definition of thermal comfort, $PMV = 0$ occurs with zero thermal body load ($L = 0$). This thermal neutrality happens when there is no accumulation of heat in the body, i.e. when the heat generated by the body minus the energy spent in mechanical processes is equal to the heat lost to the environment.

The PMV has six major influential factors related to the individual himself and the environment (ASHRAE Standard 55-2010). These are: the metabolic activity (M), the clothing insulation (I_{cl}), the air temperature (t_a), the air speed (u_a), the relative humidity (RH) and the mean radiant temperature ($\bar{t}_r$), being this last parameter the uniform temperature of an imaginary black enclosure that would exchange the same radiant heat as the one that is being exchanged in the reality.

Another way to express this index is through an indicator that gives a prediction of the percentage of thermally dissatisfied people exposed to the same environment or in other words, the Percentage of People Dissatisfied (PPD). This index is only a function of the PMV (given by equation (14)).

$$PPD = 100 - 95e^{-(0{,}03354PMV^4 + 0{,}2179PMV^2)} \ (\%) \qquad (14)$$

A study was made by (Ioannou & Itard, 2014) on the parameters of a BES model that have the highest influence on the PMV. This work focused on two residential, conditioned spaces and the sensitivity analysis could isolate three highly influential parameters. The most important was the metabolic activity, followed by clothing insulation and thermostat settings, leaving as secondary and not so influential variables the air speed and the relative humidity, which comes mainly from natural ventilation and infiltration. This study considered only the control of the temperature in both houses, which affects both air temperature (t_a) and mean radiant temperature ($\bar{t}_r$). Therefore, these two parameters, along with the activity and clothing, were found to be the most sensitive variables of the PMV.

When applying the PMV model it is important to account for some restrictions to its application, such as when a person is sleeping. Although the metabolic activity is easily obtained from tables, available for example in (ASHRAE, 2009), the thermal insulation of an individual whose activity is sleeping is impossible to predict because it depends especially on the sleeping position and bedding, which vary from one individual to another (ASHRAE Standard 55-2010). Another reason is that it is usually considered that a person is thermally comfortable when is sleeping.

Currently, there are two important standard that specify the acceptance of thermal comfort conditions: the (ASHRAE Standard 55-2010) and the (International Standard ISO 7730, 2005). Both standards establish limits for the general thermal comfort, using the analytical model of the PMV/PPD and an adaptive model.

The acceptance limits for the (ASHRAE Standard 55-2010) are a $|PMV| < 0{,}5$ which is the same as with a $PPD < 10\%$ and the (International Standard ISO 7730, 2005) considers three categories for the acceptance of the general thermal comfort. These categories vary between a stricter PMV limit (category A, Table 2) and a less strict acceptance limit, with thermal comfort for $|PMV| < 0.7$ (category C, Table 2).

Table 2: Categories of thermal comfort, adapted from (International Standard ISO 7730, 2005)

Category	PPD (%)	$\|PMV\|$
A	< 6	< 0.2
B	< 10	< 0.5
C	< 15	< 0.7

4.2 Adaptive models

The adaptive models are based on the statistical analysis of data gathered in field studies such as surveys to the occupants of a building. These models don't consider most of the factors referred in the previous section. Instead, the adaptive approach studies the link between thermal comfort and the climate, the nature of the building and time (Nicol & Humphreys, 2002). These models are strictly used to evaluate the thermal comfort in naturally ventilated buildings, where the notion of comfort is different from conditioned spaces, due to different thermal experiences, the availability of control and different expectations from the occupants (ASHRAE Standard 55-2010).

Currently, one of the most used adaptive models relates the operative temperature (t_o, evaluated as the mean between the mean radiant temperature and the air temperature) to the mean monthly outdoor air temperature t_{out} (evaluated as the arithmetic average of the mean between the daily minimum and daily maximum outdoor air temperature, for the previous thirty days). This model has two areas of comfort: a zone with 80% acceptability of the thermal conditions by the occupants; and another zone with 90% acceptability, which is used as a higher standard of the thermal comfort, as it is presented in Figure 15 (ASHRAE Standard 55-2010) where both acceptability limits are defined by equation (15).

$$\begin{cases} t_o = 0.31.t_{out} + 17.8 \pm 2.5\ (℃), & 90\%\ acceptability \\ t_o = 0.31.t_{out} + 17.8 \pm 3.5\ (℃), & 80\%\ acceptability \end{cases} \qquad (15)$$

There are some conditions to use this model, such as: the opening and closing of windows must be the primary mean of regulating the thermal conditions of the space, the physical activities must be near-sedentary ($M \in [1;\ 1.3]\ (met)$) and the occupants must be free to adapt their clothing to the thermal conditions.

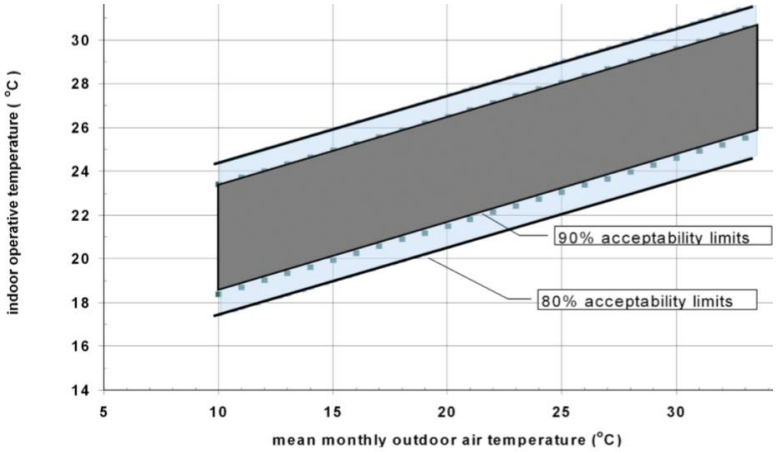

Figure 15: Acceptable operative temperature ranges of the adaptive model, taken from (ASHRAE Standard 55-2010)

5 METHODS FOR THE RETROFIT MEASURES IDENTIFICATION

Retrofit measures are the combination of measures applied to a building in order to improve its physical conditions and usability by the occupants. Most of the studies found on the literature about retrofit measures focus in finding the combination of measures that give the minimum energy consumption (ECM) with the minimum investment cost. Other studies consider also other objectives, such as maximizing the thermal comfort or the visual comfort (Carlucci, Cattarin, Causone, & Pagliano, 2015).

To find the combination of retrofit measures that satisfy only one criterion is a single-objective optimization problem and there is usually only one solution for this problem, which describes the combination of measures in which the objective function is equal to the global minimum. In contrast to single-objective optimization, multi-objective optimization (MOO) deals with several objectives or criteria, often conflicting, and searches for the optimum, simultaneously for all the objectives.

5.1 Multi-Objective Optimization

The MOO concept of optima is different from the single-objective optimization, since it is in general a set of solutions (not only one) that cannot be minimized in one of the objectives without increasing their value in the other objectives, representing therefore the *trade-off* between the objectives. These are the solutions that are not dominated by any others, i.e. there are no better solutions than the non-dominated in all objectives (Goldberg, 1989). The set of non-dominated solutions defines the *Pareto front*, which can be a two-dimensional curve (when there are two objectives) or a n dimensional surface (for n objective functions).

There are two approaches to search for the optimal solution(s) in a MOO problem. The first method scalarizes all the conflicting criteria into a single objective function, which is usually the weighted average of all the objectives, and then minimize the objective function with a single-optimization approach. In this method, the *decision-maker* (DM) needs to define what is the relative importance each objective (by assigning the weights to each objective) so, this is also known as an *a priori approach.*

The other approach is the *a posteriori* approach, which consist of searching not for one solution but for a set of solutions that are equally optimal and represent the *trade-off* between all the conflicting objectives. After finding the *Pareto front* (i.e. the location of the optima solutions), the *decision-maker* then chooses with his own criteria, one solution from the set of optimal solutions.

Several methods exist to search for the *Pareto front*. One of these methods consists of performing multiple independent parametric single-objective optimizations (Deb, 2011), where the objective function is, as in the *a priori* methods, a linear combination of all objectives and the weights of all the objectives are varied in order to search for multiple global optima. The major drawback of this method is the high computational effort, especially for objective functions computationally expensive and although each single objective solution can converge to a global optimum, a good distribution of *Pareto optimal* solutions is not guaranteed (Deb, 2011). Thus, other methods are in general preferred.

Some methods allow to search for all the *Pareto* solutions in a single optimization problem. One of the most used in BES multi-objective optimization uses the *Genetic Algorithm*, more specifically, a version that is called the *elitist non-dominated sorting GA*, NSGA-II (Deb, 2011). This version of the GA, uses the same genetic operators as in a single-objective optimization (i.e. *crossover, mutation* and *selection*), but has a different approach to evaluate the fitness of the *chromosomes* regarding the multi objectives.

After applying the genetic operators to the selected parents of the previous generation, the NSGA-II classifies all the population of chromosomes (parents and offspring) in different ranks (as it is explained in Figure 16) according to the *non-dominated* front where the *chromosome* is located: *chromosomes* that are not dominated by any others have the highest rank, followed by the *chromosomes* that are only dominated by the highest rank's *Pareto* front and so on, until all the population is ranked.

The *chromosomes* with the highest rank (i.e. highest fitness) have highest probability of being chosen for reproduction to generate the offspring of the next generation. To limit the number of chromosomes to the initial size of the population, the solutions with the worst rank are either removed from the population or used to increase the diversity of solutions. This diversity is calculated with one operator that is called the *crowding distance*, which evaluates the *spread* of the solutions in the domain of the objective functions.

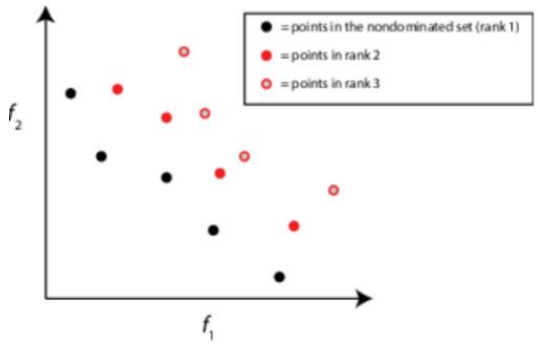

Figure 16: Example of a population with different ranks according to the non-dominated fronts (MathWorks, 2018)

The major drawback of using GAs to optimize BES models with several objectives, especially for time-costly models, is that many evaluations of the model are required to find the global *Pareto* front (Magnier & Haghighat, 2010). This might be infeasible in terms of computational effort and so, other approaches must be used.

Some alternatives to solve this problem have been proposed, such as using simplified estimation algebraic models to replace the BES program (Eskander, Sandoval-Reyes, Silva, Vieira, & Sousa, 2017). The impact of several retrofit measures - in this work the measures are: the replacement of the windows, lighting, insulation, electric equipment, HVAC and the installation of PV modules - is estimated with linear equations that give an approximation of the heat gains and losses through glazed and opaque surfaces. Then, the MOO evaluates these equations, instead of using a BES program. The problem of these models is that they over-simplify the problem and might lead to inaccurate conclusions.

The second option to avoid infeasible computational effort, commonly used, is to perform the MOO with a small number of *chromosomes* per generation or a stopping criterion that might not lead to the optimal *Pareto* front, such as a small maximum number of generations.

A third approach is to solve the problem of the computational effort without having to over-simplify the BES model or the GA. The main idea of this approach is to use models that are sufficiently complex to accurately replace the BES program without being time-costly. These models are also known as *surrogate models* (i.e. approximation or data-driven models) and they are used to approximate very complex models by only knowing the outputs of the actual model when subjected to specific inputs (i.e. a *black-box* approach) and finding the complex relations between them.

One example of a type of *surrogate model* that has been used in several BES-MOO studies and handled efficiently building retrofit multi-objective optimization problems ((Grossard, Lartigue, & Thellier, 2013), (Magnier & Haghighat, 2010) and (Asadi, Silva, Antunes, Dias, & Glicksman, 2014)), is the use of *Artificial Neural Networks* (ANNs). These models mimic the behaviour of the BE*S* program and then fully replace it in the MOO problem to evaluate the objective functions.

5.2 Artificial Neural Network

Artificial neural networks (ANNs) are algorithms inspired in the human brain to solve several kinds of problems, such as *pattern recognition, classification, optimization, function approximation* and many others (Fyfe, 2005). As in the brain, these systems are composed of many *artificial neurons* working in a parallel architecture (Shukla, Tiwari, & Kala, 2010), exchanging information from one *neuron* to another through the connections. The information flows into the system as the input of the ANN, which is then processed by the multiple *neurons* that generate then the output(s) of the network.

The most basic type of ANN, which is used especially for curve-fitting (function approximation) problems, is the multi-layer perceptron network (MLP). In this type of networks, the *artificial neurons* are arranged in layers, which can be passive or active layers depending if the *neurons* in those layers process or not the information (Shukla, Tiwari, & Kala, 2010). In the MLP networks, the flow of information only goes forward (that is the reason why these ANNs are also known as *feed-forward neural networks*), contrarily to the *recurrent neural networks* that have backward connections, allowing the information to flow cyclically with feedback between the *neurons*. This feedback introduces dynamism to the network, allowing the outputs to be time variant, in contrast to the MLP which have a static nature.

The first layer of a MLP is the input layer, which is a passive layer (it does not process the information), with the same number of *neurons* as the number of inputs of the system. The inner layers are also known as the *hidden layers* which are responsible to process the information. Finally, the information flows to the *output layer* that has the same number of *neurons* as the number of outputs of the system. The geometry of a MLP is then composed of an input and output layer with a fixed number of neurons, given by the dimension of the inputs and outputs of the problem, and a specific number of *hidden layers* with a specific number of *neurons*.

All the *neurons* that process the information basically perform two operations (Figure 17). Firstly, they calculate the weighted average between their K inputs ($\{x_1, \dots, x_K\}$) plus a constant (b, the *bias*). Each connection has a specific *weight* ($\{w_1, \dots, w_K\}$), which affects the signal that goes into the *neuron*. After calculating the weighted average between the inputs of the *neuron*, the result is evaluated by the activation function, $f_{act}(X)$ (equation (16)). Prior to this calculation, all the inputs are usually normalized between -1 and 1 for a better performance of the network (Shukla, Tiwari, & Kala, 2010)

$$o = f_{act}(\sum_{i=1}^{K} x_i . w_i + b) \qquad (16)$$

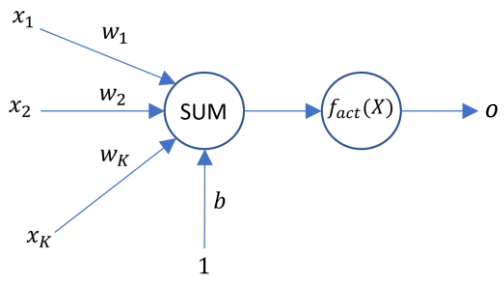

Figure 17: Operations performed by an artificial neuron

The activation function of the *hidden neurons* ($f_{act}(X)$) is usually a non-linear differentiable function, such as the log-sigmoid or the tan-sigmoid function (Figure 18 a) and b), respectively) that is responsible for the non-linear behaviour of the network.

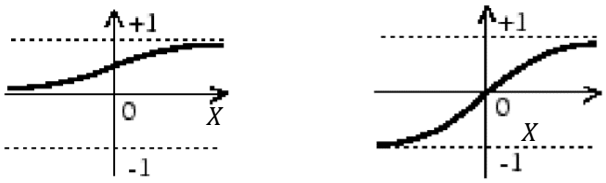

Figure 18: a) Log-sigmoid activation function, b) Tan-sigmoid activation function; adapted from (Beale, Hagan, & Demuth, 2017)

To accurately estimate the outputs when specific inputs are applied to the ANN, the network must firstly be trained with a set of inputs and the correct outputs, which are known as the *targets* (this process is also known as *supervised learning*). Training a network consists basically of performing an optimization problem, where the objective function is the error between the network's *outputs* and the *targets* in each iteration. The objective of this problem is, in a simplified way, to search for the combination of *biases* and *weights* of all connections that give the minimum *training* error. The error indicator, which analyses the performance of the network (i.e. the objective function) is usually the mean square error MSE (equation (17), where n is the number of targets (t) and outputs (o), i.e. size of the *training* data set).

$$MSE = \frac{1}{n} . \sum_{i=1}^{n} (t_i - o_i)^2 \qquad (17)$$

To train an ANN, several optimization methods exist. These methods calculate iteratively the adjustments on the network's parameters (w and b) to search for the solution with the best performance. These adjustments are usually made with the help of the derivatives of the error in respect to each parameter of the network. However, since this is a very complex task (especially for the *neurons* in the *hidden layers*), an efficient algorithm is usually used: *the back-propagation algorithm.* This algorithm is the most common method used to train the MLP networks and consists of: firstly, with a *forward pass* (from the input to the output layer), calculating the outputs of the network and the error between them and the targets. Then, it calculates the partial derivatives of the error on the output layer and propagate these derivatives with a *backward pass* to find the derivatives in the *hidden layers*.

Coupled to the *back-propagation* algorithm, several optimization methods exist, such as the *steepest gradient method*. This method, as it is explained in equation (18), updates the *weights* and *biases* of each *neuron*, using the partial derivative of the overall training error in respect to the output signal of the j neuron in the l layer (i.e. $\delta_j^{(l)}$). In this equation, $\Delta w_{ij}^{(l)}$ is the change in the weight that connects the i and j *neuron* (this latter from the l layer); $o_i^{(l-1)}$ is the output of the i neuron, which belongs to the $(l-1)$ layer; η is the *learning-rate* and it influences the speed of convergence. As it was said, the derivatives of the error ($\delta_j^{(l)}$) are firstly calculated on the output layer and then with *back-propagation*, these are calculated recursively in the hidden layers (from the layer l to the layer $l-1$ and so on, until all the derivatives in each *neuron* are calculated) (Fyfe, 2005).

$$\Delta w_{ij}^{(l)} = -\eta . o_i^{(l-1)} . \delta_j^{(l)} \qquad (18)$$

Other more robust methods are usually preferred, such as the *Levenberg-Marquardt algorithm*. This is a second order approach (it uses information about the second derivatives of the error to adjust the network's parameters). The problem of calculating the Hessian matrix H (that contains the second derivatives of the errors) is its computational cost and so, the *Levenberg-Marquardt algorithm* approximates H with the help of the Jacobian matrix J, which contains the first derivatives of all the network's errors in respect to all the *weights* and *biases* (calculated with the *back-propagation algorithm*). The vector with the updates of the parameters (Δw) in each iteration is calculated with equation (19) (Wilamowski & Chen, 1999), where J is the Jacobian matrix of the errors, μ is a learning parameter (adjusted in each iteration) and E is a vector with all the errors of the network.

$$\Delta w = -[J^T J + \mu I]^{-1} J^T E \qquad (19)$$

A problem of an ANN is called the *over-fitting*. During the *training,* when a network tries to reduce the error to fit all the training data as close as possible, the "curve" can adopt very complex shapes (Shukla, Tiwari, & Kala, 2010), which might become a problem because when the network starts to over-fit the data, it loses the ability to generalize i.e. starts to affect the data that was not used for training. To solve this problem, usually all the data set is divided in three sets: the *training, testing* and *validation data.* The first data set is used to adjust all the *weights* and *biases* of the network and therefore reduce the *training error.* The *validation data set* is to apply the principle of the early stopping, which consists of stopping the *training* when the *validation error* increases i.e. when the network starts to lose generalization. The other data set is the *testing data set* and is usually used to compare between several training algorithms.

6 CASE STUDY

This work focuses in determining the best retrofit solutions to improve a household in a residential building with poor thermal comfort conditions located in Lisbon, more specifically in Olivais Sul. The basic information about the household is summarized in the Table 3.

Table 3: Basic information of the household

Typology	T3 (5^{th} floor)
Orientation with N (°)	23
Floor area (m^2)	106.4
Location	Olivais Sul
Construction (year)	1971
HVAC	No
Nr. occupants	3
Weather file	Olivais Sul

The household's data was collected during a monitoring campaign within the *Suscity* project (SusCity Project, 2013) that occurred between the year of 2015 and 2016. This campaign involved several measurements on the outdoor and indoor environment thermal conditions that provided data to increase the accuracy of the models used in this work, more specifically on the thermal comfort predictions.

Regarding the indoor measurements, the air temperature was recorded in three areas of the house (divisions 1, 2 and 3, of Figure 19) for one year and the CO_2 air concentration was measured in only one division for a period of four days during the month of March. During this campaign, surveys were made to the occupants regarding their habits and usage patterns, such as occupation, the use of window shading, lighting and electric equipment. The outdoor measurements were performed using a weather station in the building's location that allowed to generate a weather file with hourly information on the dry bulb temperature, relative humidity, solar radiation, wind speed and direction during the entire year. All the indoor and outdoor monitored parameters are summarized in the Table 4.

Table 4: Indoor and outdoor parameters recorded during the monitoring campaign (SusCity Project, 2013)

Monitoring Parameters		Equipment
Indoor conditions	Temperature ($^{\circ}C$)	Temperature sensor
	CO_2 concentration (ppm)	Indoor Air Quality logger
Outdoor conditions	Temperature ($^{\circ}C$)	Temperature sensor
	Relative Humidity (%)	Humidity Sensor
	Solar Radiation (W/m^2)	Pyranometer
	Wind Speed (m/s)	Weather vane
	Wind Direction (°)	

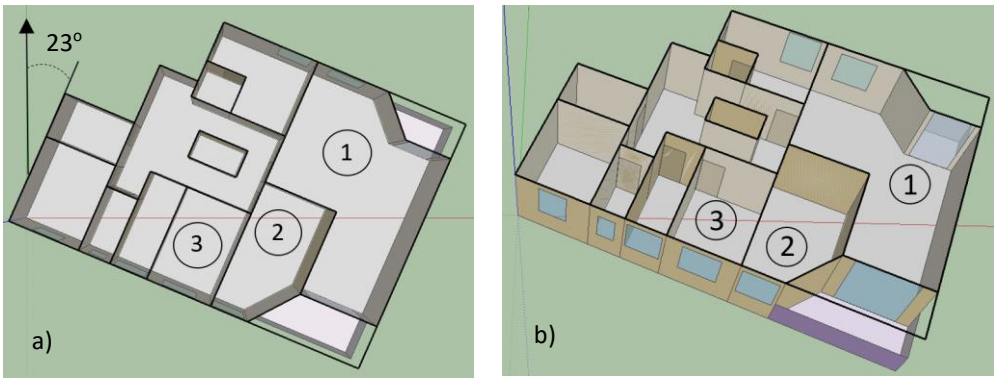

Figure 19 a) Top view of the household; b) Three-dimensional view of the house (with Google Sketchup 7)

As it was explained in Figure 1, this work includes two main stages: firstly it is presented the model calibration, which includes starting from a *baseline model* of the household, then it follows a *detailed model* and finally, a model in which the error between the simulated and measured air temperature has been minimized, using a calibration procedure.

Following the steps of the methodology of this work (Figure 1), the second stage i.e. the retrofit analysis, intends to find the optimal combination of retrofit measures for the calibrated model that satisfy two conflicting objectives in two different scenarios. As it was previously referred, a final analysis will study the differences between the optimal retrofit solutions given by the three models generated in this work (*baseline, detailed* and calibrated), which may affect the *decision-making* process.

6.1 Model Calibration

Firstly, a BES model was created using the *EnergyPlus,* by considering almost no information about the household besides the basic knowledge of the location, geometry of the house and the year of construction. This is the *Baseline model* and its input parameters were based on the legal standards, literature reviews and assumptions.

Then, a second model was generated with more detailed information that was collected during several walkthroughs to the houses. This second model is called the *detailed model* and act as the best guess of what is the actual thermal behaviour of the household that can be generated with the information available.

Finally, the *detailed model* was calibrated using a sensitivity analysis reduce the order of the uncertain parameters in the model (i.e. the number of calibrated parameters) and then, the GA was used to minimize the error until a minimum value was found. After calibrating the model, the thermal comfort was predicted and compared, between the *baseline, detailed* and *calibrated model*.

As the input properties of the model become more accurate and less uncertain, the degree of confidence on the predictions increases. Then, when no more detailed information is available besides the parameters to quantify the uncertainty of the model, calibration is used to generate a model with the smallest possible error (Figure 20).

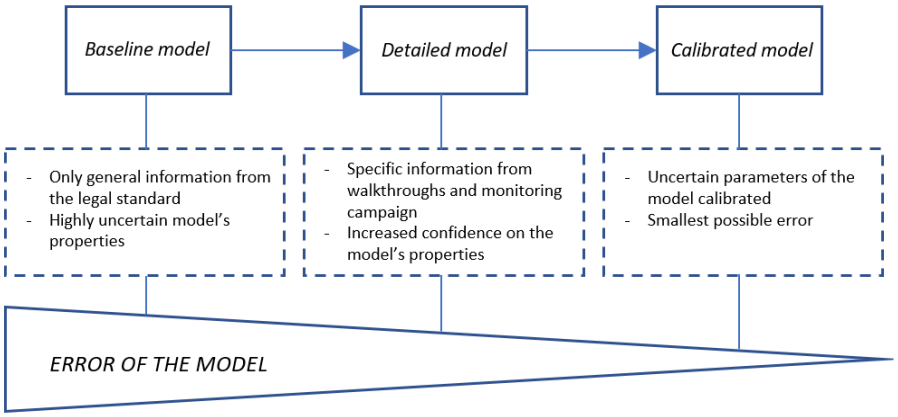

Figure 20: Model calibration

6.1.1 Baseline model

The initial model of the house was manually created in *EnergyPlus*, considering the basic information like the location, year of construction, architectural plans and a weather file created by a weather station located near the location of the house. Besides the properties of the model regarding the building envelope, internal gains and infiltration rate, it was also estimated the useful energy for the domestic hot water (DHW). The Table 3 summarizes the basic information used to develop the model and Figure 19 a) and b) represent respectively the top and three-dimensional views of the house, based on architectural plans. This information allowed to build one *baseline model* (i.e. early stage model with great uncertainty in all the parameters).

6.1.1.1 Building envelope

By knowing the year of construction of the building it was possible to assume some properties about the thermal behaviour of the opaque surfaces of the building, such as the overall heat transfer coefficient ($U\ [W/m^2.K]$). To simplify, it was considered an adiabatic floor and ceiling because the dwelling is located between two occupied floors and it was assumed that no considerable heat transfer occurs from the upper and lower floors, with the same type of use.

Default values for the heat transfer coefficients of the exterior walls and floor (Table 5) were respectively taken from the tables II.3 and III available in (ADENE, 2013). This document is useful to quantify with default values the building envelope thermal properties when the exact construction details are unknown. The information on the heat transfer coefficients is based on the year of construction and approximate thickness of walls.

The thickness of the exterior walls was assumed to be in the range of $[0.18; 0.2]\ (m)$, which is the worst-case scenario (with highest overall heat transfer coefficient), according to the tables used and corresponds to $U_{ext} = 1.7\ W/m^2.K$ (brick walls, for houses built after 1960 and with the assumed thickness). Since no default information is available regarding the thermal performance of the interior walls, they were assumed to have a thickness of half of the value of the thickness of the exterior walls ($t \approx 0.10\ m$) and their overall thermal resistance (R_{int}) was taken from (Pina dos Santos & Matias, 2006).

Using only the overall heat transfer coefficients to estimate the gains of the house may add a significant error to the simulation model, because the envelope has no mass and therefore the thermal inertia effects (which depend on the specific heat (C) and density (ρ)) are ignored. To include these effects in the household, mass was added to the opaque surfaces (walls, floor and ceiling). The standard (REH, 2013) suggests a method to calculate the total inertia of the building's envelope, which strongly depends on the exact materials, more specifically, on the superficial coating of the surfaces. Since at this early stage, no knowledge on this specific information existed, average values for the density of the walls and floor were taken from (Pina dos Santos & Matias, 2006) for ceramic bricks (walls) and concrete for the floor and ceiling, which is according to the information available in (ADENE, 2013). The specific heat was taken from (ASHRAE, 2009), considering the same materials.

Regarding the glazed surfaces, since no default values exist for the thermal performance of these surfaces, all the windows were assumed to consist of single pane sliding glass and metal frame with no thermal break. These are the most common windows for this type of house, assuming that no interventions occurred concerning the glazed surfaces. It was also assumed an exterior shading device for each window of the house (exterior plastic shutters).

To simplify the model, the thermal performance of the glazed surfaces was described by their overall heat transfer coefficient (U_g) and solar factor ($g_\perp$), which are both steady-state performance indices (ASHRAE, 2009) that include all the heat gains by conduction, convection and radiation. This last parameter ($g_\perp$) is the fraction of the solar radiation normal to the windows that is transmitted to the interior zones. The U_g, as presented in Table 5, was obtained from (Pina dos Santos & Matias, 2006), considering windows with single pane glass, metal frame with no thermal break and accounting for the exterior shutters.

The solar factor of the glazed surfaces was obtained using the methodology described in the legal standard (REH, 2013). For the calculation of $g_\perp$ this standard accounts for the type of glass, frame, shading device and direction of the surface. Since this standard focus only on estimating the energy consumption during the whole year, it assumes that the use of the shading devices is made to minimize the heating and cooling energy consumption. This means that during the heating season the devices are not used and conversely during the cooling season, these are partially used and the fraction of the time in which they are opened depends on the orientation of the surfaces. Therefore, each glazed surface has two solar factors, one for the heating season ($g_\perp^{hs}$) and another one for the cooling season ($g_\perp^{cs}$). The $g_\perp^{cs}$ is smaller than the $g_\perp^{hs}$ because the solar heat gains are desirable during the Winter to minimize the heating energy consumption (the shutters are fully opened, which increases the solar factor, according to this method). All the factors, calculated using this method, are presented in Table 5.

6.1.1.2 Internal gains

All the data for the usage schedules of the internal gains, such as electric equipment density (power per unit area), occupancy density (number of occupants per unit area) and lighting (power per unit area) was obtained using the information in (Monteiro, C., Pina, Santos, & Ferrão, 2018) and (Monteiro, 2018). The

metabolic activity was set to 72 $W/occupant$ in the bedrooms and 126 $W/occupant$ in the living-room, which correspond to activities respectively related to sleeping and standing relaxed, according to (ASHRAE, 2009).

6.1.1.3 Infiltration

The estimation of the infiltration rate $\dot{V}$ was according to the standard (REH, 2013), which suggests a method for the calculation of the number of air changes per hour (ACH) in residential buildings (accounting for the natural and mechanical ventilation and infiltration). According to this standard, the ACH depends on some factors, such as the air permeability of the glazed surfaces, the existence of air admission devices and ventilation ducts, the wind pressure coefficient and on the buoyance effect. With only the basic information, assuming high air permeability of the glazed surfaces (specifically regarding the frame and the exterior shutters) and no air admission devices, the value that was obtained for the ACH, i.e. the infiltration rate ($\dot{V}$), is presented in the Table 5.

Table 5: Properties used in the baseline model

Property	*Value*
Walls	
$U_{ext}(W/m^2.K)/R_{int}(m^2.K/W)$	$1.7^{*}/0.42^{*1}$
$\rho(kg/m^3)$	1700^{*1}
$C(J/kg.K)$	790^{*5}
Floor/Ceiling	
$U\ (W/m^2.K)$	3.1^{*}
$\rho(kg/m^3)$	2300^{*1}
$C_p(J/kg.K)$	900^{*5}
Glazed surfaces	
$U_g(W/m^2K)$	4.5^{*1}
$g_{\perp}^{hs}/g_{\perp}^{cs}$	$0.77/(0.32, 0.73^{*3})^{*2}$
Internal gains	
$p_{equip}(W/m^2)$	5.3^{*4}
$M(W)$	$72/126^{*5}$
$p_{light}(W/m^2)$	1.6^{*4}
Schedules	^{*4}
Infiltration	
$\dot{V}(h^{-1})$	1.23^{*2}

* From (ADENE, 2013)

*1 From LNEC (Pina dos Santos & Matias, 2006)

*2 From (REH, 2013)

*3 $g_{\perp}^{cs} = 0.73$ for glazed surfaces facing the north direction and $g_{\perp}^{cs} = 0.32$ in the other cases

*4 From (Monteiro, C., Pina, Santos, & Ferrão, 2018) and (Monteiro, 2018)

*5 From (ASHRAE, 2009)

6.1.1.4 Domestic hot water

Regarding the useful energy for DHW (Q_{DHW}), the estimation methodology follows the legal standard (REH, 2013) which uses equations (20) and (21) .

$$Q_{DHW} = \frac{M_{DHW} \times (4{,}187 \times 10^3) \times \Delta T_{DHW} \times n_d}{3{,}6 \times 10^6} \; [kWh/year] \qquad (20)$$

$$M_{DHW} = 40 \times N_{occupants} \times f_{eh} \; [L] \qquad (21)$$

This methodology considers that in each household the number of days of hot water consumption (n_d) is the whole year and the average temperature variation from the water supply temperature to the DHW temperature (ΔT_{DHW}) is equal to 35℃ . The hot water average daily consumption (M_{DHW}) is assumed to be $40\ L$ per occupant and the number of occupants, $N_{occupants} = 4$, since the standard suggests the number of occupants to be equal to one plus the typology of the house (number of bedrooms). Finally, it was assumed that the hydric efficiency of the shower systems (f_{eh}), was equal to 1 (basic showering system, with no certification). Using these reference values, the calculated useful energy for the DHW during the whole year is $Q_{DHW} = 2.38 \times 10^3\ kWh/\ year$.

6.1.2 Detailed model

During the monitoring campaign (SusCity Project, 2013), several *walkthroughs* on site, surveys made to the occupants and the analysis of building drawings and specifications allowed to collect more detailed information about the occupants' behaviour and building envelope properties, such as the construction materials and an estimation of the shading caused by the surrounding buildings. Other indoor parameters were also more correctly specified, such as the internal gains (plug-in loads such as lighting and electric equipment) and occupational patterns. Other assumptions made in the *baseline models* were also confirmed (e.g. assumptions made on the shading devices and the type of window). Having all this information, it was possible to develop a *detailed model* that considered more accurately some of the parameters, decreasing therefore their "degree of uncertainty".

6.1.2.1 Building Envelope

Information regarding the building envelope was taken from drawings and other documents. Despite of not knowing the exact materials of the building envelope, the type of materials (e.g. massive and drilled ceramic bricks are both from the *ceramic brick* type of material) and construction solutions (Table 7) were known from specifications (SusCity Project, 2013). With this new detailed information but still with great uncertainty on the knowledge of the specific materials, the thermal properties for each opaque material type (i.e. k, ρ and C) were taken from (Macdonald, 2002). This source provides a database quantifying the uncertainty of the most common properties of the materials used in buildings (covering all the specific materials within their material type). At this stage of the work, there was no interest in quantifying the variability of these properties and therefore, to describe this *detailed model*, the average values of the properties of the materials were used (Table 6).

Table 6: Thermophysical properties of the opaque materials (mean values for each property, from (Macdonald, 2002))

material	$k(W/m.K)$	$\rho(kg/m^3)$	$C(J/kg.K)$
Dark cement	0.78	1750	840
Ceramic brick	0.79	1720	837
Light plaster	0.53	1264	889
Screed	0.79	1481	904
Light-weight concrete	0.31	891	839
Ceramic tiles	1.06	1920	844

Table 7: Construction details from drawings and specifications

construction	Exterior wall	Interior wall	Floor	Ceiling
Material type/ $/t(m)$	Dark Cement/ 0.025	Light plaster/ 0.02	Light plaster/ 0.025	Ceramic tiles/ 0.015
	Ceramic brick/ 0.2	Ceramic brick/ 0.11	Light-weight concrete/0.25	Screed/0.05
	Light plaster/ 0.025	Light plaster/ 0.02	Screed/0.05	Light-weight concrete/0.25
			Ceramic tiles/ 0.015	Light plaster/ 0.025

The glazed surfaces, identified during the *walkthroughs* to the house, consist all in sliding windows with single pane clear glass, aluminium frame without thermal break and with light-coloured, PVC exterior horizontal shutters. This information means that the assumption made in the *baseline model* regarding the type of glazed surfaces was correct. In this new model, the thermal performance of the windows and shading devices were described separately, contrarily to the *baseline model,* where the overall heat transfer coefficient and solar factor accounted for the effects of the shutters.

Despite of knowing the type of glass and frame of the windows, there was no accurate information on the detailed properties of the window (e.g. manufacturer information) and therefore there was still some "degree of uncertainty", such as regarding the thickness of the glass, the optical properties of the glass (transmittance and reflectance), the conductivity of the glass and the thermal properties of the window's frame. To avoid errors on the inputs regarding the properties of the windows, each window was simplified (as in the *baseline model*) and again, was described only by the *steady-state* indicators ($g_{\perp}$ and U_w). The overall heat transfer coefficient of the frame and glass (U_w) was taken from (Pina dos Santos & Matias, 2006) and the solar factor of the window ($g_{\perp}$) was taken from the fenestration chapter of (ASHRAE, 2009), assuming a glass thickness of $6\,mm$. The shutters, with a known thickness and material type (PVC), were assumed to have a low transmissivity (τ_s) and medium reflectivity (ρ_s). The average conductivity of the PVC was taken from (Macdonald, 2002). All the information on the detailed properties of the glazed surfaces are summarized in Table 8.

Table 8: Properties of the glazed surfaces of the detailed model

Frame and glass	$U_w(W/m^2.K)$	6.5
	$g_\perp$	0.74
Exterior Shutters	$k\ (W/m.K)$	0.28
	τ_s	0.1
	ρ_s	0.5
	$t(m)$	0.01

6.1.2.2 Internal gains

The metabolic activity remained unchanged, since the levels of activity assumed before gave a good estimation on the actual tasks performed by the occupants in each division, as it was confirmed during the monitoring campaign by asking the occupants what their indoor habits in each thermal zone were. Complementing the information on the internal heat gains from the occupants, the radiant heat fraction ($f^r_{occupant}$, i.e. radiant fraction of the total sensible heat) was taken from (ASHRAE, 2009), assuming low air velocity ($u_a < 0.2\ m/s$) and sedentary activity ($M < 140\ W$).

During the monitoring period, it was also calculated the total power density (power per unit floor area) of the lights (p_{light}) and electric equipment (p_{equip}). The house has fluorescent lighting systems (CFL) with a suspended configuration (suspended in the ceiling) so, according to (Lighting Handbook: Reference & Application, 8th Edition, 1993), it was possible to estimate the fraction energy that goes into each thermal zone as visible radiation (f^v_{light}), the fraction of energy that goes into the zone as long-wave radiation (f^r_{light}) and the fraction of heat lost by convection (f^c_{light}).

For each internal gain, it was also created a schedule based on the information collected during the monitoring campaign. This information was given by the occupants concerning their weekly and weekend daily routine, their typical use of the electric equipment, lighting and information on the approximated periods when the shutters were opened or closed, during winter and summer.

Some assumptions had still to be made: it was considered a representative day of the weekends and this day was used during the two days of weekend; another representative day of the week was used during the whole working week; the heating (winter) and cooling (summer) season periods were defined according to the standard, which affect both the lighting and shading schedules.

Table 9: Variables regarding the internal gains used in the detailed model

Occupation	Bedrooms	$M\ (W/occupant)$	72
		$f^r_{occupant}$	0.6
	Living-room	$M\ (W/occupant)$	126
		$f^r_{occupant}$	0.6
Lighting		$p_{light}(W/m^2)$	7.2
		f^r_{light}	0.42
		f^v_{light}	0.18
		f^c_{light}	0.4
Electric equipment		$p_{equip}(W/m^2)$	38.7
		f^r_{equip}	0.38

6.1.2.3 Infiltration rate

The air infiltration rate was assumed to remain constant during the entire year. During the monitoring campaign, the infiltration rate was measured indirectly using the tracer gas method, where the traced gas was carbon dioxide. The concentration of CO_2 was measured only during the occupancy periods in one of the bedrooms of the house, for a total of four days (SusCity Project, 2013).

With all the measurements, the average infiltration was calculated for each day ($\dot{V}_i$) and then it was calculated an average of the four days ($\bar{\dot{V}}$). This was the value assumed as the infiltration rate for all thermal zones and during the entire year (Table 10). Comparing to the method used in *baseline model* (REH, 2013), the tracer gas method resulted in an infiltration rate much larger (with a difference of 76.4%).

Although this parameter was calculated through measurements, it has a great uncertainty mainly due to the non-controllable conditions of the measurements. Problems such as opening windows or doors when the CO_2 is being measured can largely affect the values of the concentration of the carbon dioxide and therefore the infiltration rate.

Table 10: Average infiltration rates (SusCity Project, 2013)

Day (Nr.)	1	2	3	4	$\bar{\dot{V}}(h^{-1})$
$\dot{V}(h^{-1})$	1.83	2.09	2.38	2.38	2.17

6.1.3 Calibrated model

The calibration of a model consists of fine tuning some of the model's most uncertain parameters and involves, as explained before, the minimization of the model error using statistical error estimators between the measured and the simulated data, such as the $cv(RMSE)$ and/or the $NMBE$.

To calibrate the *detailed model* of the house, it was minimized the error between the simulated and measured air temperature, to enable a more accurate prediction of the thermal comfort. The air temperature was recorded at the monitoring campaign during almost one year (there were some periods without recorded data) and in three thermal zones of the house (two bedrooms and the living-room).

Having all these sets of measured temperatures from different thermal zones makes calibration a very difficult task and so, to simplify the process, all the temperatures from different zones were averaged into a single vector of temperatures with a timestep of one hour. This simplification allowed to compare both measured and simulated hourly temperatures.

The average temperatures ($\bar{t}_{a,i}$, given by equation (22)) were obtained by averaging the temperature ($t_{a,i}^{J}$) of each J zone at each i hour, weighting it by the volume of the thermal zone V_J; J goes from 1 to 3, which is the number of zones with recorded temperature (living-room and two bedrooms). The error estimators that were used to evaluate the accuracy of the models, calculate the residuals between the average simulated ($\bar{t}_{a,i}^{s}$) and average measured ($\bar{t}_{a,i}^{m}$) hourly temperature. The first indicator ($NMBE$, given by equation (23)) estimates the overall *bias* of the models (i.e. its tendency to over/under-predict the temperature) and the last one ($cv(RMSE)$, given by equation (24)) is used as the global indicator of the error of the models, since it has no *cancelation effect*.

$$\bar{t}_{a,i} = \frac{\sum_{J=1}^{3} V_J . t_{a,i}^{J}}{\sum_{J=1}^{3} V_J} \text{ (°C)} \quad (22)$$

$$NMBE = \frac{\sum_{i=1}^{n} (\bar{t}_{a,i}^{m} - \bar{t}_{a,i}^{s})}{\sum_{i=1}^{n} \bar{t}_{i}^{m}} \quad (23)$$

$$cv(RMSE) = \frac{\sqrt{(\sum_{i=1}^{n} (\bar{t}_{a,i}^{m} - \bar{t}_{a,i}^{s})^2 / n)}}{(\sum_{i=1}^{n} \bar{t}_{a,i}^{m})/n} \quad (24)$$

The uncertain parameters considered for calibration were all the parameters described in the *detailed model*, which includes the envelope related variables, the internal gains of each thermal zone and the air infiltration rate, in a total of 58 uncertain parameters. To simplify, only the variables that were expected to influence minimally the error were considered in the calibration and these are the variables that are directly related to the thermal zones where the temperature was measured. For example, the heat gains from the equipment in the kitchen were not calibrated because they were not expected to influence the temperature in the bedrooms and living-room.

The schedules of lighting, electric equipment, shading and occupation were not considered in the calibration. Otherwise, all the schedules would add a lot more variables to the calibration, making it infeasible in terms of computation effort and so, to simplify, they were set equal to the base schedules (the same schedules considered in the *detailed model*). The calibration was performed with one-year simulations, to take advantage of all the recorded data. Regarding the weather file, this was not calibrated since it was considered sufficiently accurate.

A high order system with many uncertain parameters involved in calibration can contribute to the existence of many non-unique solutions. To overcome this problem, the order of the system was reduced by fixing the parameters that have small influence on the error and therefore can remain constant throughout the calibration without affecting the error of the model. The most influential parameters were found with sensitivity analysis, more specifically, the Morris method.

Ignoring the *scenario uncertainty* and the uncertainty on the *EnergyPlus* itself (*numerical uncertainty*), the only type of uncertainty that was tackled in this work was the uncertainty on the parameters introduced as inputs of the BES program (*specification uncertainty*).

6.1.3.1 Specification Uncertainty

The probability distributions considered for the sensitivity analysis should ideally be those that better fit the measured data. In this work, only the infiltration had data from measurements that were collected during the monitoring campaign. Since the sample size was too small for the data to fit a distribution, the uncertainty quantification for all parameters was based on the literature (past studies).

For all the other parameters in which relevant literature information was not found, the probability distribution represents the "degree of uncertainty" on the specific parameter. For parameters with large uncertainty, it was assumed a uniform probability distribution (u, Figure 2 c)), where all the values within a specific range are equally probable. For parameters with a smaller "degree of uncertainty", in which there was a most likely value (i.e. the mode) but the probability distribution was unknown, it was assumed a coarse probability distribution defined by the lower ($x^{(l)}$) and upper ($x^{(u)}$) bounds (less likely values) and the mode (m). This is the triangular probability distribution (Tri, Figure 2 a)).

In this work, it was used the information in (Macdonald, 2002) on the uncertainty quantification of the thermal properties of the opaque materials, since only the material types (instead of the specific materials) were known. A normal distribution (Figure 2 b)), as suggested by (Macdonald, 2002)), was assigned to the conductivity (k), density (ρ) and specific heat (C) of these materials and the range of variation for these parameters was assumed to be within one standard deviation from the average value of the variable ($\mu \pm \sigma$), where μ is the value of the parameter that was used in the *detailed model*.

A triangular (symmetrical) distribution with upper and lower bounds respectively equal to $\pm 30\%$ of mode, was assigned to the lighting and electric equipment power, overall heat transfer coefficient and solar factor of windows and thickness of all materials. The same distribution but with a larger range of variation ($\pm 50\%$) was used to describe the infiltration rates of each thermal zone, since the values obtained with the tracer-gas method (Table 10) seemed to over-estimate the air infiltration rate.

Since no information regarding the uncertainty of the fractions of radiant/convective heat was found on the literature, all the fractions of radiant heat (f^{r}_{equip} and $\mathrm{f}^{r}_{occupant}$) along with the lighting efficiency (fraction of visible energy, f^{v}_{light}) were assumed to be equally uncertain, with a large "degree of uncertainty", which reflected on a uniform probability distribution, bounded by $\mathrm{f} \pm 30\%$, where f is the fraction that was used in the *detailed model.* The optical properties of the shutters (ρ_s and τ_s), were considered as uncertain as the heat fractions referred before and so, the same type of distribution and bounds were considered.

The metabolic activity (M) is considered to be sufficiently accurate if the task described by the occupants in each thermal zone is accurately described (ASHRAE, 2009). In this work, the uncertainty of this parameter was assumed to depend only on the uncertainty in the activity performed and so, a uniform distribution was assigned

to M, bounded by $72\,W$ and $126\,W$, which are the minimum and maximum heat generation rate by a person with sedentary activity. Table 11 and Table 12 summarize the uncertain characterization for all parameters.

Table 11: Uncertainty parameters of the thermophysical variables of opaque materials, from (Macdonald, 2002)

	$k(W/m.K)$		$\rho(kg/m^3)$		$C(J/kg.K)$	
material	μ	σ	μ	σ	μ	σ
Dark cement	0.78	0.35	1750	29	840	90
Clay brick	0.79	0.26	1720	301	837	90
Light plaster	0.53	0.25	1264	425	889	122
Screed	0.79	0.34	1481	390	904	125
Light-weight concrete	0.31	0.14	891	309	839	90
Ceramic tiles	1.06	0.26	1920	349	844	34

Table 12: Uncertainty quantification

Property	$x^{(l)}$	$x^{(u)}$	Distribution
Opaque surfaces			
$k\ (W/m.K)$	$\mu - \sigma$	$\mu + \sigma$	$N{\sim}(\mu, \sigma)$
$\rho\ (kg/m^3)$	$\mu - \sigma$	$\mu + \sigma$	$N{\sim}(\mu, \sigma)$
$C\ (J/kg.K)$	$\mu - \sigma$	$\mu + \sigma$	$N{\sim}(\mu, \sigma)$
$t\ (m)$	-20%	$+20\%$	$Tri(l, u, m)$
Glazed surfaces			
$U_w\ (W/m^2.K)$	-20%	$+20\%$	$Tri(l, u, m)$
$g_\perp$	-20%	$+20\%$	$Tri(l, u, m)$
Exterior Shutters			
$k\ (W/m.K)$	$-\sigma$	$+\sigma$	$N{\sim}(\mu, \sigma)$
τ_s	-30%	$+30\%$	u
ρ_s	-30%	$+30\%$	u
$t\ (m)$	-20%	$+20\%$	$Tri(l, u, m)$
Lighting			
$P_{light}\ (W)$	-20%	$+20\%$	$Tri(l, u, m)$
f^{v}_{light}	-30%	$+30\%$	u
Electric Equipment			
$P_{equip}\ (W)$	-20%	$+20\%$	$Tri(l, u, m)$
f^{r}_{equip}	-30%	$+30\%$	u
Occupancy			
$M\ (W)$	72	126	u
$\mathrm{f}^{r}_{occupant}$	-30%	$+30\%$	u
Infiltration			
$\dot{V}\ (h^{-1})$	-50%	$+50\%$	$Tri(l, u, m)$

6.1.3.2 Sensitivity Analysis

The influential parameters were screened with the Morris method (section 3.1.1), using trajectories to explore the domain of uncertainty. All the parameters were normalized and allowed to vary between $[0; 1]$. Before evaluating the objective function, which is the overall error ($cv(RMSE)$), each parameter was mapped with its probability distribution to account for its uncertainty (Table 12). This was done using the inverse of the cumulative distribution function of the uncertain parameters, truncated by the lower ($x^{(l)}$) and upper ($x^{(u)}$) bounds.

The base points for the trajectories were generated not with random sampling (i.e. original version of the method) but using the Latin Hypercube sampling (LHS) as proposed by (Sohier, Farges, & Piet-Lahanier, 2014), because it guarantees a better representativeness of the trajectories in the domain.

The method that was used to create the trajectories was adapted from (Saltelli, et al., 2008) and is described in Figure 21, where X^* is the base point for each trajectory, X^{m+1} is the subsequent point that is

incremented or decremented (with the same probability) with the finite quantity Δ to X^m, r is the number of trajectories, K the total number of uncertain parameters and Ω the unitary hypercube-K.

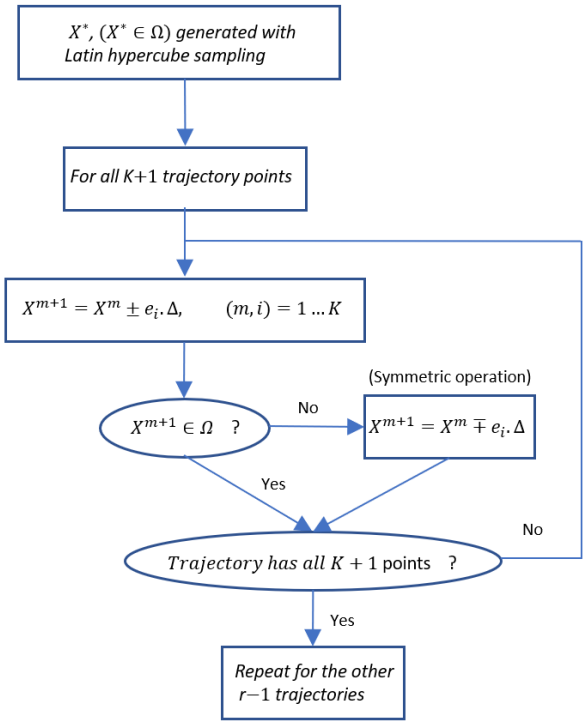

Figure 21: Flowchart describing the procedure used to create the trajectories

Since the *EnergyPlus* allows the inputs to be written in a text file (i.e. files with extension "*. idf*"), *Matlab®* was used to perform this method and interact with *EnergyPlus*, due to its simplicity in writing, reading and organizing large quantity of data in matrices.

After the trajectories were randomly generated in *Matlab* using the method in Figure 21, each solution of each trajectory was written in the "*. idf*" file and the *EnergyPlus* ran that solution automatically. Finally, *Matlab* collected the temperature results from a file with extension "*.csv"* (where the *EnergyPlus* writes all the simulation outputs) and calculated the overall error between the simulated and measured average temperatures (equation (24)). Each elementary-effect was then calculated, using two consecutive solutions of each trajectory, as it is shown in equation (25), where Δ is the increment (in this work, $\Delta = \frac{p}{2(p-1)}$ because it ensures all the p levels to be explored with the same probability) and $EE_i(X_0)$ is the elementary-effect associated to the i variable, around the point X_0.

$$EE_i(X_0) = \frac{cv(RMSE)[(x_1^0, x_2^0, \dots, x_i^0 + \Delta, \dots, x_K^0) - cv(RMSE)(x_1^0, x_2^0, \dots, x_i^0, \dots, x_K^0)}{\Delta} \qquad (25)$$

This procedure was repeated until the solutions of all trajectories were calculated, so that the sensitivity measures could be calculated for each uncertain variable. These were the mean and standard deviation of the distribution G_i , i.e. the distribution of the absolute value of the elementary-effects $|EE_i|$.

The order of the influential variables was graphically identified by the sample mean (μ_i^*) which is the overall sensitivity measure of this method. All the steps of this methodology are explained in the annex 10.1.

6.1.3.3 Single-objective optimization

After identifying the most influential parameters, the annual error of the *detailed* models ($cv(RMSE)$) was minimized between the measured and simulated average temperatures. This was performed as an *automated calibration*, using the *genetic algorithm* (GA) to adjust the uncertain influential parameters within their boundaries (the same as in Table 12) and reduce the error. This problem is in the scope of a single-objective optimization, where all the K variables found with the Morris method are continuous and can vary within the bounded constraints (equation (26)).

To solve this optimization problem, the *Matlab* function "*ga*", available in the global optimization toolbox, was used with the default *chromosome's* encoding type (RCGA), *crossover, mutation* and *selection* functions and a fixed *crossover probability* of 0.9. The procedure that was used in this optimization to evaluate the objective function was very similar to the one used in the sensitivity analysis, but instead of calculating the error in all of the points of the pre-created random trajectories, the function "*ga"* chose the points to run the BES program, according to the genetic operations performed in the *chromosomes* of each *generation*.

Several variations on the number of *chromosomes* per generation were tested and during all simulations it was considered a fixed stopping criterion in which the GA stopped if the error of fittest solution per generation didn't evolve during 20 generations.

Minimize: $$F_{obj}(X) = \frac{\sqrt{(\sum_{i=1}^{n}(\bar{t}_{a,i}^{m} - \bar{t}_{a,i}^{s})^2/n)}}{(\sum_{i=1}^{n}\bar{t}_{a,i}^{m})/n} \times 100\ (\%), \qquad X \in R^K \tag{26}$$

Subject to: $$x_i^{(l)} \leq x_i \leq x_i^{(u)}, \qquad i = 1 \dots K$$

Considering the problem of indeterminacy of calibration, not only one solution was assumed as calibrated, but instead, it was considered as calibrated a set of solutions collected from the last generations of the several optimizations, whose error was similarly small.

To conclude this part, the calibrated solutions were analysed in terms of comfort and compared to predictions of thermal comfort of the *detailed* and *baseline model.*

6.2 Thermal Comfort

This study used two indicators for thermal comfort related to the PMV and another one related to the notion of adaptive thermal comfort, which were all calculated through *EnergyPlus.*

The first one gives an indication of the severity of the discomfort in the house, i.e. the cumulative number of occupied hours in which the PMV is higher than the acceptance criteria ($N_{static0.7}$, given by equation (27)). It was assumed that the acceptable conditions for thermal comfort were given by the least rigid criteria

over the two standards, so it was assumed that there is discomfort in a specific period if $|PMV| \geq 0.7$ in that period, which corresponds to a $PPD \geq 15\%$ (Category C of thermal comfort, given by (International Standard ISO 7730, 2005)).

Besides the discomfort, it was considered another indicator for thermal comfort. This is the average $|PMV|$ over the whole year $|PMV|_{avg}$, which corresponds to the average of the absolute value of the Predicted Mean Vote weighted by the time spent in each thermal zone, as explained in equation (28), were $N_{occupied_J}$ is the number of occupied periods on the J thermal zone. Each period (Δt_j^J) is the time step of the PMV output of *EnergyPlus* (in this work $\Delta t_j^J = 1h$) in the J thermal zone, Z is the total number of occupied thermal zones, $|PMV|_j^J$ the absolute value of the PMV at the hour j and finally, α_J is the weight of the occupation at each J zone that is proportional to the total time spent there (equation (29)).

While evaluating the thermal comfort on the non-retrofitted models (*baseline, detailed* and *calibrated*), both indicators ($N_{static0.7}$ and $|PMV|_{avg}$) are used and supported by another indicator related to the adaptive thermal comfort (which is considered to be more accurate for naturally ventilated buildings than the PMV model). This indicator is equivalent to $N_{static0.7}$, but determines the cumulative number of hours in which there is discomfort according to the adaptive method given by (ANSI/ASHRAE Standard 55-2010, 2010) where it was again considered the less strict criteria, i.e. the 80% acceptability limits, presented in Figure 15. This thermal comfort parameter ($N_{adapt80\%}$) is defined by equation (30).

Conversely, the evaluation of the thermal comfort on models with HVAC system is made only with the $N_{static0.7}$ and the $|PMV|_{avg}$, since the adaptive model is strictly used in naturally ventilated buildings.

$$N_{static0.7} = [\sum_{J=1}^{Z} \sum_{j=1}^{N_{occupied_J}} \Delta t_j^J]: \ |PMV|_j^J \geq 0.7 \tag{27}$$

$$|PMV|_{avg} = \sum_{J=1}^{Z} (\alpha_J . \frac{\sum_{j=1}^{N_{occupied_J}} |PMV|_j^J}{N_{occupants_J}}) \tag{28}$$

$$\alpha_J = \frac{N_{occupied_J}}{N_{occupied_1} + N_{occupied_2} + \cdots + N_{occupied_Z}}, J = \{1, \dots, Z\} \tag{29}$$

$$N_{adapt80\%} = [\sum_{J=1}^{Z} \sum_{j=1}^{N_{occupied_J}} \Delta t_j^J]: \begin{cases} t_o \geq 0.31.t_{out} + 17.8 + 2.5 \ (℃) \\ t_o \leq 0.31.t_{out} + 17.8 - 2.5 \ (℃) \end{cases} \tag{30}$$

The occupation was only considered in the main thermal zones of the house, i.e. the living-room and three bedrooms ($Z = 4$), because the time spent in the kitchen and in other thermal zones is negligible comparing to the time spent in the main areas. In the living-room, all the occupied periods were relevant to the

calculation of the thermal comfort. Conversely, to avoid the wrong use of the PMV index (more specifically when the occupants are sleeping), only specific hours were considered inside the bedrooms. These are the hours in which the occupants are awaken in the bedroom. Although no information is available regarding these periods, they were assumed to be one hour before going to sleep after entering the bedroom and another hour before leaving the bedroom, as it can be seen in Figure 22, where "$t = X$" is the hour the occupant enters the bedroom, "$t = Y$" the hour he leaves the bedroom and in blue, the periods considered to estimate the thermal comfort.

Regarding the variables that directly affect the PMV, such as the air speed (u_a) and the metabolic activity (M), these were kept constant during the whole year and respectively equal to $0.1\ ms^{-1}$ and $126\ W$ (sedentary activity). Moreover, it was assumed that these parameters were the same for all the bedrooms and living-room. The level of clothing was assumed to vary between $0.5\ clo$ and $1\ clo$ during the whole year, being equal to $0.5\ clo$ during the cooling season and $1\ clo$ during the heating season. The starting and ending periods for both heating and cooling season were according to the Portuguese Standard (heating season from 01/10 to 30/05 and cooling season from 01/06 to 30/09 (REH, 2013)).

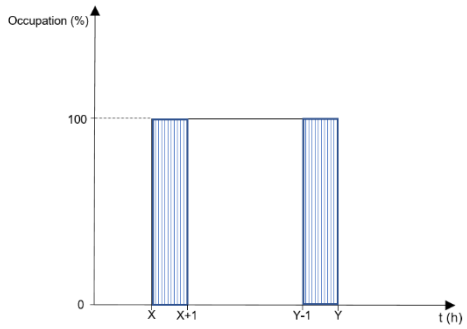

Figure 22: Occupied periods in the bedrooms considered to analyse the thermal comfort

6.3 Retrofit Analysis

The methodology for the retrofit analysis is presented in Figure 23. The *calibrated model* was firstly replaced by an *artificial neural network* that after *trained* and *validated,* was ready to be used as the objective function for the different decision variables, using a multi-objective GA (MOGA). After obtaining the *Pareto solutions,* these were analysed and compared to the solutions given by the *baseline* and *detailed models.*

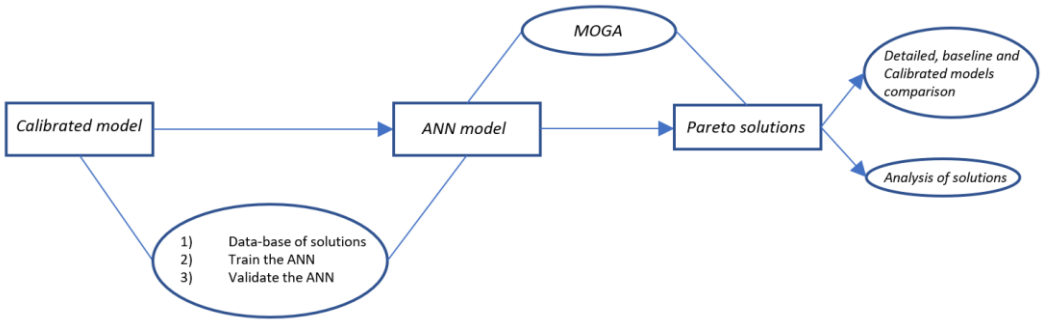

Figure 23: Flowchart explaining the methodology of the retrofit analysis

6.3.1 Retrofit measures

The studied retrofit measures are the typical residential energy conservation measures that fit this specific house (e.g. solar PV panels are not included in this study due the physical constraint of installing it in the building rooftop) and have impact not only on the energy consumption but also on the thermal comfort, since this is the focus of this work.

The considered measures are not only related to the replacement or introduction of new equipment (such as insulation, windows, lighting, HVAC and DHW equipment), but are also related to the settings of the HVAC equipment, more specifically to the thermostat and humidistat setpoints, since these are known to have great influence on both thermal comfort and energy consumption (Magnier & Haghighat, 2010). With these criteria in mind for choosing the possible measures, market information from catalogues and past studies was gathered to estimate the investment cost (acquisition and installation cost) of each measure.

Each considered measure is a decision variable of the proposed MOO problems, with different possible values within its range of variation. The variables can be binary, integer or continuous, depending on their nature. In this work, 12 decision variables were chosen, from which 1 is binary, 5 are integer and the remaining 6 are continuous (Table 14).

The binary variable has a logical meaning since it describes the choice of the type of lighting (x_{11}). If $x_{11} = 1$, the current lighting (CFL lighting) will be replaced by a more efficient system (LED lighting), otherwise the lighting system will remain unchanged and no investment cost regarding the lighting is considered. Only one alternative is proposed because the current lighting is already highly efficient. The efficacy (luminous flux per unit rated lighting power (lm/W)) of CFL and LED lighting was taken from (NREL, 2018), so as the average cost of LED lighting per unit lumen (€$/lm$).

Regarding the first four integer variables ($\{x_1, x_2, x_3, x_{12}\}$), several options were considered for each one, including the "0" option, which is when the measure is not used (except with the HVAC system choice (x_3) because if it's not used, there will always be discomfort and $N_{static0.7} \neq 0$ %). The first integer non-physical decision variable is the type of insulation (x_1). In this work, the insulation consists of expanded polystyrene (EPS) boards installed in the exterior walls. This type of organic insulation material was preferred to others (e.g. XPS or inorganic insulation) because of its smaller cost for similar thermal performance (conductivity ($k_{insulation}$) and thickness ($t_{insulation}$)) that have impact on the thermal comfort and energy consumption of the HVAC system. Different values of x_1 reflect the different thickness of the insulation for the same thermal conductivity ($k_{insulation} = 0.03\ W/m.K$, taken from (CYPE Ingenieros, 2018)).

The second non-physical integer valued variable (x_2) is the window type, which includes the frame and the glass. As before, the thermal performance of the glazed surfaces is described by the *steady-state* indicators (i.e. the solar factor ($g_\perp$) and the overall heat transfer coefficient (U_w)). Eight types of windows were considered (Table 13) and taken from (Costa, 2016), provided that their U_w or $g_\perp$ were smaller than the current type of

window (better thermal performance on at least one parameter). Just like the insulation, these parameters are expected to influence both on the thermal comfort and HVAC energy consumption.

Table 13: Retrofit measures proposed, regarding the glazed surfaces

x_2	description	U_w	$g_\perp$
1	Metal frame (no TB), double glazing, argon, (4/10/4) (mm)	3.67	0.77
2	Metal frame (no TB), double glazing, argon, (6/10/6) (mm)	3.6	0.75
3	Metal frame (no TB), double glazing, air, low ε, (4/6/6) (mm)	3.46	0.41
4	Metal frame (no TB), double glazing, argon, low ε, (4/6/6) (mm)	2.69	0.39
5	PVC frame, double glazing, argon, (4/10/4) (mm)	2.56	0.77
6	PVC frame, double glazing, argon, (6/10/6) (mm)	2.49	0.75
7	PVC frame, double glazing, air, low ε, (4/6/6) (mm)	2.36	0.41
8	PVC frame, double glazing, argon, (6/12/6) (mm)	1.58	0.39

As for the type of HVAC system (x_3), there are 3 possible values for this variable ($\{1, 2, 3\}$), i.e. three different HVAC systems. Each HVAC system is an air-source heat pump with a multi-split system, typical of the residential sector, and it was assumed that only the efficiency varies. This, along with the investment cost, was the only criterion for choosing the options of the heat-pumps. More specifically, it is only considered the overall efficiency during the whole year, i.e. the seasonal efficiency for heating and cooling (respectively the $SCOP$ and $SEER$, given by equation (31)). Three heat-pumps were considered, and their efficiencies and investment costs were taken from (CYPE Ingenieros, 2018).

$$SEER = \frac{Q_C}{E_C} \qquad SCOP = \frac{Q_H}{E_H} \tag{31}$$

The choice of the DHW systems is given by the discrete variable x_{12}, which describes systems with different efficiencies, including the original ($x_{12} = 0$). The three types of DHW systems that can be chosen (two natural gas tankless heaters and one heat pump for DHW) have different efficiencies (η_{wh}), which were taken from (JUNKERS, 2018) along with their acquisition cost.

Finally, the 6 remaining continuous decision variables ($\{x_5, \dots, x_{10}\}$) are the parameters related to the HVAC system control and their main objective is to optimize the use of the other variables. It was assumed that the HVAC system only works outside a range of heating and cooling temperatures (i.e. outside the range of the thermostat *deadband*) and these ranges are different for the heating and cooling season. The variables related to the heating setpoints for the heating and cooling seasons, are respectively the continuous variables x_5 and x_7 (i.e. T_H^{hs} and T_H^{cs}), while the variables related to the *deadband* of the same respective seasons are (also continuous variables) x_6 and x_8 (i.e. ΔT_{db}^{hs} and ΔT_{db}^{cs}).

The HVAC is assumed to have only dehumidification and again, there are two dehumidification setpoints (continuous variables): one for the heating season, x_9 (i.e. RH^{hs}) and another one for the cooling season, x_{10} (i.e. RH^{cs}).

Additionally, pre-heating and cooling periods were considered because they have impact on both energy consumption and thermal comfort and so, the discrete variable x_4 (i.e. Δt_{pre}) controls the advance in time in which the HVAC system starts working before the occupation periods referred in the Figure 22. It was considered the same Δt_{pre} for heating and cooling to simplify the problem, which can go up to $60\ min$.

Table 14: Retrofit decision variables

Variable	Type	Description	Variation
x_1	integer	Insulation Type	$\{0, 1, 2, 3, 4, 5\}$
x_2	integer	Window Type	$\{0, 1, 2, 3, 4, 5, 6, 7, 8\}$
x_3	integer	HVAC type	$\{1, 2, 3\}$
x_4	integer	Δt_{pre}	$[0;\ 60]\ [min]$
x_5	continuous	T_H^{hs}	$[19;\ 23]$ [°C]
x_6	continuous	ΔT_{db}^{hs}	$[0.5;\ 3]$ [°C]
x_7	continuous	T_H^{cs}	$[21;\ 26]$ [°C]
x_8	continuous	ΔT_{db}^{cs}	$[0.5;\ 3]$ [°C]
x_9	continuous	RH^{hs}	$[30;\ 60]$ [%]
x_{10}	continuous	RH^{cs}	$[30;\ 60]$ [%]
x_{11}	binary	CFL replaced by LED	$\{0, 1\}$
x_{12}	integer	DHW equipment	$\{0, 1, 2, 3\}$

The household is currently equipped with a natural gas tankless heater, with an estimated efficiency (η_{wh}, useful to final energy ratio) equal to 0.6 (REH, 2013). By knowing the efficiencies of all the other DHW systems and the useful energy for this household (Q_{DHW}, equations (20) and (21)) it is possible to estimate the final energy consumption for DHW (equation (32)) for all the options of the decision variable x_{12} (Table 15).

$$E_{DHW} = \frac{Q_{DHW}}{\eta_{wh}}\ (kWh/year) \qquad (32)$$

Table 15: Final energy consumption of DHW systems (variable x_{12})

x_{12}	0	1	2	3
$E_{DHW} \times 10^{-3}$ $(kWh/year)$	3.96	3.13	2.86	1.98

The decision variables that involve investment costs, i.e. x_1, x_2. x_3, x_{11} and x_{12} - respectively, the insulation, the window type, the HVAC system, the lighting system and the DHW system - are described in Table 16, along with their investment cost (I).

Table 16: Investment cost of each measure

Variable	Value	Description	I ($€/m^2$, unless specified)
x_1	0	No insulation	0
	1	20*	6.6
	2	40*	8.4
	3	60*	10.1
	4	80*	12.3
	5	120*	15.3
x_2	0	No new window	0
	1	3.67/0.77*[1]	106.1
	2	3.6/0.75*[1]	128.3
	3	3.46/0.41*[1]	169.5
	4	2.69/0.39*[1]	176.1
	5	2.56/0.77*[1]	219.4
	6	2.49/0.75*[1]	241.6
	7	2.36/0.41*[1]	282.8
	8	1.58/0.39*[1]	294.8
x_3	1	3.85/5.38*[2]	3279 €
	2	4.41/5.99*[2]	4551 €
	3	4.41/6.19*[2]	4300 €
x_{11}	0	No new lighting (55 lm/W)*[4]	0 $€/W$
	1	LED lighting (80 lm/W)*[4]	0.38 $€/W$*[4]
x_{12}	0	No new DHW system	0 €
	1	0.76*[3]	393 €
	2	0.83*[3]	476 €
	3	1.2*[3]	2225 €

* thickness of the insulation, $t_{insulation}$ (mm)

*[1] U_w $(W/m^2K)/g_\perp$

*[2] $SCOP/SEER$

*[3] η_{wh}

*[4] taken from (NREL, 2018)

To generate the Pareto front using the GA, a large number of simulations must be performed, which involves a high computational effort, especially using annual simulations on the *EnergyPlus* to optimize the model, which last approximately 20 seconds per simulation.

Simplifying the GA by reducing the number of *chromosomes* or the number of generations would be one option to reduce the effort but, as it was stated before, this could lead to *Pareto fronts* far away from the

optimal front (even with a small number of 20 chromosomes per generation and a small number of 50 generations, the optimization would take about 6 hours, a considerably high computational effort).

To avoid this simplification, the simulation program was replaced by a *surrogate model* that approximates the outputs of the BES program (equation (33)). The *artificial neural network* (ANN) was chosen to derive this model. These models have shown in past studies ((Magnier & Haghighat, 2010) and (Asadi, Silva, Antunes, Dias, & Glicksman, 2014)) to handle successfully multi-objective optimizations using the GA, inducing only small errors between the network's outputs and the BES program.

$$Output_{ANN}(X) \approx Output_{BES}(X) \qquad (33)$$

6.3.2 Artificial Neural Network

To create an ANN model, three major steps were followed: the first was to obtain a sample of representative solutions inside the domain of the problem; the second consisted in *training* the ANN with an appropriate *training* algorithm; finally, the *validation* step consisted in validating the network with a sample of solutions that were not used in the *training*.

Some decision variables of the MOO problem were not included in the ANN because they have effects that were considered to be insignificant for the calculation of the thermal loads and thermal comfort (done by the *EnergyPlus*), therefore they were introduced externally in the MOO. These variables are x_3 (the HVAC type), x_{11} (the replacement or not of the current CFL bulbs by LEDs) and finally x_{12} (the replacement or not of the DHW system).

The HVAC and DHW type were considered irrelevant to the *EnergyPlus*, since modelling the air-conditioning equipment is out of the scope of this work and so, an ideal HVAC type was chosen to calculate the thermal loads (the ideal HVAC system of *EnergyPlus* is a system that supplies heating or cooling air to a thermal zone in sufficient quantity to meet the zone loads (EnergyPlus Engineering Reference, 2013)). Then, depending on the heating and cooling seasonal efficiency of each equipment, the annual consumed energy was calculated outside the BES program (equation (31)). The same happened with the annual consumed energy for DHW, that was assumed to depend only on the efficiency of the equipment (Table 15).

Changing the lights to LEDs was also assumed to have a negligible thermal effect and it impacts only on different energy consumptions, which were calculated outside the *EnergyPlus.*

After excluding x_3, x_{11} and x_{12}, there are 9 variables left from which, 6 are continuous ($\{x_5, x_6, x_7, x_8, x_9, x_{10}\}$) and 3 are discrete ($\{x_1, x_2, x_4\}$). The ANN was found to present smaller errors if almost all the variables were kept continuous, so all the discrete variables except for x_4 were converted in continuous values. For this, x_2 (the type of window) was split in x_2' (the window heat coefficient, U_w) and x_2'' (the solar factor, $g_\perp$) which became continuous variables along with the thickness of the insulation boards (x_1).

These 10 variables ($\{x_1, x_2', x_2'', x_4, x_5, x_6, x_7, x_8, x_9, x_{10}\}$) were used as the inputs of the network. To *train* the network, 2000 retrofit solutions were randomly chosen using the *Latin Hypercube Sampling* (LHS) to

guarantee that the sample represents the actual variability of the whole population of solutions, inside the domain of the problem. The training set is considered sufficiently large comparing to other studies using ANN as *surrogate models* of a BES program, as for example in (Magnier & Haghighat, 2010).

The desired outputs of the LHS (i.e. the *targets* used to train the network) were the annual heating load (Q_H), the annual cooling load (Q_C), the cumulative number of hours in which the conditions are not thermally acceptable ($N_{static0.7}$) and the average $|PMV|$ over the whole year ($|PMV|_{avg}$).

The *validation* of the network was performed with 200 solutions different than the training data set (solutions that were never seen during the training). To validate a network, it is also important to consider solutions representative of the domain of the problem and so, these were again generated with the LHS, by discretizing each variable in 200 equally spaced levels.

Since the outputs: $Q_H, Q_C, N_{static0.7}$ and $|PMV|_{avg}$ are constant quantities (i.e. are not time-series), the ANN used was the *multi-layer perceptron* MLP (with only *feed-forward* connections). This type of network must have at least 3 layers (input, output and at least one *hidden layer*). The number of *hidden layers* and *hidden neurons* was found by trial and error in such a way that the network had the best possible *performance* (i.e. the smallest validation error, without significant over-fitting) with the simplest possible configuration. The input layer had a fixed number of 10 neurons, an output layer with a fixed number of 4 neurons, as it is shown in Figure 24, where the dots represent the unknown number of *hidden layers*, at this early stage.

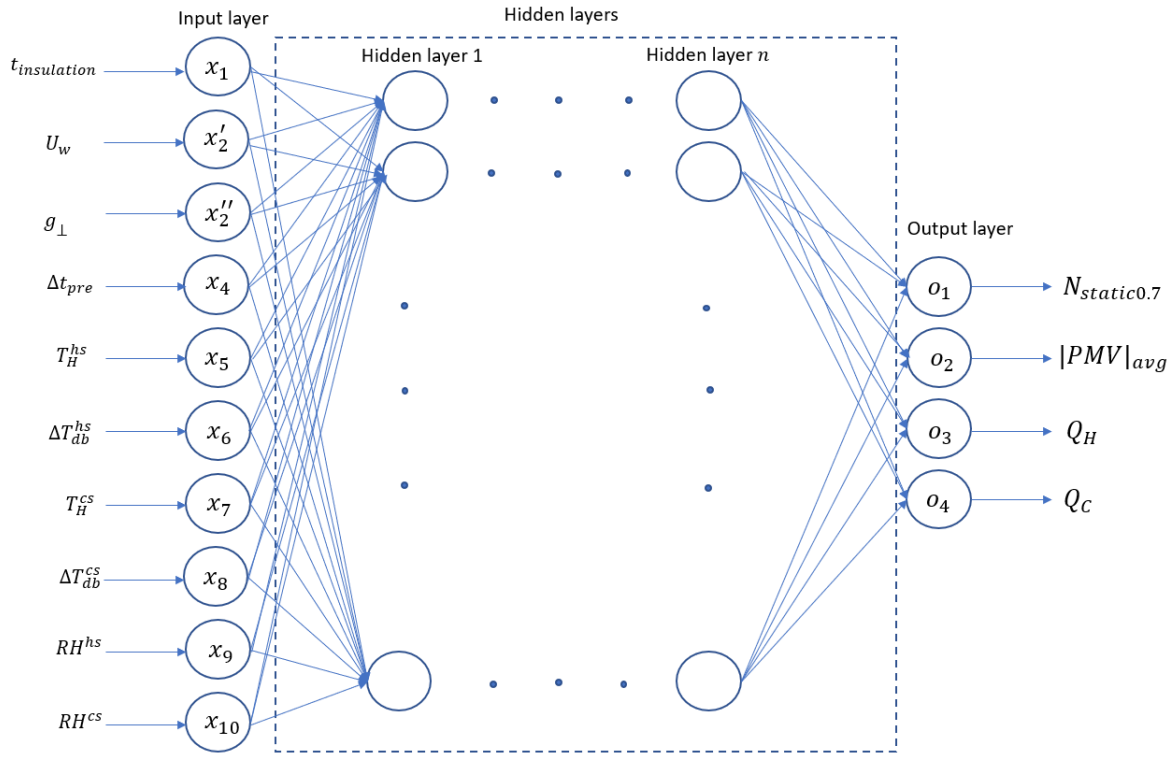

Figure 24: Multi-layer feed-forward ANN used in this study

To *train* and generate the network, it was used the "*fitnet*" function of the "*Neural Network Toolbox*" of *Matlab* (Neural Network Toolbox User's Guide, 2017), which is used for function approximation (*curve-fitting*).

The method used to *train* the network was the *back-propagation* method, using the *Levenberg-Marquardt* algorithm. The transfer functions used in the neurons of the hidden layers were hyperbolic tangent sigmoid functions, i.e. tan-sigmoid (to add non-linear behaviour to the network) and linear functions in the neurons of the output layer, which are typical of *curve-fitting* problems.

The *performance function* (the error function to be minimized during the *training*) was the *mean square error* (MSE) between the all the *outputs* and *targets* and the *training* stopped using the *early stopping* method. As it was stated before, this method is useful to prevent the over-fitting of the network (i.e. the inability to generalize well the output, for inputs not used for *training*) and consists of stopping the *training* when the ANN starts over-fitting the data, which is detected if the *validation error* increases for a specific number of iterations.

The *"fitnet"* function requires the specification of the data for *training, testing* and *validation* (The testing data is usually used to compare between different training methods). After *training* the ANN, all the validation data (inputs and *outputs*) was collected and used to analyse the generalizing ability of the network (ability to give accurate outputs for non-trained inputs). This was done by calculating the linear regression between the validation outputs and targets and the statistical distribution of the *validation errors.*

6.3.3 Multi-Objective Optimization

6.3.3.1 First and Second scenarios

After validating the ANN, the calibrated *surrogate model* was optimized. Two different scenarios corresponding to different optimization problems were studied and depending on the problem, the considered criteria were the annual energy cost $C_E\,(X)$ $[€/year]$, the investment cost of the retrofit measures $I(X)$ [€] and the thermal comfort $|PMV|_{avg}(X)$. It was also considered the percentage of cumulative time without thermal comfort, i.e. $N_{static0.7}(X)$ [%]. In all these criteria, X is a vector with all the decision variables ($X = \{x_1, x_2, \dots, x_{12}\}$).

The annual energy cost is the cost of electricity for the HVAC system and lighting plus the energy cost of DHW (which can be electricity or natural gas, depending on the type of system). This objective function is given by equation (34), where c_e and c_{DHW} are respectively, the unitary cost of electricity and the unitary cost of final energy for DHW, in $€/kWh_F$ (these values are presented in Table 17); E_{DHW} is the final energy consumption for DHW in $(kWh/year)$, as presented in Table 15; E_{light} is the final energy consumption for lighting; Q_H and Q_C are respectively the heating and cooling loads given by the ANN*;* and $SCOP$ and $SEER$ are respectively the seasonal efficiency for heating and cooling.

The investment cost is simply the sum of the acquisition and installation costs of each measure (summarized in Table 16).

$$C_E(X) = c_e\left(\frac{Q_H}{SCOP} + \frac{Q_C}{SEER} + E_{light}\right) + c_{DHW}.(E_{DHW})\ [€/year] \qquad (34)$$

Table 17: Final energy unitary cost, from (Gomes, et al., 2018)

$c_e\ (€/kWh_F)$	0.2
$c_{NG}\ (€/kWh_F)$	0.065

As stated before, two scenarios were considered for optimization. Both scenarios admit that thermal discomfort can never happen, i.e. $N_{static0.7}(X) = 0\ \%$. This, along with the bounds for each variable and the integer constraints (for the integer variables) defines a feasible zone to search for the *Pareto front.*

The first and second scenarios are respectively:

1. The minimization of $f(X) = [C_E\ (X); I(X)]$ with $N_{static0.7}(X) = 0\ \%$, i.e. the optimal retrofit solutions in terms of annual energy consumption and investment cost, that satisfy the "zero discomfort" condition;
2. The minimization of $f(X) = [C_E\ (X); |PMV|_{avg}(X)]$, i.e. the solutions with the best thermal comfort and annual energy cost, simultaneously, again with the no discomfort constraint;

These two problems are defined in equation (35), where $F_{obj}(X)$ is a vector of the objective functions to be minimized, $x_i^{(l)}$ and $x_i^{(u)}$ are respectively the lower and upper bounds of the variable x_i (summarized in Table 14), x_j represents the real variables (continuous), x_k represents the integer constrained variables and $N_{static0.7}(X) = 0\ \%$ is the non-linear equality constraint.

$$\begin{aligned} &\text{Minimize:} && F_{obj}(X) \\ &\text{Subject to:} && x_i^{(l)} \le x_i \le x_i^{(u)}, i = \{1, \dots, 12\} \\ & && x_j \in \mathbb{R}, j = \{5,6,7,8,9,10\} \\ & && x_k \in \mathbb{Z}, k = \{1,2,3,4,11,12\} \\ & && N_{static0.7}(X) = 0\ \% \end{aligned} \qquad (35)$$

The MOO was implemented using *Matlab* by adapting the function "*gamultiobj*" to the problem that uses real-coded variables to encode the chromosomes (RCGA). This *Matlab* function uses a variant of the NSGA- II with better convergence (Deb & Goel, 2001). The main difference between this variant and the original NSGA-II is that this version has less elitism than its predecessor, such that within a certain population, the fronts with higher *ranks* (i.e. dominated by other fronts) are not discarded from the population to increase the diversity of solutions, not only inside the non-dominated front but also in worst ranked fronts. This "less elitist" NSGA-II is also known as the *controlled elitist* NSGA-II, because it allows to restrict the number of individuals in the current best *ranked* front and then, the subsequent ranks are also restricted until the population has its initial size.

The *Matlab* function "*gamultiobj*" controls the elitism by using a constant that is known as the *Pareto fraction.* This is a constant between 0 and 1 and it is the fraction of *chromosomes* of a population that are included in best *ranked* front (corresponds also to the maximum number of solutions in the final *Pareto front*). Therefore, lower values of the *Pareto fraction* increase the diversity by exploring more space than the confined optimal points of each population and higher *Pareto fractions* focus more in the current non-dominated front.

Due to the inability of this *Matlab* function to optimize integer valued multi-objective problems, special crossover and mutation functions had to be created. These functions were the *arithmetic crossover* and *uniform mutation*, since these basic GA operators handled well all the optimizations, and had a truncation operator that guaranteed the integer constraints to be satisfied. All the basic steps of the "gamultiobj" function, are explained in the flowchart of the annex 10.3.

A drawback of using this adapted *Matlab* function is that non-linear constraints are not satisfied, such as the equality non-linear restriction. To solve this problem, the equality constraint was handled externally to the GA, with a penalty function approach, which adds a term related to the infeasibility of the solutions to the original objective functions and thus, removes the constraint from the problem. This way, infeasible solutions were penalized, guaranteeing the *Pareto front* to have all the solutions with $N_{static0.7}(X) = 0\ \%$.

The penalty term used was $(1 + N_{static0.7})$ and it was included in all the objective functions, as it is shown in equation (36), so that infeasible solutions have fitness values $(1 + N_{static0.7})$ times higher than the original objective function $F_{obj,i}(X)$ and are never *non-dominant* solutions.

$$F_{obj,i}^{pen}(X) = \begin{cases} F_{obj,i}(X).\,(1 + N_{static0.7}(X)) & ,N_{static0.7}(X) \neq 0\ \% \\ F_{obj,i}(X) & ,N_{static0.7}(X) = 0\ \% \end{cases} \qquad (36)$$

6.3.3.2 Baseline, detailed and calibrated models

The objective of the *Pareto front* on the topic of the retrofit measures is to consider not only one, but all the feasible and optimal retrofit solutions in all objectives (investment cost, annual energy cost, thermal comfort). Thus, an accurate *Pareto front* might be decisive for the *decision-maker* (DM) to choose the combination of optimal retrofit measures for his project. Inaccuracy on the *Pareto front* might lead to wrong choices. For example, the cost of investing in one solution that the DM thought would fit his project, but another solution with a much smaller investment achieves the same operational costs and level of comfort. This cost may even be reflected on a solution that is believed to give acceptable thermal comfort conditions, but in the reality, that solution does not comply with the thermal comfort desired conditions.

The first two models (*baseline* and *detailed*) were also optimized, considering the annual energy cost, the investment cost and the thermal discomfort penalty. The *Pareto solutions* of these models were then compared to the solutions given by the *calibrated model*, which is the most accurate model, to study the impact of choosing an optimal solution based on an inaccurate model, which can be an early stage model with a large uncertainty (i.e. *baseline model*) or a model created after *walkthroughs* to the house, with a reduced uncertainty but still, not calibrated (i.e. *detailed model*).

To optimize the *baseline* and the *detailed model*, the procedure used in the *calibrated model* was again applied. Firstly, it was created an artificial neural network to replace the *EnergyPlus* in the MOO (for each model). The ANNs of the two models had to have a sufficiently small error for the comparison between the three models to take place. Again, 2000 random retrofit solutions were generated using the LHS (to have representative solutions) to *train,* another set of 200 to *validate* and 200 to *test* the network.

Regarding the geometry of the networks, the ANN of the *detailed model* has the same number of *input neurons* as the network of the *calibrated model* because the retrofit measures are described by the same parameters in both models. However, one of the retrofit measures of the *baseline model* is described by different parameters than the other two models. In particular, the glazed surfaces of the *baseline model* have a solar factor ($g_{\perp}$) that depends on the orientation of the window and season (to account for the exterior shutters, there is one solar factor for the heating and another for the cooling season), so each type of window (Table 13) originates three solar factors, one for the heating season and for all windows ($g_{\perp}^{hs}$) and two other for the cooling season ($g_{\perp}^{cs}$), i.e. for windows facing north and for windows facing south. Again, to keep almost all the variables continuous, each of the solar factors had to represent a different input parameter of the ANN. To sum up, the network of the *baseline model* has 12 input parameters (2 additional variables to the other models) and therefore, 12 *neurons* on the *input layer.*

After generating the 2000 retrofit solutions, the same method was used to generate the ANN. Firstly, all the data (*inputs* and *targets*) was divided in three different sets (*training, testing* and *validation set*) and then, the networks were trained with the *Levenberg-Marquardt* algorithm, with the geometry (number of *hidden layers* and *hidden neurons*) that gave the minimum validation error and with the early stopping criterion.

7 RESULTS AND DISCUSSION

This chapter presents the results regarding the model calibration and the retrofit analysis

7.1 Model Calibration

For the model calibration, the $cv(RMSE)$ and $NMBE$ of the *baseline* and *detailed model* are presented, considering the errors on a monthly and annual basis. Then, after comparing the errors between the two types of model, the results of the sensitivity analysis using the Morris method are presented for the *detailed model.* The influential uncertain parameters are graphically identified and only these are calibrated, using the GA. A final set of solutions that have approximately the same overall error are presented, instead of only the optimal calibrated solution. Finally, the thermal comfort ($N_{static0.7}$, $|PMV|_{avg}$ and $N_{adapt0.7}$) is presented for all the models (*baseline, detailed* and *calibrated*) and the results are analysed.

7.1.1 *Baseline* and *detailed* models

The baseline BES model of the household was generated with the information presented in the Table 5, which allowed us to build a model based on generic information. The overall error and overall bias-error of the model were calculated in a yearly basis (Table 18) and showed that overall, the *baseline model* over-predicts the indoor temperature, since the $NMBE$ is negative.

Knowing what are the months that most contribute to the differences between the simulated and measured temperatures can help to understand better the model and to know what the most probable causes are for the error. A finer error analysis was performed with the same error indicators but, instead of accounting for the whole year, these errors were calculated separately for each month (Figure 25).

The results show months with $cv(RMSE) > 15$ %, even though the annual $cv(RMSE)$ is 12.3 %. From Figure 25 it is possible to see that the curve of the $cv(RMSE)$ is approximately symmetrical to the curve of the $NMBE$ which happens because there are small cancelation effects (over-estimation of the temperature during almost the whole year). Also, from Figure 25, there is a noticeable difference on the error between June and September and the other months, which is coherent with the description of the glazed surfaces in the model. These are the months when, according to the standard (REH, 2013), the shading devices are used. In the remaining months (the heating season) it was considered that the shading devices are not used at any hour of the day (also according to the standard), which may be the reason for the large increase of the error.

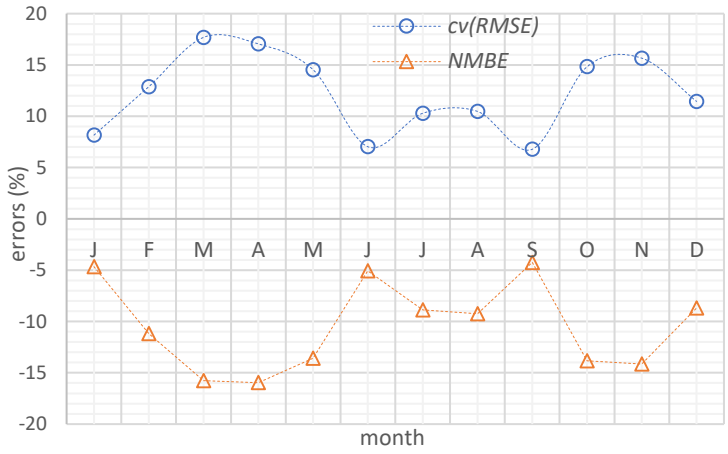

Figure 25: Monthly error of the baseline model

The detailed model was generated with the information in Table 6 (properties of opaque materials), Table 7 (construction details), Table 8 (properties of glazed surfaces), Table 9 (internal gains) and Table 10 (infiltration rate). The overall error and bias of this model improved significantly comparing to the baseline model, with a difference of 5 % of the $cv(RMSE)$ and 13.3 % of the $NMBE$ (Table 18). Contrarily to the baseline model, the $cv(RMSE)$ is approximately the same for every month (Figure 26) and the model under-predicts the temperature almost in every month, except during July and August, in which the $NMBE < 0$ %.

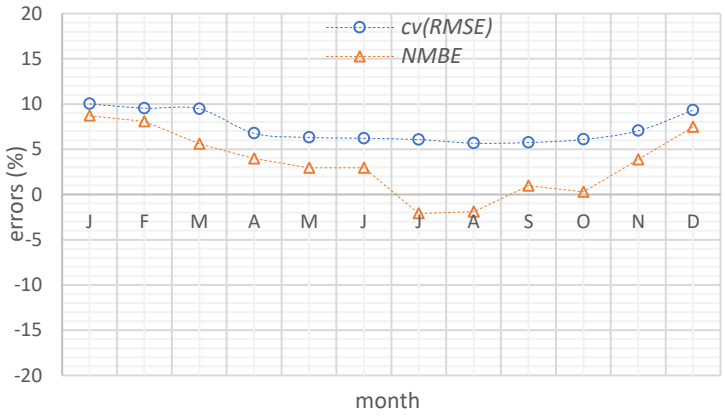

Figure 26: Monthly error of the detailed model

Although the standard criteria for validation is only valid for calibrations with measured energy data, the errors of these models were compared to the standards (Table 1, using the hourly calibration criteria). Using the criteria of (ASHRAE, 2002), the *baseline model* has only the $cv(RMSE)$ inside the validation ranges ($cv(RMSE)_{max} = 30$ %), while the $NMBE$ is slightly out of range ($|NMBE|_{max} = 10$ %). The *detailed model* has both errors inside the validation range.

To sum up, using the (ASHRAE, 2002) validation criteria with indoor air temperature data, both models are considered validated to reliably estimate the energy consumption and savings in a retrofit project.

Table 18: Overall errors of the baseline and detailed model

model	$cv(RMSE)$ (%)	$NMBE$ (%)
Baseline	12.3	-10.2
Detailed	7.3	3.1

7.1.2 Sensitivity Analysis

To screen the most influential parameters of the *detailed model,* the *elementary-effects method* or *Morris method* was used with *Latin hypercube sampling* (LHS) to ensure the representativeness of the trajectories when exploring the high-dimensional domain.

Firstly, 50 trajectories were used ($r = 50$). Since the sampling method was the LHS, each variable had to be discretized in the grid with the same number of equally spaced levels as the number of sampled points (the base points of the trajectories). To calculate all the elementary effects (50×58 elementary-effects), the value of Δ was fixed to approximately 0.51 using the expression $\Delta = \frac{50}{2(50-1)}$, as suggested by (Saltelli, et al., 2008). This simulation required running the BES program $r \times (K + 1) = 2950$ times, which took approximately 12 hours.

The results of this first analysis are presented in Figure 27, where the standard deviation of the absolute value of the elementary effects (σ) is plotted against the overall sensitivity measure (μ^*). As it is shown in Figure 27, eight variables are easily identified as the most influential (variables inside the dashed circle, in Figure 27) due to their high μ^* comparing to the other 50 parameters. This set of 50 variables form a cluster of parameters near the origin, with small μ^* and σ, which indicates that they have respectively small overall influence on the $cv(RMSE)$ and also small non-linear behaviour and/or small interaction between variables, except for the variable x_{40} (U_w) that has higher σ than the remaining non-influential but since this parameter has very small overall influence (μ^*), its impact on the $cv(RMSE)$ is negligible.

Remember that the overall sensitivity measure μ^* is the same as the average absolute value of the elementary-effects of a certain variable, which means that all the variables that were considered not important have $\mu^* < 1 \times 10^{-3}$ (as it can be seen in Figure 27). This means that when the Δ quantity is varied on the non-influential parameters, the error of the model ($cv(RMSE)$) will vary on average less than 0.05%, which is a very small variation compared to the most influential variable (x_{41}) that varies on average $\approx 0.5\%$ (10 times more) whenever Δ is changed.

The 8 most influential variables not only have a higher μ^* than the remaining 50, but also show increasing non-linear and/or interaction behaviour, due to the increase in σ. This means that as the relative influence of the parameters increases, there is also an increasing interaction behaviour between other variables and/or increasing curvature (non-linear) effects.

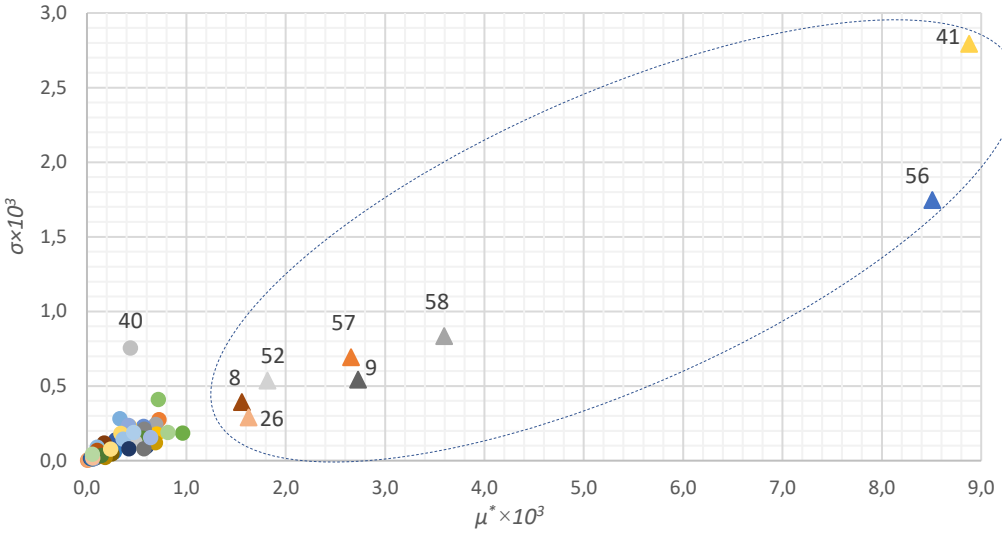

Figure 27: Sensitivity measures using 50 trajectories

In this model, all the uncertain variables were numbered from 1 to 58 (i.e. $\{x_1, \dots, x_{58}\}$) and the physical meaning of each of the most influential variables is presented in Table 19, where the parameters are sorted in decreasing order of importance (according to the previous graphical analysis). The parameters with the highest influence on the error are (not by order): the solar factor ($g_\perp$), which varies the temperature by varying the solar heat gains; the infiltration rate in each main thermal zone (living-room, $\dot{V}_S$ and bedrooms, $\dot{V}_{Q_1}$ and $\dot{V}_{Q_2}$); the conductivity and thickness of the bricks ($k_{brick_{ext}}$ and $t_{brick_{ext}}$), which are related to the heat transfer by conduction on the exterior walls; the density of the concrete ($\rho_{concrete}$) which affects the thermal inertia of the floor and ceiling; and finally, the stand-by electric equipment power (P_{sb}) which affects the temperature because it is assumed to be releasing heat during the whole year.

Table 19: Most influential parameters found with the Morris method

x_i	parameter
x_{41}	$g_\perp$
x_{56}	$\dot{V}_S$
x_{58}	$\dot{V}_{Q_1}$
x_9	$k_{brick_{ext}}$
x_{57}	$\dot{V}_{Q_2}$
x_{52}	P_{sb}
x_{26}	$\rho_{concrete}$
x_8	$t_{brick_{ext}}$

Although the *Latin Hypercube Sampling* was used to increase the representativeness of the trajectories in the domain, a *sampling error* may still exist. To increase the robustness of the results of the first analysis, the number of trajectories was increased to 100 (which took approximately 50 hours), and the overall sensitivity measure (μ^*) was calculated.

The results, presented in Figure 28 for the 20 most influential parameters, show that the screened parameters are the same, whether 50 or 100 trajectories are used. There are only some differences on the relative order of some of these parameters ($\dot{V}_{Q_1}$, $\dot{V}_{Q_2}$ and $k_{brick_{ext}}$), which does not affect the results, since the top 8 influential parameters still have a higher μ* than the remaining non-influential (so the screened parameters are the same). With this analysis, it was considered that the search domain was well sampled.

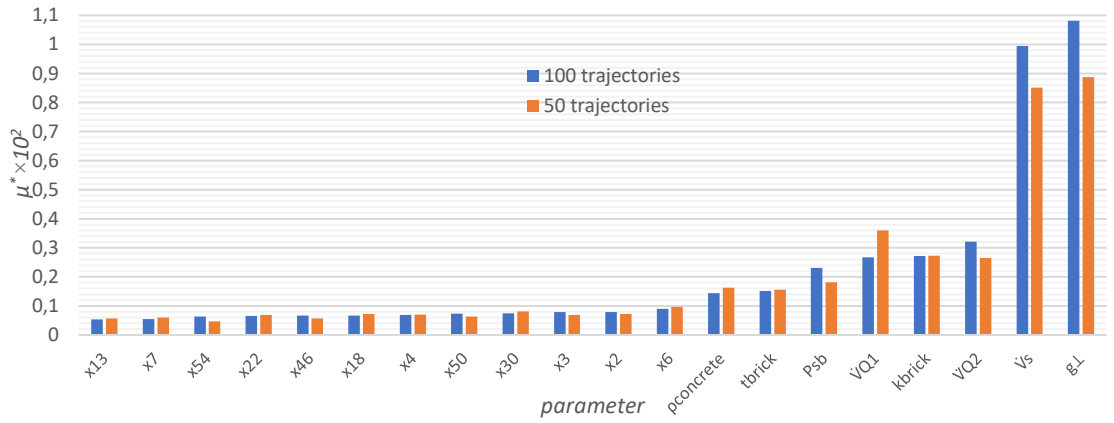

Figure 28: Overall sensitivity of the 20 most influential parameters screened with 50 and 100 trajectories

7.1.3 Calibration of the *detailed model*

To minimize the $cv(RMSE)$ and calibrate the *detailed model*, the variables related to the infiltration rates of each of the main divisions (living-room and bedrooms) were kept constant in such a way that there is only one infiltration rate parameter for the whole house ($\dot{V}$) that varies in the same range specified in Table 12 ($\pm 50\%$ around the infiltration estimated with the tracer gas method). This means that instead of 8 variables (the 8 uncertain parameters screened with the *elementary-effects method*), only 6 were calibrated (i.e. $t_{brick_{ext}}$, $k_{brick_{ext}}$, $\rho_{concrete}$, $g_{\perp}$, P_{sb}, $\dot{V}$). The objective function and feasible searching zone is defined by equation (37).

$$\text{Minimize:} \quad F_{obj}(X) = \frac{\sqrt{\left(\sum_{i=1}^{n}\left(\bar{t}_{a,i}^{m} - \bar{t}_{a,i}^{s}\right)^2/n\right)}}{\left(\sum_{i=1}^{n}\bar{t}_{a,i}^{m}\right)/n} \times 100\ (\%)\ , X \in R^6 \qquad (37)$$

Subject to:

$$0.016 \leq x_1 \leq 0.024\ (m)$$
$$0.528 \leq x_2 \leq 1.05\ (W/m.K)$$
$$582 \leq x_3 \leq 1200\ (kg/m^3)$$
$$0.592 \leq x_4 \leq 0.89$$
$$28 \leq x_5 \leq 52\ (W)$$
$$1.09 \leq x_6 \leq 3.26\ (h^{-1})$$

The *crossover probability* was set constant ($p_c = 0.9$) during all optimizations and only three different combinations of population sizes were tested (due to the high computational effort of each optimization) to study the differences on the results between a small population (20 *chromosomes* per generation) and populations with more *chromosomes* (50 and 100 *chromosomes*).

The defined stopping criterion was the following: if there is no improvement on the fittest solution of each generation over 20 generations with a tolerance of $\Delta F_{obj} = 10^{-2}$ (%) between the fittest chromosomes of the 20 generations (with the lowest $cv(RMSE)$ (%)), the GA stopped.

The GA found the minimum solution with 50 *chromosomes* per generation, in which the $cv(RMSE)_{min} = 5.93\%$. The other minimum solutions for the remaining runs of the *GA*, with 20 and 100 *chromosomes* per generation, were respectively 6% and 5.94% (approximately the same error). The values of the 6 tuned parameters for the solution with the smallest error are those presented in the Table 20.

Although the error of the best solution did not change considerably when comparing to the *detailed model* (only changed approximately 1.4%) the values of the most influential parameters varied significantly, in particular the infiltration rate for the whole house, which is the variable with the largest variation compared to the *detailed model* (decreased almost in 50%). The performance of the glazed surfaces increased, since the solar factor $g_{\perp}$ (the most influential parameter in the model) decreased in approximately 18%, which might mean that the properties of the glass were incorrectly assumed in the *detailed model* (reflecting the uncertainty present in this model).

Table 20: Calibrated parameters of the detailed model

Variable	Parameter	*Detailed model* value	Best solution value	Δ(%)
x_1	$t_{brick_e}(m)$	0.20	0.24	20.0
x_2	$k_{brick_e}(W/mK)$	0.79	0.6	−24.1
x_3	$\rho_{concrete}(kg/m^3)$	891	1177	32.1
x_4	$g_{\perp}$	0.74	0.61	−17.6
x_5	$P_{sb}(W)$	40	38.3	−4.3
x_6	$\dot{V}(h^{-1})$	2.17	1.13	−47.9
$cv(RMSE)(\%)$		7.3	5.93	−18.8
$NMBE$ (%)		3.11	−0.48	−115.0

All these variations on the influential parameters (Table 20) decreased the annual error and the monthly error in the majority of the months, as it is presented in Figure 29. Although the annual error only decreased approximately 1.4%, there are some months still with considerable differences, such as January, February and December. There are also some months in which the $cv(RMSE)$ remained approximately equal or increased by a small amount (July and August) but these increases are considered negligible, compared to the improvement on the other months.

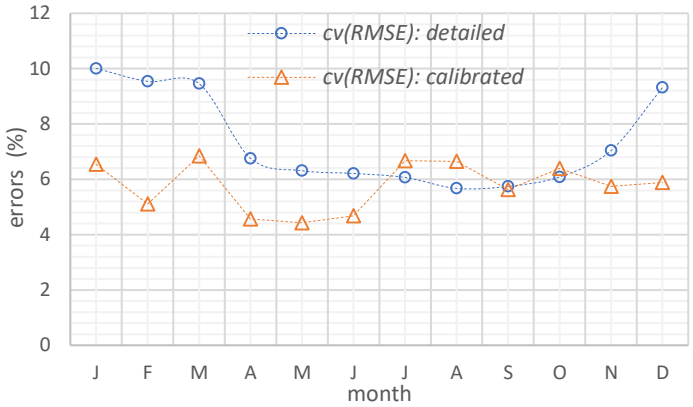

Figure 29: Monthly error of the solution with the smallest error

7.1.4 Thermal Comfort

Although there is only one solution with the smallest error in each run of the GA, the calibration is known as an indeterminate problem (i.e. several different solutions with sufficiently small $cv(RMSE)$ can accurately represent the actual air temperature of the house) so, the solutions having approximately the same error were considered equally calibrated.

The several runs of the GA allowed to collect several solutions with different comfort and approximately the same annual $cv(RMSE)$. These solutions were taken from the last generations of the GA, where almost all *chromosomes* had similar fitness values. The criteria for choosing the solutions was the following: from the three last generations of each GA (first with 20, then with 50 and finally, with 100 *chromosomes*), all the different solutions with $cv(RMSE) < 6\%$ were chosen.

As for the thermal comfort indicators related to the PMV used in this work (equations (27) and (28)), the *calibrated solutions* have a percentage of cumulative thermally dissatisfied hours ($N_{static0.7}$) approximately in the range of $[40.4; 41.4]$ $(\%)$, which is equivalent to the range of $[1939;\ 1986]$ hours of discomfort in the year and a mean average absolute predicted mean vote ($|PMV|_{avg}$) in the range of $[0.62; 0.63]$.

Comparing the thermal comfort predictions of all the models, the *detailed model* estimates the highest $N_{static0.7}$, with $\approx 3\%$ more discomfort hours than the calibrated model (which is equivalent to a difference of approximately 144 hours), while the *baseline model* has the most optimistic estimation of the number of hours in discomfort ($N_{static0.7} = 30.7\%$), which corresponds to a difference of $499\ h$ of discomfort regarding the *calibrated model* (Figure 30 a)). The same estimations are valid for the $|PMV|_{avg}$ (Figure 30 b), i.e. the *baseline model* estimates the lower $|PMV|_{avg}$, followed by the *calibrated model*, while the worst level of comfort is the given by the *detailed model.*

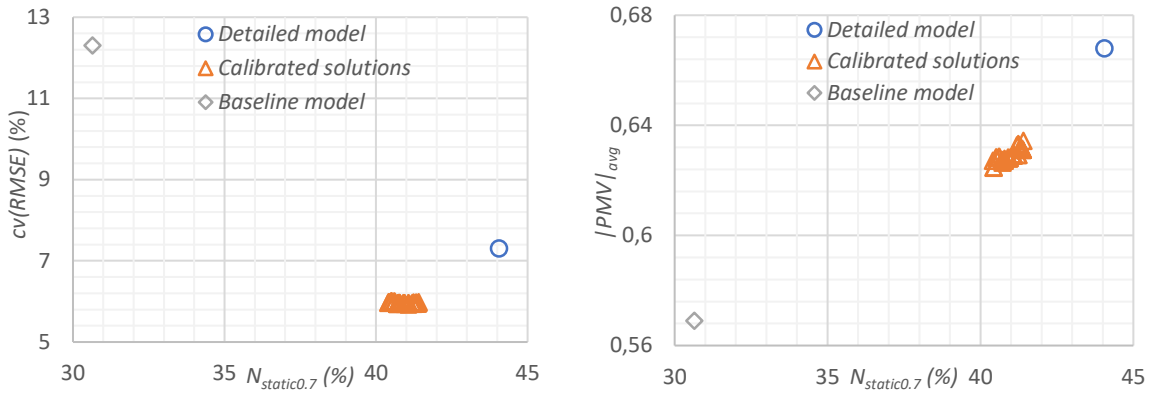

Figure 30 a) and b): Thermal comfort prediction of the baseline, detailed and calibrated solutions

Since the adaptive model is considered to be more accurate for naturally ventilated buildings than the PMV model, this was also considered for the estimation of the percentage of cumulative discomfort hours, according to the 80 % acceptability criteria ($N_{adapt80\%}$, given by equation (30)). The adaptive thermal comfort was analysed during the same occupied hours as the PMV on the previous analysis, to compare both comfort thermal comfort models.

Using the adaptive model, the cumulative percentage of discomfort hours $N_{adapt80\%}$ showed very similar results for the *detailed* and *calibrated models* as the $N_{static0.7}$ indicator (Table 21), but it is considerably smaller for the *baseline model* with a difference of 9.5 % hours in discomfort (which is equal to a difference of 456 hours).

To sum up, the *baseline model* estimates the number of hours in discomfort in a very optimistic way, especially if the adaptive model is used. Conversely, a more accurate model as the *detailed* presents considerably higher discomfort than the *baseline*. Finally, a model that was calibrated with the real household's temperature and is believed to predict more accurately the thermal comfort, decreased the number of discomfort hours comparing to the *detailed model*, but still very far away from the estimation of the *baseline model.*

Table 21: Comparison between the thermal comfort predictions of the adaptive and static models

	baseline	*detailed*	*calibrated*
$N_{static0.7}$ (%)	30.7	44.1	41.1
$N_{adapt80\%}$ (%)	21.2	44.3	37.7

For the rest of this work, the thermal comfort was evaluated only with the $N_{static0.7}$ and the $|PMV|_{avg}$ because all the retrofit measures include a HVAC system, which excludes the use of the adaptive model for the thermal comfort evaluation.

7.2 Retrofit Analysis

For the retrofit analysis (i.e. *artificial neural network* and *multi-objective optimization*), one possibility was to create ANNs for all the solutions and then optimize each one and analyse the uncertainty of the several

Pareto fronts. Since this analysis would require a high computational effort to create a database of retrofit scenarios for each *calibrated solution*, only one solution was chosen from the set of *calibrated solutions* (orange triangles in Figure 30 a) and b)). This option followed a conservative approach, i.e. the worst possible case in terms of discomfort hours and therefore the chosen solution has $N_{static0.7} = 41.4\ \%$ and $|PMV|_{avg} = 0.63$. In this solution, some of the parameters have slightly different values than the values presented in the Table 20 (for the solution with the smallest error), namely the infiltration rate ($\dot{V} = 1.19\ h^{-1}$) and the conductivity of the bricks of the exterior wall ($k_{brick_{ext}} = 0.73\ W/m.K$).

7.2.1 Artificial Neural Network

A total of 2000 retrofit scenarios generated with the LHS were used to *train* the network and other 200 representative solutions (generated again, with the LHS) were used to calculate the *validation error* and apply the early stopping principle. Additionally, 200 solutions were used to calculate the *testing errors* in each iteration (to compare to the *validation errors*). All the inputs and targets were firstly normalized between $[0;\ 1]$ and the network performance error was evaluated in this range.

After several trials, the configuration of the network with the best performance and without significant *over-fitting* had a more complex geometry than it was expected, with 2 *hidden layers,* with 15 neurons on the first *hidden layer* and 11 on the second one.

The *training* of the model ended after 113 iterations, which took approximately 5 minutes. The overall *training* MSE was 3.4×10^{-4}, very similar to the overall *validation* and *testing error* (with $MSE_{valid} = 3.5 \times 10^{-4}$), so no considerable over-fitting has occurred. Concerning each individual output, all the regressions (Figure 31 a) and b) and Figure 32 a) and b)) show a very good agreement between the *validation targets* (which were not used for *training*) and the outputs of the network, with coefficients of determination R^2 very close to 1.

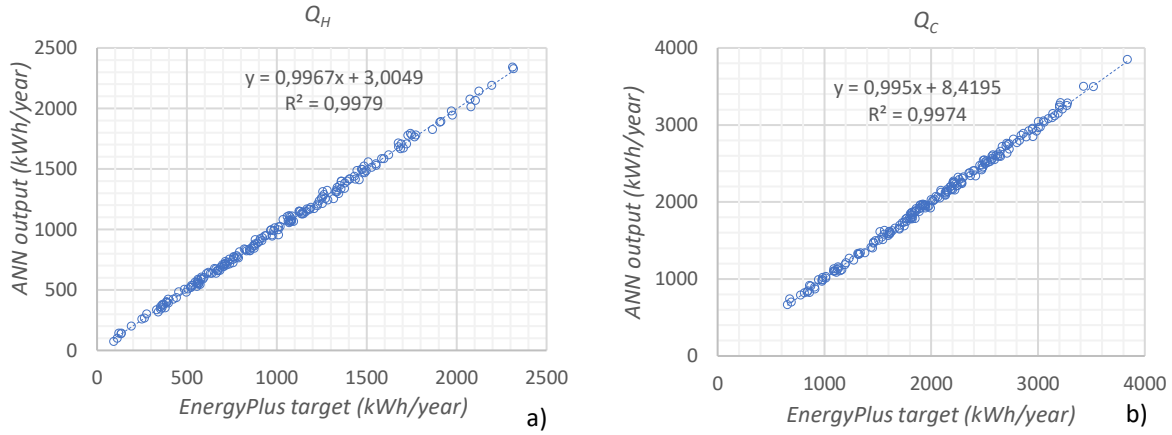

Figure 31: Linear regressions of the validation data: a) Heating loads (Q_H); b) Cooling loads (Q_C);

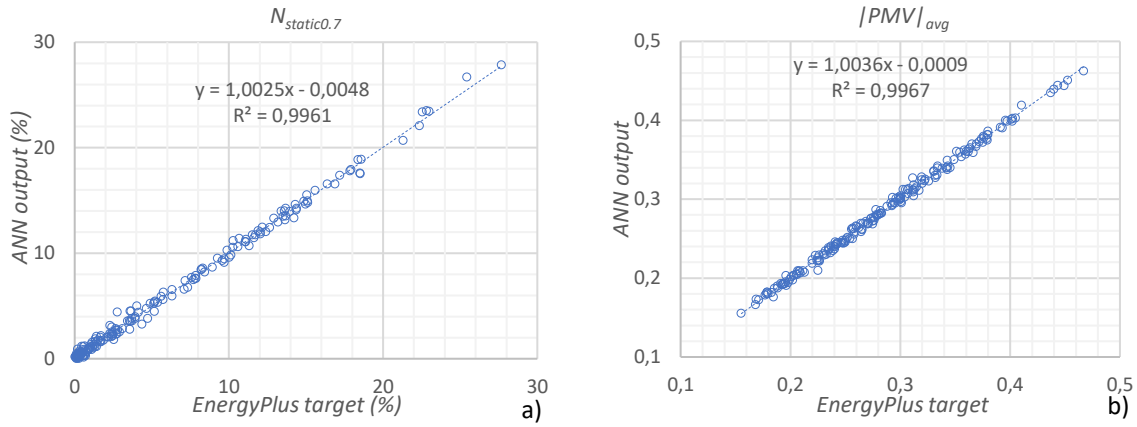

Figure 32: Linear regressions of the validation data: a) Percentage of cumulative discomfort ($N_{static0.7}$); b) $|PMV|_{avg}$

The statistical distribution of the relative errors of the *validation* data set was also calculated for $|PMV|_{avg}$, Q_H and Q_C (Table 22, where $F_X(e)$ is the cumulative frequency of the relative error (e)) and showed very small errors, especially for the $|PMV|_{avg}$, with an average relative error of only $1.09\ \%$. The errors of the HVAC loads are also very small and less than $3\ \%$ both for the heating and cooling loads. Since the output relative to the number of discomfort hours $N_{static0.7}$ has *targets* with 0 hours of discomfort, instead of the relative error, it was calculated the absolute error to avoid infinite errors. The statistical distribution of these absolute errors was also calculated (Table 22) and showed positively small errors, with an average of $0.30\ \%$ which corresponds only to 14 hours per year, on average. This table presents the frequency, on the *validation* data set, in which the error is smaller or equal than $F_X(e)$.

Table 22: Statistical distribution of the validation errors

$F_X(e)(\%)$	1	2.5	5	10	25	$\bar{e}(\%)$
$N_{static0.7}$*	98.5	100	100	100	100	0.30
$\|PMV\|_{avg}$**	56.5	94.5	99.5	100	100	1.09
Q_H**	29	66.5	95.5	98.5	100	2.19
Q_C**	40	83.5	98.5	100	100	1.49

*absolute error; **relative error;

7.2.2 Multi-Objective Optimization

7.2.2.1 First scenario

The first scenario involves the minimization of the investment cost of the combination of retrofit measures and the annual energy cost and imposes the condition of zero hours with discomfort as an equality constraint. As it is described by equation (38), the constraint is introduced with a penalty approach by increasing the value of both objective functions whenever a solution has $N_{static0.7} \neq 0\ \%$. The ANN, contrarily to the *EnergyPlus,* gives outputs without any physical meaning and so it is possible to occur negative hours in discomfort. However, since the ANN had very small errors, negative hours do not occur frequently (or if they do, the deviation is very small), so whenever a solution had $N_{static0.7} < 0\ \%$, the output was converted into $N_{static0.7} = 0\ \%$.

Minimize: $$F_{obj}^{pen}(X) = \begin{cases} [I;\ C_E] & ,N_{static0.7} = 0\ \% \\ [I.(1+N_{static0.7});\ C_E.(1+N_{static0.7})] & ,N_{static0.7} > 0\ \% \end{cases} \quad (38)$$

Subject to: $$x_i^{(l)} \leq x_i \leq x_i^{(u)}, i = \{1, \dots, 12\}$$
$$x_j \in \mathbb{R}, j = \{5,6,7,8,9,10\}$$
$$x_k \in \mathbb{Z}, k = \{1,2,3,4,11,12\}$$

A first run of the GA with 20 *chromosomes* per generation and a *Pareto fraction* of 0.5, found very unsatisfactory solutions (blue circles in Figure 33) compared to other runs with more *chromosomes.* By increasing the population size to 50 and with the same *Pareto fraction*, both objectives improved but are still far from the other fronts, obtained with 100, 200 and 300 *chromosomes*. These fronts were generated with larger populations and a smaller *Pareto fraction* (0.2) to increase the exploration of the domain (by increasing the diversity of the solutions).

The first four fronts (i.e. with 20, 50, 100 and 200 *chromosomes*) were stopped by the default *spread* stopping criteria of the function "*gamultiobj*", while the last front with 300 *chromosomes* (green triangles) and with the best results was stopped after a larger number of generations (Figure 33). This last front, which involved a significantly higher computational effort (more than 600000 evaluations of the ANN) than all the other curves, shows only small improvements in both objectives comparing to the simulation with 200 *chromosomes* (this latter with 92% less evaluations of the objective functions) but since all the solutions of the front with more *chromosomes* and largest number of *generations* are the fittest, the latter is assumed to be the *optimal front*.

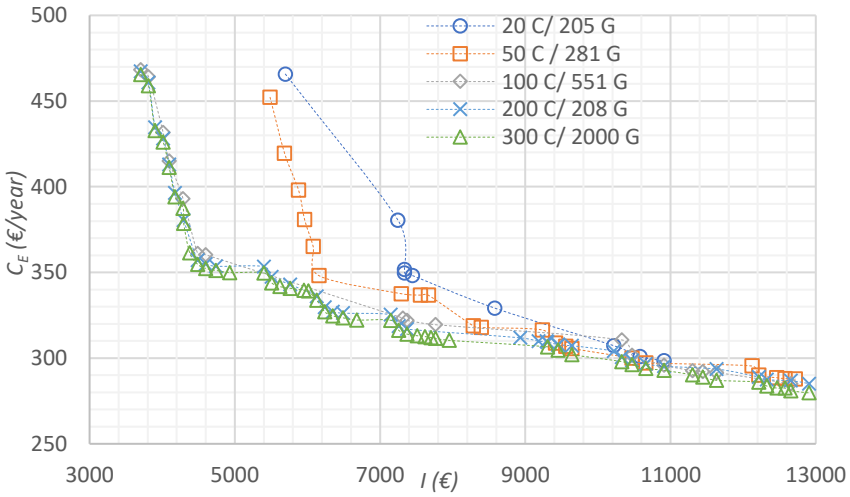

Figure 33: Pareto fronts of the first scenario for different population sizes; "C" is the number of chromosomes and "G" is the number of generations before stopping

All the 48 solutions (out of 60, which validates the choice of the *Pareto fraction*) of the *Pareto front* are feasible solutions (with $N_{static0.7} = 0\ \%$) and go from 3703 to 12907 € in terms of investment cost (I), and from 280 to 466 $€/year$ in terms of annual energy cost (C_E).

To validate these solutions as being very close to optimal, all the retrofit solutions of the *Pareto front* were evaluated by the *EnergyPlus* (blue circles in Figure 34) and showed a maximum deviation of 0.29% on the annual energy cost, which corresponds to a difference of only 0.86 $€/year$. In terms of thermal comfort, the

ANN generated only feasible solutions ($N_{static0.7} = 0\ \%$), which evaluated by the *EnergyPlus* correspond to solutions with a number of discomfort hours very close to the objective (with a maximum deviation of $0.27\ \%$ of discomfort hours, i.e. a maximum difference of 13 hours during the whole year).

Regarding the HVAC "setpoint variables", all the solutions have different optimized values for these parameters depending on the combination of retrofit solutions because for each solution, these variables will adjust to provide zero hours in discomfort with the least possible HVAC energy consumption. The ranges of each of these variables are presented in Table 23.

Table 23: Optimal solutions for the "setpoint variables"

Variable	Min. value	Max. value
$\Delta t_{pre}\ (min)$	10	30
T_H^{hs}(°C)	19.1	20.1
ΔT_{db}^{hs}(°C)	1.2	3.0
T_H^{cs}(°C)	22.0	22.6
ΔT_{db}^{cs}(°C)	1.4	1.8
$RH^{hs}(\%)$	60^*	
$RH^{cs}(\%)$	60^*	

Two distinct areas are visible in the *Pareto front.* The first area has approximately 10 solutions, in which the annual energy cost decreases approximately linearly when the investment cost increases. The retrofit solutions in this area go from the solution with the minimum investment cost and zero discomfort (solution "A", in Figure 34, with $I = 3703$ € and $C_E = 466\ €/year$) to a solution with 4488 € of investment where the annual energy cost is $355\ €/year$ (solution "B").

The GA did not find any feasible solutions only with HVAC system, so besides the investment on the HVAC, solution "A" has $x_1 = 1$, i.e. the insulation with the smallest thickness ($t_{insulation} = 0.02\ m$). This means that to guarantee $N_{static0.7} = 0\ \%$, the solution with the smallest investment requires insulation.

What the solutions in this area have in common is that they all have the least efficient HVAC system (i.e. $x_3 = 1$) and the original windows ($x_2 = 0$). The insulation of these solutions varies between $x_1 = 1$ and $x_1 = 2$, which along with x_{11} (choice of the lighting) and x_{12} (choice of the DHW) decreases the annual energy cost with a higher slope than the second area. This latter has solutions in which larger investment costs are needed to vary the annual energy cost, comparing to the first area.

Inside the first area is the first solution of the front which allows to match the annual energy cost of the original non-retrofitted model (the solution on the blue horizontal line, in Figure 34). This solution requires an investment cost of 4379 € and gives approximately the same annual cost as the original household (i.e. $C_{E,original} = 362$ €) and the main difference is that the original house has no HVAC system but $41.4\ \%$ of the cumulative occupied time has thermal discomfort. This is the solution in which the energy spent in the HVAC, to remove the discomfort, starts to be compensated by the smaller energy consumption in lighting and DHW due to more efficient systems than in the original model.

All the solutions under the blue line (Figure 34) have lower C_E than the non-retrofitted model (i.e. solutions that have annual energy savings). However, a *payback* analysis does not make sense in this case because it would always originate *payback periods* (considering the simple calculation) of the order of magnitude of 10^2 years, which occurs because the original model has no HVAC system (and therefore significant discomfort). The solutions that include savings go from the solution "B" (Figure 34) to a solution "C", with the minimum energy annual cost ($C_E = 280$ €). The investment of these solutions varies from 4488 € in "B" to 12907 € in "C".

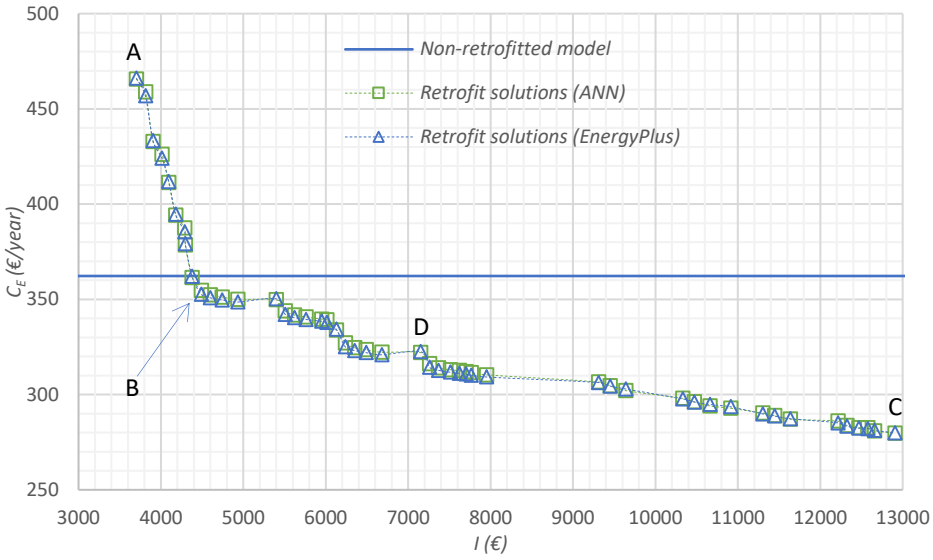

Figure 34: Retrofit solutions and annual energy cost of the non-retrofit household

The values of the decision variables for the three optimal solutions referred in the previous paragraphs are presented in the Table 24: solution "A" with the minimum investment cost, solution "B" with the minimum annual savings and solution "C" with the minimum annual energy cost (maximum annual savings). Solution "A" requires the smallest investment because its cost only includes the less efficient HVAC system ($x_3 = 1$) and minimum thickness insulation ($x_1 = 1$) , while solution "C" requires the maximum investment and includes all the solutions with the highest efficiency (i.e. windows with the smallest U_w and $g_\perp$, thermal insulation with the largest thickness and the most efficient lighting, DHW and HVAC system).

The pre-heating and cooling advance (Δt_{pre}) was set on $30\ min$ for solutions "A" and "B" and reduced to $10\ min$ in the solution with the minimum energy cost, i.e. solution "C". The choice of the "setpoint variables" in all the *Pareto* solutions is only related to the retrofit decision variables that influence the thermal comfort (and the energy consumption), which are the insulation (x_1) and window type (x_2). In other words, solutions with the same type of window and insulation will have the same values for the "setpoint variables", as for example solutions "A", "B" and "D" (Table 24) have exactly the same temperature, humidity setpoints and pre-heating/pre-cooling advance period, since the window type and insulation is the same for both cases. Although the HVAC system is more efficient in solution "D", the same *setpoint variables* that minimize the HVAC energy consumption in this case also apply to solutions "A" and "B" without increasing the discomfort (because the window and insulation do not change).

When comparing solutions "A", "B" or "D" to solution "C", the window was changed from the original type to the window with the best performance ($x_2 = 8$) and the insulation was changed from the minimum thickness to the largest ($x_1 = 5$), which in order to keep zero discomfort and decrease the energy consumption, allowed to decrease Δt_{pre} in more than 50% and to increase the *deadbands* of the heating (ΔT_{db}^{hs}) and cooling (ΔT_{db}^{cs}) seasons.

Table 24: Decision variables for solutions "A", "B", "C" and "D"

solution	Ins.	Win.	HVAC	Δt_{pre} (min)	T_H^{hs} (°C)	ΔT_{db}^{hs} (°C)	T_H^{cs} (°C)	ΔT_{db}^{cs} (°C)	RH^{hs} (%)	RH^{cs} (%)	lighting	DHW
A	1	0	1	30	20.1	1.2	22.0	1.6	60	60	0	0
B	1	0	1	30	20.1	1.2	22.0	1.6	60	60	1	2
C	5	8	3	10	19.1	3.0	22.1	1.8	60	60	1	3
D	1	0	2	30	20.1	1.2	22.0	1.6	60	60	1	3

7.2.2.2 Second scenario

The second scenario involves maximizing the overall thermal comfort ($|PMV|_{avg}$) while minimizing the annual energy consumption (C_E). A level of comfort of $|PMV|_{avg} < 0.7$ doesn't mean that all occupied hours have each hour with $|PMV| < 0.7$ and so, the non-linear constraint that guarantees all hours to be inside the acceptable thermal comfort zone, was used. The problem is more formally described by equation (39)

$$\text{Minimize:} \quad F_{obj}^{pen}(X) = \begin{cases} [|PMV|_{avg}; C_E] & , N_{static0.7} = 0\ \% \\ [|PMV|_{avg}.(1 + N_{static0.7}); C_E.(1 + N_{static0.7})] & , N_{static0.7} > 0\ \% \end{cases} \quad (39)$$

$$\text{Subject to:} \quad x_i^{(l)} \leq x_i \leq x_i^{(u)}, i = \{1, \dots, 12\}$$
$$x_j \in \mathbb{R}, j = \{5,6,7,8,9,10\}$$
$$x_k \in \mathbb{Z}, k = \{1,2,3,4,11,12\}$$

The GA was used with a population of 300 *chromosomes*, crossover and mutation probabilities of respectively 0.9 and 0.1 and a *Pareto fraction* of 0.3. The results of this optimization are presented in Figure 35.

The *Pareto front* shows solutions with a good spread between the two extremes, with results of the $|PMV|_{avg}$ in the range of $[0.118; 0.285]$ and with annual energy costs (C_E) in the range of $[280; 370]$ $(€/year)$. All the solutions found in this optimization have the most efficient HVAC, DHW and lighting system (i.e. $x_3 = 3, x_{12} = 3$ and $x_{11} = 1$), the windows with the best thermal performance ($x_2 = 8$) and the insulation with the highest thickness ($x_1 = 5$), which means that they all have the same investment cost ($I = 12907$ €). This is the same cost as the investment of the solution with the minimum energy consumption found on the first optimization (*first scenario*). This solution "C" (see Table 24) has also approximately the same annual energy cost as the solution with the highest $|PMV|_{avg}$ in Figure 35.

In all the solutions of Figure 35, from the right to the left, the HVAC "setpoint variables" make the thermal comfort increase at the cost of increasing the HVAC energy consumption (i.e. increasing C_E). The *Pareto* front in Figure 35 shows two areas approximately linear with different slopes. The first area, with higher $|PMV|_{avg}$ (dashed ellipse on the right, in Figure 35) has the smallest slope and suggests that a small increase on

C_E leads to a high reduction of the $|PMV|_{avg}$ (up to approximately $|PMV|_{avg} = 0.14$), while the second area (dashed ellipse on the left) shows that even higher level of thermal comfort is possible to obtain (up to $|PMV|_{avg} = 0.118$), but with a much larger increase on the HVAC energy consumption. This means that the energy consumption can vary significantly even without significant improvements on the thermal comfort.

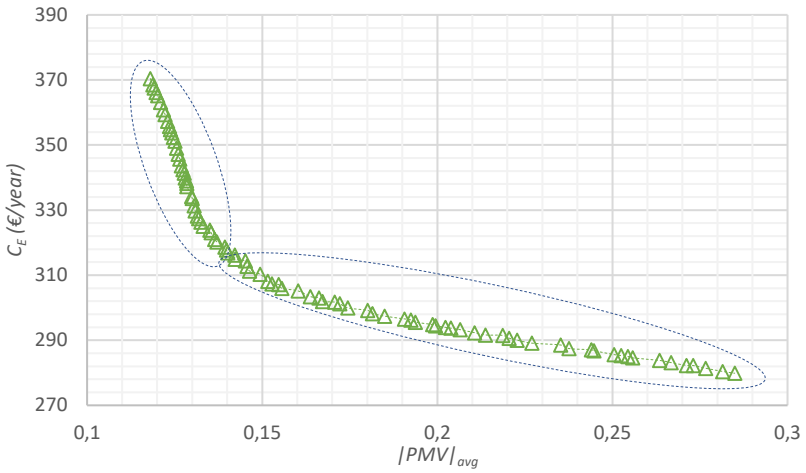

Figure 35: Pareto solutions of the second scenario

The analysis of the decision variables of the *Pareto solutions*, presented in Figure 36, shows that the differences on these two areas is mainly caused by an abrupt variation on the relative humidity setpoint of the heating season, RH^{hs}, which decreases from approximately $60\ \%$ to $30\ \%$, causing a great impact on the energy consumption (increased dehumidification) and moving the thermal comfort towards the minimum $|PMV|_{avg}$. This, along with the decrease of the temperature *deadband* during the heating season, increases the thermal comfort at the cost of increased energy consumption. The thermostat temperatures and humidistat setpoint for the cooling season are approximately constant for all solutions.

The thermostat ranges that provide the maximum comfort ($|PMV|_{avg} = 0.118$) were found to be $T \in [21.7; 22.3]$ (℃) for the heating season and $T \in [22.5; 23.8]$ (℃) for the cooling season, the relative humidity always below $30\ \%$ for the heating season and below $60\ \%$ for the cooling season. Additionally, $\Delta t_{pre} \approx 60\ min$ for this solution.

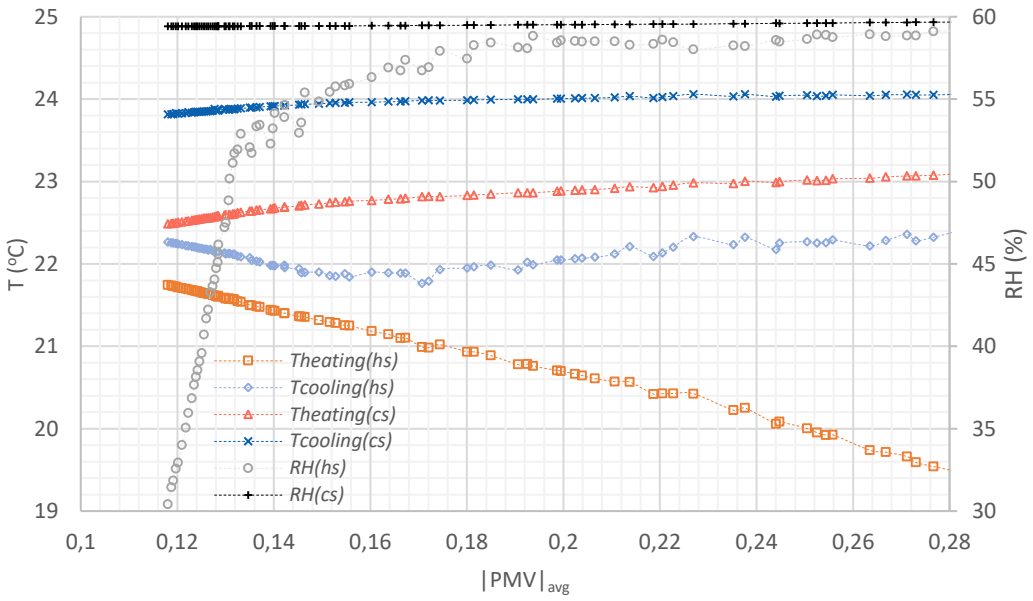

Figure 36: "Setpoint variables" for the second scenario

7.2.2.3 Baseline, detailed and calibrated models

The number of *hidden layers* and *hidden neurons* of the ANN used for the *baseline* and *detailed models*, like in *calibrate* model, were found by trial and error. For the *detailed model,* the network with the smallest error (and simplest geometry) had one less *neuron* in the second *hidden layer* than the network used on the *calibrated* model (i.e. 2 *hidden layers* with 15 and 10 *neurons*). After the *training* (which occurred after 150 iterations), this network showed positively small *validation errors*, with an overall *validation* MSE_{valid} of 2.8×10^{-4} (even smaller than the MSE of the *calibrated model*) again, very close to the *training* and *testing* MSE (i.e. no considerable over-fitting happened).

The network of the *baseline model* has a slightly different geometry (12 i*nput neurons*, instead of 10) and presented the smallest error again with two *hidden layers*: the first layer with 15 *neurons* and the second with 10 *neurons* (like the network of the *detailed model*). The *training* of this network stopped after 137 iterations with a very small MSE_{valid} (2.1×10^{-4}) and close to the *training* and *testing errors*, so no considerable over-fitting occurred. The average errors were also calculated for both trained networks, considering the representative *validation data* set (with 200 solutions), in which the relative average error was calculated for Q_H, Q_C and the absolute average error was calculated for $N_{static0.7}$. The results, presented in Table 25, show small errors in both models.

Table 25: Average validation errors

	$N_{static0.7}$	Q_H	Q_C
Detailed (e(%))	0.13*	1.42**	1.35**
Baseline (e(%))	0.31*	2.23**	1.17**

* average absolute error

** average relative error

Both optimizations (investment cost $I(€)$ and annual energy cost $C_E(€/year)$) were only performed using 300 *chromosomes* per generation with a *Pareto fraction* of 0.2 (i.e. a maximum of 60 solutions) and with the same *crossover* and *mutation probabilities* used in the *calibrated model* (i.e. $p_c = 0.9$ and $p_m = 0.1$). The stopping criterion was after 2000 generations since this number of generations showed convergence in the *Pareto fronts* of the previous MOO problems. The results of these two optimizations are presented in Figure 37, along with the *Pareto front* of the *calibrated model* for this same problem (first scenario of the previous MOO problems).

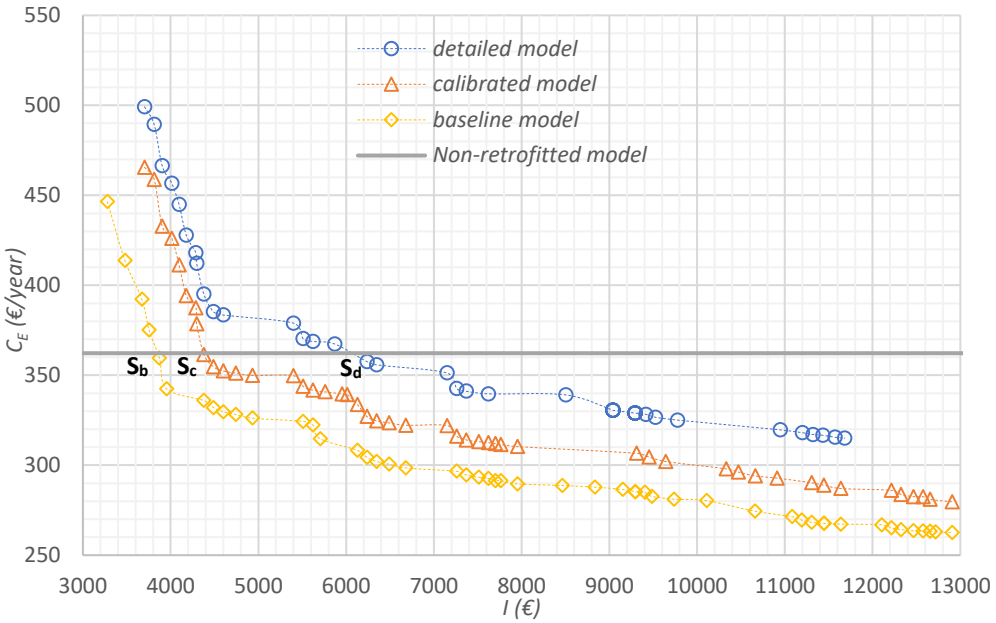

Figure 37: Pareto fronts of the detailed, baseline and calibrated models

For the *detailed model*, a similar shaped curve to the *Pareto front* of the *calibrated model* was found (curve with the blue circles, Figure 37), but with larger values for the annual energy cost ($C_E \in [315\,,499]$ (€)). This curve is almost parallel to the two other fronts in Figure 37 and maintains an approximately constant distance from the *calibrated model's front* of $\Delta C_E \approx 30\ €/year$. The maximum investment for this curve ($I = 11682$ €), is smaller than in the *calibrated front*, which means that the GA did not find optimal solutions without discomfort from this investment due to the insulation (x_1) and window type (x_2) that were not set to their maximum performance.

The difference between the *calibrated* and *detailed fronts* can be explained due to the variations of the 6 calibrated parameters, which allowed to decrease the HVAC energy consumption for the same level of comfort ($N_{static0.7} = 0\ \%$). Firstly, regarding the exterior wall of the household, the conductivity of the wall's bricks ($k_{brick_{ext}}$) decreased and their thickness ($t_{brick_{ext}}$) increased, which increased the thermal resistance of the wall's bricks in approximately $30\ \%$ and therefore reduced the heat gains and losses by conduction, comparing to the *detailed model.* The solar factor $g_\perp$ of the original windows was also reduced in $22\ \%$, which reduced the solar heat gains through the glazed surfaced in the *detailed model* and explains the differences between the annual energy cost of the optimal *calibrated* and *detailed* solutions that both consider the original windows ($x_2 = 0$). Another parameter responsible for the differences between the curves is the infiltration rate ($\dot{V}$) that

decreased by $45\ \%$. Reduced infiltration means less sensible and latent heat gains in the house, which reduces the HVAC energy consumption (lower sensible and latent loads) and therefore, the annual energy cost.

Conversely, the curve of the *baseline model* (Figure 37) estimates smaller annual energy costs ($C_E \in [263, 446]$ (€)) than the *calibrated model*, which corresponds to a smaller C_E in ≈ 25 €$/year$ for the same investment cost. This was the model that largely under-estimated the thermal comfort, so it was expected that the optimal retrofit solutions to remove the discomfort have also low HVAC energy consumption. This front has approximately the same shape as the fronts of the two other models (i.e. two areas with different slopes), but it is the only curve with a range of investment that goes from the smallest to the largest possible investment cost, which means that the combination of measures with the minimum investment ($I = 3279$ €, i.e. least efficient HVAC system ($x_3 = 1$), original windows ($x_2 = 0$), lighting ($x_{11} = 0$) and DHW system ($x_{12} = 0$) and no insulation ($x_1 = 0$)) is, contrarily to the two other curves in Figure 37, a feasible solution of this model (with $N_{static0.7} = 0\ \%$). The solution with the maximum investment ($I = 12907$ €) cost is also an optimal solution like in the *calibrated model's* front and contrarily to the *detailed model*.

The *detailed model*, being completely independent of the *baseline*, originated a *Pareto front* that over-estimates the annual energy cost (compared to the *calibrated model*). However, after being calibrated, it moves back towards the *baseline model*. This might happen because, after the influential parameters were calibrated, some of them were tuned to values close to the parameters of the *baseline model*, such as the infiltration rate of the *baseline model*, that is only $3.4\ \%$ larger than the calibrated infiltration rate and the overall heat transfer coefficient of exterior walls of the *baseline model* that is only $6\ \%$ smaller than the same parameter in the *calibrated model* (after calculated on the *EnergyPlus*). The other parameters, such as the assumed ρ and C (related to the thermal inertia), the internal gains and the parameters of the glazed surfaces, especially the solar factor (calculated from the standard, which assumes that the shading devices are used to minimize the heating and cooling loads), are responsible for lowering the HVAC energy consumption and therefore, the annual energy cost.

All the *solutions* of a *Pareto front* are equally optimal, so it is up for the *decision-maker* (DM) to evaluate them and choose what is the solution that best fits his project. The DM might want to choose a solution that for instance, allows to have thermal comfort all the time and to save a specific amount of money each year. It is then fundamental to include in the retrofit project a set of optimal solutions that can make the most accurate approximation of what will happen in the reality, which can be achieved with a *calibrated model.* To understand what are the implications of choosing the retrofit solution based on a model that is not calibrated, two scenarios are proposed: the first is if the retrofit solution had been chosen based on the *baseline model* and the second, based on the *detailed model*.

7.2.2.3.1 Baseline model

If neither the *detailed* nor the *calibrated model* were available to find the optimal solutions in terms of investment and energy annual cost, the retrofit project would have to be based on the *Pareto front* given by a model based only on simple information about the house, i.e. the *baseline model*.

As an example, it is given the case in which the DM wants to choose the solution with the smallest investment that allows him to match the annual energy cost of the non-retrofitted household (grey straight line, in Figure 37). With this criterion, the DM would choose the solution "S_b", from Figure 37, which requires an investment cost of approximately 3872 € (investment on the least efficient HVAC system ($x_3 = 1$), LED lighting system ($x_{11} = 1$) and natural gas tankless boiler for DHW with $\eta_{hw} = 0.76$ ($x_{12} = 1$)). The same solution, but evaluated by the *calibrated model*, estimates an annual energy cost of 376 €$/year$, i.e. no savings would occur. Although this solution might appear to *dominate* the other solutions of the *calibrated model's front*, it has a $N_{static0.7} \approx 1.4$ % (i.e. the *calibrated model* estimates that this solution has approximately $67\ h$ in discomfort, so it is not a feasible solution).

This represents a loss of comfort and annual savings that would not occur if the DM had chosen the solution based on the *calibrated model's front*. However, for the same criteria, the solution chosen with this latter front would require the extra investment of 507 €.

Although the increase of the energy cost would not substantial (up to 17 €$/year$), the loss of comfort could reach up to $143\ h$, which is a considerable amount of time in which the conditions would not be acceptable in terms of thermal comfort. This occurs mainly due to non-optimal values of the HVAC setpoint parameters that don't estimate discomfort in the *baseline model* but estimate in the *calibrated model.*

7.2.2.3.2 Detailed model

If, instead of the *baseline model*, the project had been based on the *detailed model* (with more detailed information on the actual properties of the house), it is given the example where the DM would want to choose the solution with the minimum investment that allows to save money each year.

Again, the solution would be the first point below the grey line (Figure 37), i.e. solution "S_d", which requires $I = 6238$ € and has $C_E = 358$ €$/year$. The same solution, when evaluated by the *calibrated model*, has approximately $N_{static0.7} = 0$ %, but a smaller C_E (in ≈ 32 €$/year$). Although this solution would have smaller energy cost than it was expected, the DM invested on a much more expensive combination of measures than he would need based on the proposed criterion.

If, with the same criteria (i.e. minimum investment with money savings and $N_{static0.7} = 0$ %), the solution was based on the *calibrated Pareto front*, the investment required would be much smaller than the 6238 € spent if the solution was chosen with the *detailed Pareto front.* Instead of 6238 €, the DM would choose a solution that has approximately zero savings and $I = 4379$ € (solution "S_c", in Figure 37) and therefore would save 1859 € of investment. To sum up, the solutions given by the *detailed model* represent a bad investment when analysed under the *calibrated model*, because a much smaller investment (estimated by the *calibrated Pareto front*) achieves the annual cost that was expected to occur, for the same level of comfort.

8 CONCLUSIONS

This work introduces a methodology to determine the best retrofit measures for residencial households based on building energy simulation models. To do this, the work is composed of two parts. In the first part, a model of the household is developed and calibrated and then, in the second part, a multi-objective optimization algorithm is implemented to determine the best retrofit solutions.

The first part involved the development of a BES model, from an early design stage (*baseline model*, i.e. with only general information about the house) to a *calibrated model*, in which the parameters of the middle stage model (i.e. the *detailed model*) were tunned to minimize the error of the model.

The GA proved to be a powerful tool in automated calibration procedures, since only a few number of generations were needed to achieve to stop the GA, with very small errors. In order to reduce the order of the optimization problem, the elementary-effects method was used, which allowed to exclude $87\ \%$ of the uncertain variables of the model due to their small influence on the error. After the calibration of the model, it was collected not only one optimal solution, but a set of solutions with the smallest errors, which recognizes the indeterminacy of the calibration

Although some of the properties of the *detailed model* were tuned for more accurate predictions of the indoor temperatures of the household, some of the simplifcations made in this procedure represent a source of error. The main limitation of this calibration work was the infiltration rate that was considered equal for the all thermal zones of the house and constant through the whole year. This simplification ignores, for example, occasional windows or doors' openings, which vary the renewable air rate (through natural ventilation). Although this effect was neglected, the infiltration air rate parameter may be seen as an average reneweable air rate that accounts for the overall effect of natural ventilation.

Another limitation of this work is the fact that the schedules were not allowed to vary during the calibration and sensitivity analysis. One possibility to overcome this problem, without increasing too much the number of variables, would be to generate several variations for each usage schedule and then calibrate them in such a way that, for instance, the lighting schedule chosen for the living-room was the one that led to the smallest error. This solution was assumed to be as realistic as the one that was adopted because between two schedules that are constant through the whole year, one schedule represents the reality as accurately as the other. This hypotesis was also discarded because through sensitivity analysis, it was confirmed that the internal gains (associated to occupation, lighting and equipment schedules) don't have substancial impact on the $cv(RMSE)$.

Although the overall error of the model did not evolve considerably, the small variation of approximatelly $1.4\ \%$ of the $cv(RMSE)$ was sufficient to calibrate the most influential parameters in such a way that the *detailed* and *calibrated* models show substantial differences on the thermal comfort predictions, with a difference on the discomfort of $144\ h$ given by the static (PMV) model and $317\ h$ given by the adaptive model.

For the second part of the work, the use of artificial neural networks was fundamental to develop *surrogate models* to mimic the behaviour of the *EnergyPlus.* Even with a static ANN like the MLP, the errors of

the optimal solutions found in the MOO problems are very small compared to the BES program, so they are believed to be very close to optimality. The *Pareto fronts* generated in the first scenario with the largest populations (300 *chromosomes*) and number of generations (2000 generations) took approximately $1.5\ h$ each and required 6×10^5 evaluations of the network. The same number of simulations using *EnergyPlus* was estimated to take the infeasible computational effort of 153 days with only slightly improvements on the accuracy of the results. Even using smaller population sizes and number of generations, such as the generated *Pareto front* in Figure 33 (with 20 *chromosomes*), this would take $25\ h$ on *EnergyPlus* and the results would be very far from what is believed to be the true *Pareto front.*

Regarding the multi-objective optimizations, a wide range of optimal solutions were found for the two scenarios in the particular household of this work's case-study. Considering the first scenario (*Pareto front* of Figure 34), a good choice for the optimal combination of retrofit measures would be solution "B" of Figure 34 because it has considerably smaller energy cost than the solution with the minimum investment (solution "A", Figure 34) due to more efficient lighting and DHW systems installed with only a small increase of investment cost, contrarily to solution "C" (Figure 34) that requires almost three times more investment than solution "B" and achieves only a small decrease in the energy cost, comparing to solution "B".

All the *Pareto fronts* generated have low annual energy cost for all the investments because the HVAC system was only assumed to be working during very small periods, i.e. in the bedrooms only one hour before leaving and another hour after entering the bedroom, which originates low HVAC energy consumption. Even though, the three models (*baseline, detailed* and *calibrated*) show substantial differences on the optimal *Pareto solutions.* The difference on the curves (Figure 37) indicates that different models of the same household, with a different uncertainty degree, can lead to a set of solutions that over-estimate (i.e. *detailed model*) or under-estimate (*baseline model*) the annual energy cost. Since the decision-making process may consider this cost, trusting the retrofit project on a model that was not calibrated can lead to bad investments (on the case of the *detailed model*). It may also lead to higher annual costs than it was expected or even to the existence of thermal discomfort (*baseline model*).

Some other limitations of this work include the simplifications that were made when modelling the HVAC and DHW system that affect both energy consumption and thermal comfort. In the MOO problems, the choice of the HVAC and DHW systems was reflected only on different efficiencies, which affect in an simplified way the heating and cooling loads (calculated with the *EnergyPlus,* using an ideal HVAC system) and also the usefull energy for DHW (calculated with equations (20) and (21), from the standard). An interesting future study would be to model with more detail the HVAC and DHW systems in order to, more accurately, search for the optimal retrofit solutions on a calibrated model.

This work proved the added value of the calibration process to estimate more accurately the household's temperature and therefore, the thermal comfort. Since this latter was always considered on the retrofit analysis, the calibration helped to increase the confidence on the optimal solutions, which can be decisive for an adequate choice of the measures.

9 REFERENCES

ADENE. (2013). Coeficientes de transmissão térmica de elementos opacos da envolvente dos edifícios.

America, I. E. (1993). *Lighting Handbook: Reference & Application, 8th Edition.* New York.

ANSI/ASHRAE Standard 55-2010. (2010). *Thermal Environmental Conditions for Human Occupancy*.

Asadi, E., Silva, M. G., Antunes, C. H., Dias, L., & Glicksman, L. (2014). Multi-objective optimization for building retrofit: A model using genetic algorithm and artificial neural network and an application. *Energy and Buildings*, 444-456.

ASHRAE. (2002). *Guideline 14-2002.* Atlanta, GA 30329: American Society of Heating, Refrigerating and Air-Conditioning Engineers.

ASHRAE. (2009). ASHRAE 2009 Fundamentals (SI Edition). Em *Energy Estimating and Modelling Methods* (pp. 19.1-19.33).

ASHRAE Standard 55-2010. (2010). *Thermal Environmental Conditions for Human Occupancy*.

Bae, N. R. (2016). *Influence of Uncertainty in User Behaviors on the Simulation-Based Building Energy Optimization Process and Robust Decision-Making.*

Beale, M. H., Hagan, M. T., & Demuth, H. B. (2017). *Neural Network Toolbox User's Guide.* Natick, MA: The MathWorks, Inc.

Bertagnolio, S. (2012). *Evidence-Based Model Calibration For Efficient Building Energy Services.* Liège.

Carlucci, S., Cattarin, G., Causone, F., & Pagliano, L. (2015). Multi-objective optimization of a nearly zero-energy building based on thermal and visual discomfort minimization using a non-dominated sorting genetic algorithm (NSGA-II) . *Energy and Buildings*, 378-394.

Chong, A., Xu, W., & Lam, K. P. (2015). UNCERTAINTY ANALYSIS IN BUILDING ENERGY SIMULATION: APRACTICAL APPROACH. *14th Conference of International Building Performance Simulation Association.* Hyderabad, India.

Coakley, D., Raftery, P., & Keane, M. (2014). A review of methods to match building energy simulation models to measured data. *Renewable and Sustainable Energy Reviews, 37* , 123-141.

Costa, P. C. (2016). *Otimização multiobjetivo para a promoção dos edifícios de balanço energético quase nulo em Portugal.*

CYPE Ingenieros, S. (. (2018). *Gerador de Preços.* Obtido de http://www.geradordeprecos.info/

De Wit, M. S. (2001). *Uncertainty in Predictions of thermal comfort in buildings.* Delft, NL: Technische Universiteit Delft.

Deb, K. (2000). An efficient constraint handling method for genetic algorithms. *Computer methods in applied mechanics and engineering 186*, 311-338.

Deb, K. (2011). *Multi-Objective Optimization Using Evolutionary Algorithms: An Introduction.*

Deb, K., & Goel, T. (2001). Controlled Elitist Non-dominated Sorting Genetic Algorithms for Better Convergence. *EMO 2001, LNCS 1993*, 67-81.

Deep, K., Singh, K. P., Kansal, M., & Mohan, C. (2009). A real coded genetic algorithm for solving integer and mixed integer optimization problems. *Applied Mathematics and Computation 212*, 505-518.

ENERGYPLUS. (2013). *EnergyPlus Engineering Reference.*

Eskander, M. M., Sandoval-Reyes, M., Silva, C. A., Vieira, S., & Sousa, J. M. (2017). Assessment of energy efficiency measures using multi-objective optimization in Portuguese households . *Sustainable Cities and Society*, 764-773.

European Directive 2010/31/EU. (2010). European Directive 2010/31/EU on the Energy Performance of Buildings. *Official Journal L 153, 18/06/2010 (2010)*.

Fanger, P. O. (1970). *Thermal Comfort.* McGraw-Hill.

Fyfe, C. (2005). Artificial Neural Networks. Em C. Fyfe, *Artificial Neural Networks* (pp. 57-79). Springer.

Goldberg, D. E. (1989). *Genetic Algorithms in Search, Optimization, and Machine Learning.* Reading, MA: Addison-Wesley Publishing Company, Inc.

Gomes, R., Ferreira, A., Azevedo, L., Neto, R. C., Aelenei, L., & Silva, C. (2018). Retrofit measures evaluation considering thermal comfort by using Building Energy Simulation - Lisbon households.

Grossard, D., Lartigue, B., & Thellier, F. (2013). Multi-objective optimization of a building envelope for thermal performance using genetic algorithms and artificial neural network. *Energy and Buildings*, 253-260.

Haupt, S. E., & Haupt, R. L. (2004). *Practical Genetic Algorithms.* Hoboken, New Jersey: John Wiley & Sons, Inc.

International Standard ISO 7730. (2005). *Ergonomics of the thermal environment — Analytical determination and interpretation of thermal comfort using calculation of the PMV and PPD indices and local thermal comfort criteria*.

Ioannou, A., & Itard, L. (2014). Thermal comfort in residential buildings: sensitivity to building parameters and occupancy. *Fifth German-Austrian IBPSA Conference.*

JUNKERS. (2018). *Água Quente.* Obtido de JUNKERS : https://www.junkers.pt/consumer/produtos_consumidor/category_256

Lara, R. A., Naboni, E., Pernigotto, G., Cappelletti, F., Zhang, Y., Barzon, F., . . . Romagnoni, P. (2017). Optimization Tools for Building Energy Model Calibration. *Energy Procedia 111*, 1060-1069.

Macdonald, I. A. (2002). *Quantifying the Effects of Uncertainty in Building Simulation.* Strathclyde: University of Strathclyde.

Magnier, L., & Haghighat, F. (2010). Multiobjective optimization of building design using TRNSYS simulations, genetic algorithm, and Artificial Neural Network. *Building and Environment*, 739-746.

MathWorks. (2018). *gamultiobj Algorithm.* Obtido de MathWorks: https://www.mathworks.com/help/gads/gamultiobj-algorithm.html

Mitchell, M. (1999). *An Introduction to Genetic Algorithms.* Cambridge, Massachusetts: MIT Press.

Monteiro, C. S. (2018). *Building Energy Modeling at Urban Scale Using Multi-Detail Archetypes: Addressing the Uncertainties and Applications.* Lisboa: IST.

Monteiro, C. S., C., C., Pina, A., Santos, M., & Ferrão, P. (2018). An Urban Building Database (UBD) supporting a Smart City Information System. *Energy and Buildings, V. 158*, 244-260.

Morris, M. D. (1991). Factorial Sampling Plans for Preliminary Computational Experiments. *Technometrics, Vol.33, No2.*, 161-174.

Nguyen, A., & Reiter, S. (2015). A performance comparison of sensitivity analysis methods for building energy models. *Building Simulation, Vol. 8, No. 6*, 651-664.

Nicol, J., & Humphreys, M. (2002). Adaptive thermal comfort and sustainable thermal standards for buildings. *Energy and Buildings*, 563-572.

NREL. (2018). *NREL.* Obtido de National Residential Efficiency Measures Database: https://remdb.nrel.gov/group_listing.php

Pina dos Santos, C., & Matias, L. (2006). *Coeficientes de Transmissão Térmica dos Elementos da Envolvente dos Edifícios .* Lisboa: LNEC.

Reddy, A. T., Maor, I., & Panjapornpon, C. (2011). Calibrating Detailed Building Energy Simulation Programs with Measured Data—Part I: General Methodology (RP-1051). *HVAC&R Reasearch,13:2*, 221-241.

Reddy, A. T., Maor, I., & Panjapornpon, C. (2011). Calibrating Detailed Building Energy Simulation Programs with Measured Data—Part II: Application to Three Case Study Office Buildings (RP-1051). *HVAC&R Research, 13:2*, 243-265.

REH. (2013). *Decree-Law 118/2013 "Regulamento de Desempenho Energético dos Edifícios de Habitação", from 20th of August 2013*.

Roberti, F., Oberegger, U. F., & Gasparella, A. (2015). Calibrating historic building energy models to hourly indoor air and surface temperatures: Methodology and case study. *Energy and Buildings 108*, 236-243.

Rodríguez, G. C., Andrés, A. C., Muñoz, F. D., López, J. M., & Zhang, Y. (2013). Uncertainties and sensitivity analysis in building energy simulation using macroparameters. *Energy and Buildings 67*, 79-87.

Saltelli, A., Ratto, M., Andres, T., Campolongo, F., Cariboni, J., Gatelli, D., . . . Tarantola, S. (2008). *Global Sensitivity Analysis, The Primer.* England: John Wiley & Sons, Ltd.

Shukla, A., Tiwari, R., & Kala, R. (2010). Artificial Neural Networks. Em A. Shukla, R. Tiwari, & R. Kala, *Towards Hybrid and Adaptive Computing* (pp. 31-58). Springer.

Sohier, H., Farges, J.-L., & Piet-Lahanier, H. (2014). Improvement of the Representativity of the Morris Method for Air-Launch-to-Orbit Separation. *Proceedings of the 19th World Congress The International Federation of Automatic Control .* Cape Town, South Africa.

SusCity Project. (2013). SusCity: Urban Data Driven Models for Creative and Resourceful Urban Transitions. *FCT*. Obtido de https://www.fct.pt/apoios/projectos/consulta/vglobal_projecto.phtml.en?idProjecto=137220&idE 2013

Tian, W. (2013). A review of sensitivity analysis methods in building energy analysis. *Renewable and Sustainable Energy Reviews*, 411-419.

Wilamowski, B. M., & Chen, Y. (1999). Efficient Algorithm for Training Neural Networks with one Hidden Layer.

10 ANNEXES

10.1 Matlab code of the sensitivity Analysis

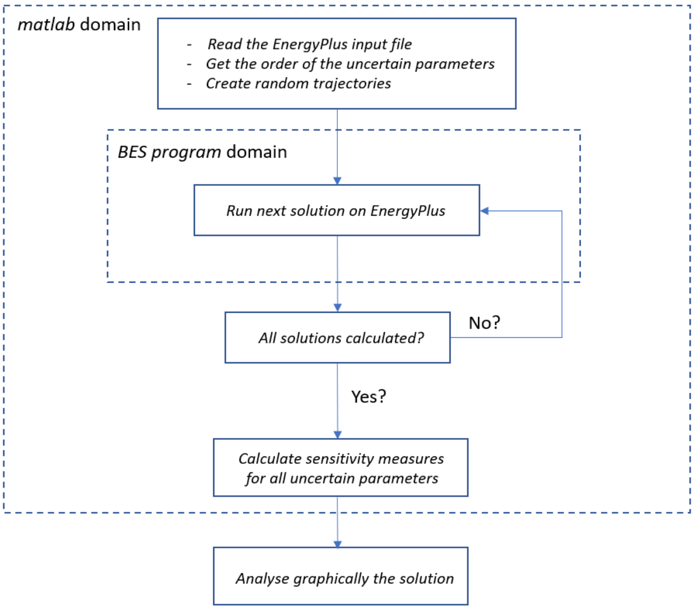

10.1.1 Main script

```
%%%%%%%MAIN SCRIPT%%%%%%%%%%%%%%%%%%%%%%%%%%%%%%%%%%%%%%%%%%%%%%%%%%%%%%%
[actual, order,Dist, IDF, UB, LB,var,TRI,UNI,NORM,commonF,commonF2]=ANALISE;
[Tre_media] = LeReaisASS;
k=length(actual);
P = input('divisões:');
R = P;
delta=P/(2*(P-1)); %increment
%%%INITIAL POINTS CREATED WITH LATIN HYPERCUBE SAMPLING%%%%
out=0;
d=1/R;
mini=0;
maxi=1;
coord = 0:R-1;
for i = 1:k
pontos(1:R,i) = coord(randperm(length(coord)));
end
pontos = pontos/(R-1);
%%%%GENERATION OF THE R-TRAJECTORIES FROM EACH BASE POINT CREATED WITH LHS
for t = 1:R
    out=0;
    out2=0;
    Xbase=pontos(t,:);
    E=zeros(1,k);
    traj(t).B=zeros(k+1,k);
    a=Xbase;
    %%%%%%FIRST POINT OF THE TRAJECTORY%%%%%%%%%
    %%%%%%%%%%%50% PROB. OF ADDING AND 50% PROB. OF SUBTRACTING%%%%%%%%
    ran1=randi([1 2],1,1);
            for j=1:2
                if ran1==2
                sinal=-1;
                else
                sinal=1;
                end
            end
    %%%%%%%%%%%%%%%%%RANDOM ORDER OF THE CHANGED VAR%%%%%%%%%
```

```
            orderr=randi([1 k],1,1);
            E(orderr)=1;
            a=a+sinal*delta*E;
            for l=1:k
                if a(l)>1||a(l)<0
                    out=1;
                end
            end
            if out == 1
                a=a-2*sinal*delta*E;
            end
            traj(t).B(1,1:end)=a;
            ordemm=randperm(k);
            I=0;
        %%%%%%%OTHER K POINTS OF EACH TRAJECTORY%%%%%%
        %%%%SAME PROCESS%%%%
            for i = 2:k+1
                out2=0;
                I=I+1;
                ran2=randi([1 2],1,1);
                for j=1:2
                    if ran2==2
                        sinal=-1;
                    else
                        sinal=1;
                    end
                end
                e=zeros(1,k);
                e(ordemm(I))=1;
                a=a+sinal*delta*e;
                for l=1:k
                    if a(l)>1||a(l)<0
                    out2=1;
                    end
                end
                if out2 == 1
                    a=a-2*sinal*delta*e;
                end
                traj(t).B(i,1:end)=a;
            end
        end
        %%%%%%%%%%%%%%%ORGANIZING THE POINTS TO CALCULATE THE ELEMENTARY EFFECTS%%%%
        for i =1:k
            M(i).pts=[];
            M(i).EE=[];
        end
        %%%%%%MAPPING THE EQUALLY SPACED LEVELS FOR THE SPACE OF THE PROB.
        %%%%%%DISTRIBUTION OF EACH PARAMETER%%%%%%%%%%%%%%%%%%%%%%%%%%%%%%
        for i = 1:R
            for kk = 1:k+1
                for l = 1:k
                    traj(i).B(kk,l)=round(traj(i).B(kk,l),4);
                    if UNI(l)==1
                        %INVERSE CUMULATIVE UNIFORM
                        a(l)=traj(i).B(kk,l)*(UB(l)-LB(l))+LB(l);
                    elseif NORM(l)==1
                        %INVERSE CUMULATIVE NORMAL
                        a(l)=traj(i).B(kk,l)*(UB(l)-LB(l))+LB(l);
                        a(l)=norminv(a(l),Dist(l,1),Dist(l,2));
                    elseif TRI(l)==1;
                        %INVERSE CUMULATIVE TRIANGULAR
                        a(l)= Tri_inverse(traj(i).B(kk,l),LB(l),actual(l),UB(l));
                    end
                end
                traj(i).cvRMSE(kk)=
Y(a(1:k),commonF,commonF2,order,IDF,Tre_media,var);
            end
            for j=2:k+1
```

```
            vector=traj(i).B(j,:)-traj(i).B(j-1,:);
            for P=1:k
                if vector(P)~=0
                    ORDEM=P;
                end
            end
            m= horzcat(traj(i).B(j-1,:),traj(i).B(j,:));
            n= (traj(i).cvRMSE(j)-traj(i).cvRMSE(j-1))/delta;
            M(ORDEM).pts = [M(ORDEM).pts; m];
            M(ORDEM).EE = [M(ORDEM).EE; n];
        end
    end
    %%%%%CALCULATE THE SENSITIVITY MEASURES%%%%%%%%%
    for  i = 1:k
        M(i).media=sum(M(i).EE)/length(M(i).EE);
        M(i).media_abs=sum(abs(M(i).EE))/length(M(i).EE);
        soma=0;
        for j=1:length(M(i).EE)
           soma=soma+(abs(M(i).EE(j))-M(i).media_abs)^2;
        end
        M(i).DP=(1/(length(M(i).EE)-1))*soma;
    end
```

10.1.2 Objective function

```
    %%%%%%%%%%%%%%%% OBJECTIVE FUNCTION FOR THE SENSITIVITY ANALYSIS%%%%%%%
    function cvRMSE = Y(X,commonF,commonF2,order,IDF,Tre_media,var)

    %%%%%%%%%%%%%REPLACE ON THE IDF VECTOR THE VALUES WHERE THE TRAJECTORIES
    %%%%%%%%%%%%%EXPLORE%%%%%%%%%%%%%%%%%%%%%%%%%%%%%%%%%%%%%%%%%%%%%%%%%%
    for i = 1:length(order)
            if strcmp(strtok(var{i},'_'),'Metabolismo')
            oldstrval=sscanf(IDF{order(i)},'%f;');
            IDF{order(i)}=strrep(IDF{order(i)},num2str(oldstrval),num2str(X(i)));

            elseif strcmp(var{i},'Luz_Quarto_Princ--f_v')
            oldstrval=sscanf(IDF{order(i)},'%f,');
            IDF{order(i)}=strrep(IDF{order(i)},num2str(oldstrval),num2str(X(i)));
            IDF{order(i)-1}=strrep(IDF{order(i)-
1},num2str(oldstrval),num2str((1/1.9524)*(1-X(i))));

            IDF{commonF}=strrep(IDF{commonF},num2str(oldstrval),num2str(X(i)));
            IDF{commonF-1}=strrep(IDF{commonF-
1},num2str(oldstrval),num2str((1/1.9524)*(1-X(i))));

            IDF{commonF2}=strrep(IDF{commonF2},num2str(oldstrval),num2str(X(i)));
            IDF{commonF2-1}=strrep(IDF{commonF2-
1},num2str(oldstrval),num2str((1/1.9524)*(1-X(i))));

            else
            oldstrval=sscanf(IDF{order(i)},'%f,');
            IDF{order(i)}=strrep(IDF{order(i)},num2str(oldstrval),num2str(X(i)));
            end
    end
    %%%%%%%%%%CHANGE DIRECTORY%%%%%%%%%%%%%%%%%%%%%%%%%%%%%%%%%%%%%%%%%%%
    cd('C:\EnergyPlusV8-1-0');
    %%%%%%%%%%% WRITE THE IDF VECTOR ON THE IDF FILE%%%%%%%%%%%%%%%
    fid=fopen('ASSbase_DETALHADO_LUIS.idf','wt');
    if fid == -1
        fprintf('erro na abertura do ficheiro\n')
    else
        for i = 1:length(IDF)
           fprintf(fid,'%s\n',IDF{i});
        end
    end
    fclose(fid);
    %%%%%%%%%%%%%RUN THE ENERGYPLUS%%%%%%%%%%%%%%%%%%%%%%%%%%%%%
    dos('RunEPlus.bat ASSbase_DETALHADO_LUIS Suscity2015_2016');
```

```
        %%%%%%%%%%%%OPEN THE OUTPUT CSV.FILE%%%%%%%%%%%%%%%%%%%%%%%
        fid = fopen('ASSbase_DETALHADO_LUIS.csv','r');
        if fid == -1
            fprintf('erro na abertura do ficheiro\n')
        else
            cabecalho = fgetl(fid);
            i=0;
            TsimQ1 = [];
            TsimS=[];
        %%%%%%%%%%%READ LINE-BY-LINE ALL THE CONTENT OF THE CSV. OUTPUT FILE: THE
TEMPERATURES%
            while~feof(fid)
                linha = fgetl(fid);
                i=i+1;
                    [a resto]= strtok(linha,',');
                    [a resto]= strtok(resto,',');
                    [a resto]= strtok(resto,',');
                    [a resto]= strtok(resto,',');
                    [a resto]= strtok(resto,',');
                    [a resto]= strtok(resto,',');
                    [a resto]= strtok(resto,',');
                   TsimQ2(i)=str2double(a);
                    [a resto]= strtok(resto,',');
                    [a resto]= strtok(resto,',');
                    [a resto]= strtok(resto,',');
                    [a resto]= strtok(resto,',');
                    [a resto]= strtok(resto,',');
                   TsimS(i)=str2double(a);
                    [a resto]= strtok(resto,',');
                   TsimQ1(i)=str2double(a);
                end
            end
            TsimQ2=TsimQ2';
            TsimQ1=TsimQ1';
            TsimS=TsimS';
            fclose(fid);
        %%%%%CHANGE DIRECTORY%%%%%%%%%%%
        cd('C:\Users\Luís\Desktop\TESE 2017-2°SEM\TESE\TESE 2017-
2°SEM\TESE\new_AS\ASS');
        %%%%%ZONE VOLUMES%%%%%%%%%%%%%%%%%%%
        V_S=91.55;
        V_Q1=33.93;
        V_Q2=24.7;
        %%%%%%%%%%%%WEIGHTED AVERAGE OF THE TEMPERATURE IN EACH ZONE%%%%%%%%%%
        Tsim_media=(1/(V_S+V_Q1+V_Q2))*(V_S*TsimS+V_Q1*TsimQ1+V_Q2*TsimQ2);
        %%%%%%CALCULATE CVRMSE WITH THE CURRENT SIMULATED TEMPERATURES%%%%%%%%%%
        j=0;
        for i = 1:length(Tre_media)
            if ~isnan(Tre_media(i))
                j=j+1;
                ordem2(j)=i;
            end
        end
        f=0;
        x=0;
        for k = 1:length(ordem2)
            x = x + Tre_media(ordem2(k));
            g=(Tre_media(ordem2(k))-Tsim_media(ordem2(k)))^2;
            f=f+g;
        end
        media = x/length(ordem2);
        cvRMSE=(sqrt(f/length(ordem2)))/(media);
        end
        %%%%%%%%%%%%%%%%%%%%%%%%%%%%%%%%%%%%%%%%%%%%%%%%%%%%%%%%%%%%%%%%%%%%%%%
```

10.1.3 Auxiliary functions

```
        %%%%%%READ THE CURRENT IDF FILE AND CREATE VECTOR IDF%%%%%%%
        function [IDF] = LeIDF
```

```
        cd ('C:\EnergyPlusV8-1-0');
        name='ASSbase_DETALHADO_LUIS.idf';
        fid = fopen(name,'r');
        if fid == -1
            fprintf('erro na abertura do ficheiro\n')
        else
            i1=0;
            while ~feof(fid)
                linha=fgetl(fid);
                i1=i1+1;
                IDF{i1}=linha;
            end
        end
        fclose(fid);
        cd('C:\Users\Luís\Desktop\TESE 2017-2°SEM\TESE\TESE 2017-
2°SEM\TESE\new_AS\ASS');
        end
        %%%%%%%%%%%%%%%%%%%%%%%%%%%%%%%%%%%%%%%%%%%%%%%%%%%%%%%%%%%%
        %%%%%%READ PARAMETERS OF THE PROBABILITY DISTRIBUTION FOR EACH VARIABLE%%
        function [ mu,sigma,VARIAVEIS ] = LeDist
        nome='nonuniform.xlsx';
        fid = fopen(nome,'r');
        if fid==-1
            fprintf('erro na abertura do ficheiro\n')
        else
          [~, VARIAVEIS]= xlsread(nome,1,'A4:A38');
          mu.k=xlsread(nome,1,'B4:B38');
          mu.ro=xlsread(nome,1,'D4:D38');
          mu.Cp=xlsread(nome,1,'F4:F38');
          sigma.k=xlsread(nome,1,'C4:C38');
          sigma.ro=xlsread(nome,1,'E4:E38');
          sigma.Cp=xlsread(nome,1,'G4:G38');
        end
        fclose(fid);
        end
        %%%%%%%%%%%%%%%%%%%%%%%%%%%%%%%%%%%%%%%%%%%%%%%%%%%%%%%%%%%%%%%%%%%%%%%%
        %%%%%%%%%%%%%%%%READ FROM THE IDF FILE THE ORDER OF EACH UNCERTAIN
        %%%%%%%%%%%%%%%%PARAMETER%%%%%%%%%%%%%%%%%%%%%%%%%%%%%%%%%%%%%%%%%%%%%
        function [actual, order,Dist, IDF, UB,
LB,var,TRI,UNI,NORM,commonF,commonF2]=ANALISE
        [IDF] = LeIDF;
        [ mu,sigma,VARIAVEIS ] = LeDist;
        Zones={'Quarto_1','Sala','Quarto_2'};
        l=0;
        k=0;
        iv=1;
        c=0;
        luz=0;
        vidro=0;
        TRI=[];
        UNI=[];
        NORM=[];
        %%%MATERIALS OF OPAQUE SURFACES%%%%%
        MAT= {'pinho35mm';'Arg_Cimento_Escura_25';'Tijolo_Furado_20';...
            'Estuque_Claro_25';'Estuque_Claro_20';'Tijolo_Furado_11';...
            'Laje Aligeirada_25';'Betonilha de Acentamento_5'...
            ;'Ladrilho Ceramico'};
        for i = 1:length(IDF)
            %%%%%%%%%%%%%%%%%OPAQUE SURFACES%%%%%%%%%%%%%%%%%%
            if strcmp(IDF{i},'Material,')
                    if strcmp(strtrim(strtok(IDF{i+1},',')),'pinho35mm')
                        %%%%%CONDUCTIVITY%%%%%
                        l=l+1;
                        actual(l)=sscanf(IDF{i+4},'%f,');
                        var{l}='pinho35mm--CONDUTIVIDADE';
                        order(l)=i+4;
                        LB(l)=0.7*actual(l);
                        UB(l)=1.3*actual(l);
```

```
            TRI(l)=0;
            UNI(l)=1;
            NORM(l)=0;
            %%%%%%%%%DENSITY%%%%%%
            l=l+1;
            actual(l)=sscanf(IDF{i+5},'%f,');
            var{l}='pinho35mm--DENSIDADE';
            order(l)=i+5;
            LB(l)=0.7*actual(l);
            UB(l)=1.3*actual(l);
            TRI(l)=0;
            UNI(l)=1;
            NORM(l)=0;
            %%%%%%%%%SPECIFIC HEAT%%%%%%
            l=l+1;
            actual(l)=sscanf(IDF{i+6},'%f,');
            var{l}='pinho35mm--Cp';
            order(l)=i+6;
            LB(l)=0.7*actual(l);
            UB(l)=1.3*actual(l);
            TRI(l)=0;
            UNI(l)=1;
            NORM(l)=0;
        end
    for ii = 1:length(MAT)
            if strcmp(strtrim(strtok(IDF{i+1},',')),MAT{ii})
                l=l+1;
                actual(l)=sscanf(IDF{i+3},'%f,');
                LB(l)=0.8*actual(l);
                UB(l)=1.2*actual(l);
                var{l}=strcat(MAT{ii},'--ESPESSURA');
                order(l)=i+3;
                Dist(l,1:2)=0;
                TRI(l)=1;
                UNI(l)=0;
                NORM(l)=0;
                for iii = 1:length(VARIAVEIS)
                    if strcmp(VARIAVEIS(iii),MAT(ii))
                        l=l+1;
                        Dist(l,1)=mu.k(iii);
                        Dist(l,2)=sigma.k(iii);
                        actual(l)=sscanf(IDF{i+4},'%f,');
                        var{l}=strcat(MAT{ii},'--CONDUTIVIDADE');
                        order(l)=i+4;
                        LB(l)=0.1587;
                        UB(l)=0.8413;
                        TRI(l)=0;
                        UNI(l)=0;
                        NORM(l)=1;
                    end
                end
                for iii = 1:length(VARIAVEIS)
                    if strcmp(VARIAVEIS(iii),MAT(ii))
                        l=l+1;
                        Dist(l,1)=mu.ro(iii);
                        Dist(l,2)=sigma.ro(iii);
                        actual(l)=sscanf(IDF{i+5},'%f,');
                        var{l}=strcat(MAT{ii},'--DENSIDADE');
                        order(l)=i+5;
                        LB(l)=0.1587;
                        UB(l)=0.8413;
                        TRI(l)=0;
                        UNI(l)=0;
                        NORM(l)=1;
                    end
                end
                for iii = 1:length(VARIAVEIS)
                    if strcmp(VARIAVEIS(iii),MAT(ii))
```

```
                        l=l+1;
                        Dist(l,1)=mu.Cp(iii);
                        Dist(l,2)=sigma.Cp(iii);
                        actual(l)=sscanf(IDF{i+6},'%f,');
                        var{l}=strcat(MAT{ii},'--Cp');
                        order(l)=i+6;
                        LB(l)=0.1587;
                        UB(l)=0.8413;
                        TRI(l)=0;
                        UNI(l)=0;
                        NORM(l)=1;
                    end
                end
            end
    end
%%%%%%%%%%%%% GLAZED SURFACES %%%%%%%%%%%%%%%%%%%%%%%%%%
 elseif strcmp(IDF{i},'WindowMaterial:SimpleGlazingSystem,')
    l=l+1;
    actual(l)=sscanf(IDF{i+2},'%f,');
    LB(l)=0.8*actual(l);
    UB(l)=7;%%1.2*actual(l);
    var{l}='W01--U';
    Dist(l,1:2)=0;
    order(l)=i+2;
    TRI(l)=1;
    UNI(l)=0;
    NORM(l)=0;
    l=l+1;
    actual(l)=sscanf(IDF{i+3},'%f,');
    LB(l)=0.8*actual(l);
    UB(l)=1.2*actual(l);
    var{l}='W01--SHGC';
    Dist(l,1:2)=0;
    order(l)=i+3;
    TRI(l)=1;
    UNI(l)=0;
    NORM(l)=0;
%%%%%%%%%EXTERNAL SHUTTERS%%%%%%%%%%%%%
 elseif strcmp(IDF{i},'WindowMaterial:Shade,')
    %%%%TRANSMISSIVITY%%%
    l=l+1;
    actual(l)=sscanf(IDF{i+2},'%f,');
    LB(l)=0.7*actual(l);
    UB(l)=1.3*actual(l);
    order(l)=i+2;
    var{l}='shade--tau';
    Dist(l,1:2)=0;
    TRI(l)=0;
    UNI(l)=1;
    NORM(l)=0;
    %%%%%%REFLECTIVITY%%%%%
    l=l+1;
    actual(l)=sscanf(IDF{i+3},'%f,');
    LB(l)=0.7*actual(l);
    UB(l)=1.3*actual(l);
    order(l)=i+3;
    var{l}='shade--ró';
    Dist(l,1:2)=0;
    TRI(l)=0;
    UNI(l)=1;
    NORM(l)=0;
    %%%%%THICKNESS%%%%%%%%%
    l=l+1;
    actual(l)=sscanf(IDF{i+8},'%f,');
    LB(l)=0.8*actual(l);
    UB(l)=1.2*actual(l);
    order(l)=i+8;
    var{l}='shade--t';
```

```
                Dist(l,1:2)=0;
                TRI(l)=0;
                UNI(l)=1;
                NORM(l)=0;
                %%%%%%CONDUCTIVITY%%%%%%%%%
                l=l+1;
                actual(l)=sscanf(IDF{i+9},'%f,');
                LB(l)=0.1587;
                UB(l)=0.8413;
                order(l)=i+9;
                var{l}='shade--k';
                TRI(l)=0;
                UNI(l)=0;
                NORM(l)=1;
                Dist(l,1)=0.283;
                Dist(l,2)=0.188;
            %%%%%%%%%%INTERNAL GAINS%%%%%%%%%%%%%%%
            %%%%%%%%LIGHTING EQUIPMENT%%%%%%%%%%
             elseif strcmp(IDF{i},'Lights,')
                if
strcmp(strtrim(strtok(IDF{i+2},',')),'Quarto_1')||strcmp(strtrim(strtok(IDF{i+2},',
')),'Sala')||strcmp(strtrim(strtok(IDF{i+2},',')),'Quarto_2')
                    luz=luz+1;
                    Lname{luz}=strtrim(strtok(IDF{i+1},','));
                    l=l+1;
                    actual(l)=sscanf(IDF{i+5},'%f,');
                    LB(l)=0.8*actual(l);
                    UB(l)=1.2*actual(l);
                    var{l}=strcat(Lname{luz},'--P');
                    order(l)=i+5;
                    Dist(l,1:2)=0;
                    TRI(l)=1;
                    UNI(l)=0;
                    NORM(l)=0;
                    l=l+1;
                    actual(l)=sscanf(IDF{i+10},'%f,');
                    LB(l)=0.7*actual(l);
                    UB(l)=1.3*actual(l);
                    var{l}=strcat(Lname{luz},'--f_v');
                    order(l)=i+10;
                    Dist(l,1:2)=0;
                    TRI(l)=0;
                    UNI(l)=1;
                    NORM(l)=0;
                end
             %%%%%%%ELECTRIC EQUIPMENT%%%%%%%%%%%%%%%%%%
             elseif strcmp(IDF{i},'ElectricEquipment,')
                if strcmp(strtrim(strtok(IDF{i+1},',')),'Televisão Sala')
                    l=l+1;
                    actual(l)=sscanf(IDF{i+5},'%f,');
                    LB(l)=0.8*actual(l);
                    UB(l)=1.2*actual(l);
                    var{l}='Televisão_Sala--P';
                    order(l)=i+5;
                    Dist(l,1:2)=0;
                    TRI(l)=1;
                    UNI(l)=0;
                    NORM(l)=0;
                    l=l+1;
                    actual(l)=sscanf(IDF{i+9},'%f,');
                    LB(l)=0.7*actual(l);
                    UB(l)=1.3*actual(l);
                    var{l}='Televisão_Sala--f_r';
                    order(l)=i+9;
                    Dist(l,1:2)=0;
                    TRI(l)=0;
                    UNI(l)=1;
                    NORM(l)=0;
```

```
        elseif strcmp(strtrim(strtok(IDF{i+1},',')),'standby Sala')
            l=l+1;
            actual(l)=sscanf(IDF{i+5},'%f,');
            LB(l)=0.7*actual(l);
            UB(l)=1.3*actual(l);
            var{l}='standby_Sala--P';
            order(l)=i+5;
            Dist(l,1:2)=0;
            TRI(l)=0;
            UNI(l)=1;
            NORM(l)=0;
            l=l+1;
            actual(l)=sscanf(IDF{i+9},'%f,');
            LB(l)=0.7*actual(l);
            UB(l)=1.3*actual(l);
            var{l}='standby_Sala--f_r';
            order(l)=i+9;
            Dist(l,1:2)=0;
            TRI(l)=0;
            UNI(l)=1;
            NORM(l)=0;
        end
%%%%%%%%%%%%%%%INFILTRATION RATE%%%%%%%%%%%%%%%%%%%%%%%
    elseif strcmp(IDF{i},'ZoneInfiltration:DesignFlowRate,')
        if strcmp(strtrim(strtok(IDF{i+1},',')),'InFiLTrac Quarto Sec')
           l=l+1;
           actual(l)=sscanf(IDF{i+8},'%f,');
           LB(l)=0.7*actual(l);
           UB(l)=1.3*actual(l);
           order(l)=i+8;
           ACH = order(l);
           var{l}= 'Inf_QS';
           Dist(l,1:2)=0;
           TRI(l)=1;
           UNI(l)=0;
           NORM(l)=0;
        elseif strcmp(strtrim(strtok(IDF{i+1},',')),'InFiLTrac Sala')
           l=l+1;
           actual(l)=sscanf(IDF{i+8},'%f,');
           LB(l)=0.7*actual(l);
           UB(l)=1.3*actual(l);
           order(l)=i+8;
           ACH = order(l);
           var{l}= 'Inf_S';
           Dist(l,1:2)=0;
           TRI(l)=1;
           UNI(l)=0;
           NORM(l)=0;
        elseif strcmp(strtrim(strtok(IDF{i+1},',')),'InFiLTrac Quarto Princ')
           l=l+1;
           actual(l)=sscanf(IDF{i+8},'%f,');
           LB(l)=0.7*actual(l);
           UB(l)=1.3*actual(l);
           order(l)=i+8;
           ACH = order(l);
           var{l}= 'Inf_QP';
           Dist(l,1:2)=0;
           TRI(l)=1;
           UNI(l)=0;
           NORM(l)=0;
        end
%%%%%%%%%%%%%%%INTERNAL GAINS 2: PEOPLE%%%%%%%%%%%%%%%%%
    elseif strcmp(IDF{i},'People,')
        if strcmp(strtrim(strtok(IDF{i+1},',')),'Pessoas_SaLa')
            l=l+1;
            order(l)=i+8;
            actual(l)=sscanf(IDF{i+8},'%f,');
            LB(l)=0.7*actual(l);
```

```
            UB(l)=1.3*actual(l);
            var{l}= 'Pessoas_SALA--f_r';
            Dist(l,1:2)=0;
            TRI(l)=0;
            UNI(l)=1;
            NORM(l)=0;

        elseif strcmp(strtrim(strtok(IDF{i+1},',')),'People_Quarto 1')
            l=l+1;
            order(l)=i+8;
            actual(l)=sscanf(IDF{i+8},'%f,');
            LB(l)=0.7*actual(l);
            UB(l)=1.3*actual(l);
            var{l}= 'Pessoas_Q1--f_r';
            Dist(l,1:2)=0;
            TRI(l)=0;
            UNI(l)=1;
            NORM(l)=0;
    elseif strcmp(strtrim(strtok(IDF{i+1},',')),'People_Quarto_Principal')
            l=l+1;
            order(l)=i+8;
            actual(l)=sscanf(IDF{i+8},'%f,');
            LB(l)=0.7*actual(l);
            UB(l)=1.3*actual(l);
            var{l}= 'Pessoas_Q1--f_r';
            Dist(l,1:2)=0;
            TRI(l)=0;
            UNI(l)=1;
            NORM(l)=0;
    end
     elseif strcmp(IDF{i},'Schedule:Compact,')
        if strcmp(strtrim(strtok(IDF{i+1},',')),'Actividade Quartos')
        l=l+1;
        order(l)=i+6;
        actual(l)=str2double(strtrim(strtok(IDF{i+6},';')));
        UB(l)=126;
        LB(l)=72;
        var{l}='Metabolismo_QS';
        Dist(l,1:2)=0;
        TRI(l)=0;
        UNI(l)=1;
        NORM(l)=0;
        elseif strcmp(strtrim(strtok(IDF{i+1},',')),'Actividade Quartos_2')
        l=l+1;
        order(l)=i+6;
        actual(l)=str2double(strtrim(strtok(IDF{i+6},';')));
        UB(l)=126;
        LB(l)=72;
        var{l}='Metabolismo_QP';
        Dist(l,1:2)=0;
        TRI(l)=0;
        UNI(l)=1;
        NORM(l)=0;
        elseif strcmp(strtrim(strtok(IDF{i+1},',')),'Actividade_Sala')
        l=l+1;
        order(l)=i+6;
        actual(l)=str2double(strtrim(strtok(IDF{i+6},';')));
        UB(l)=126;
        LB(l)=72;
        var{l}='Metabolismo_sala';
        Dist(l,1:2)=0;
        TRI(l)=0;
        UNI(l)=1;
        NORM(l)=0;
        end
    end
end
```

```
for i=1:length(order)
    if strcmp(var{i},'Luz_Sala--f_v')
        commonF=order(i);
        F=i;
    elseif strcmp(var{i},'Luz_Quarto_1--f_v')
        commonF2=order(i);
        F2=i;
    end
end
actual([F,F2])=[];
order([F,F2])=[];
Dist(F,:)=[];
Dist(F2,:)=[];
UB([F,F2])=[];
LB([F,F2])=[];
var([F,F2])=[];
TRI([F,F2])=[];
UNI([F,F2])=[];
NORM([F,F2])=[];
%%%%%%%%%%%%%%%%%%%%%%%%%%%%%%%%%%%%%%%%%%%%%%%%%%%%%%%%%%%%
%%%%%%%%%%%%READ MEASURED TEMPERATURES%%%%%%%%%%%%%%%%%%%%%%
%%%%%%%%%%%%%%%%%%%%%%%%%%%%%%%%%%%%%%%%%%%%%%%%%%%%%%%%%%%%
function [Tre_media] = LeReaisASS
nome = 'ASStemps.xlsx';
fid = fopen(nome,'r');
if fid == -1
    fprintf('erro na abertura do ficheiro\n')
else
    TreQ2 = xlsread(nome,1,'C3:C8762');
    TreS = xlsread(nome,1,'D3:D8762');
    TreQ1 = xlsread(nome,1,'E3:E8762');
end
fclose(fid);
V_S=91.55;
V_Q1=33.93;
V_Q2=24.7;
Tre_media=(1/(V_S+V_Q1+V_Q2))*(V_S*TreS+V_Q1*TreQ1+V_Q2*TreQ2);
end
%%%%%%%%%%%%%%%%%%%%%%%%%%%%%%%%%%%%%%%%%%%%%%%%%%%%%%%%%%%%
```

10.2 Matlab code of the model calibration

10.2.1 Main script

```
%%%%%%%%%%%%SINGLE OBJECTIVE OPTIMIZATION WITH THE GA%%%%%%%%
tic;
[Tre_media] = LeReaisASS;
[actual, order, IDF, UB, LB,var]=ANALISE;
nvars=length(actual);
rng(0,'twister')
Crossover_prob=input('crossover probability=');
Pop_Size=input('population size=');
options=
gaoptimset('CrossoverFraction',Crossover_prob,'PopulationSize',Pop_Size,'TolFun',1e
-2,'StallGenLimit',20,'PlotFcns',{@gaplotbestf,@gaplotstopping});
[xop,fop,exitflag,output,populations,scores]=ga(@(X)fitfunction(X,order,IDF,T
re_media),nvars,[],[],[],[],LB,UB,[],[],options);
toc;
%%%%%%%%%%%%%%%%%%%%%%%%%%%%%%%%%%%%%%%%%%%%%%%%%%%%%%%%%%%%
```

10.2.2 Objective function and auxiliary functions

For the model calibration, the objective function is the same as in 10.1.2 and the auxiliary functions the same as in 10.1.3, with the difference that only the influential parameters found with the elementary-effects method are written on the "*.idf*" file.

10.3 Matlab code of the multi-objective optimization

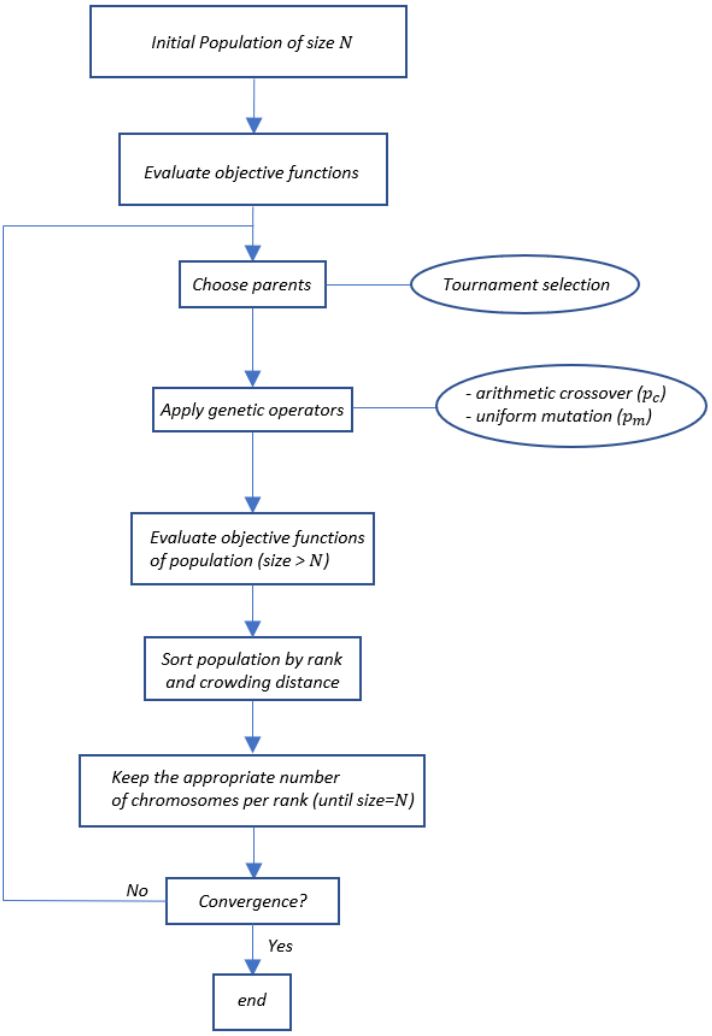

10.3.1 Main script

```
%%%%%%%%%%%%%%%%%%%%%%%%MULTI-OBJECTIVE OPTIMIZATION WITH THE GA%
nvars=12;
load('PS1_c.mat');
load('PS2_c.mat');
load('ANN_c.mat')
lb=[0.5,0.8,0.8,0,19,0.5,21,0.5,30,30,0.8,0.8];
ub=[6.2,9.2,3.2,59,23,3,26,3,60,60,2.2,4.2];
Bound = [lb; ub];
populationSize = 400;
stallGenLimit = 100;
generations = 2000;
Pfrac=input('Max. fraction of chromosomes on the first front=');
G=input('Max number of generations=');
options =
gaoptimset('ParetoFraction',Pfrac,'PopulationSize',populationSize,...
    'CreationFcn', @int_pop,...
    'MutationFcn', @int_mutationuniform,...
    'CrossoverFcn',@int_crossoverarithmetic,...
    'Generations', G,...
    'StallGenLimit', stallGenLimit,...
    'PopulationSize',populationSize,...
    'PopInitRange', Bound,'PlotFcns',@gaplotpareto,'CrossoverFraction',0.9);
options.DistanceMeasureFcn = {@distancecrowding,'genotype'};
```

```
        options.TolFun = 1e-7;
        [x,fval,exitflag,output,population,scores] =
gamultiobj(@(X)fit_fnc2(X,ps1,ps2,net),...
        nvars,[],[],[],[],lb,ub,[],options);
        %%%%%%%%%%%%%%%%%%%%%%%%%%%%%%%%%%%%%%%%%%%%%%%%%%%%%%%%%%%%%%%%%%%%%%%
```

10.3.2 Objective functions of Multi-Objective Optimization problems

```
        %%%%%%%%%%%%%%%%%OBJECTIVE FUNCTIONS OF THE MOO PROBLEM%%%%%%%%%%
        function [E_T, Ndiss] = fit_fnc2(X,ps1,ps2,net)
        X_nn=X(1:10);
        cNG=0.065;
        cE=0.2;
        if X(1)==1
            X_nn(1)=1e-03;
            Inv_ins=0;
        elseif X(1)==2
            X_nn(1)=0.02;
            Inv_ins=63.8*6.64;
        elseif X(1)==3
            X_nn(1)=0.04;
            Inv_ins=63.8*8.36;
        elseif X(1)==4
            X_nn(1)=0.06;
            Inv_ins=63.8*10.1;
        elseif X(1)==5
            X_nn(1)=0.08;
            Inv_ins=63.8*12.32;
        elseif X(1)==6
            X_nn(1)=0.12;
            Inv_ins=63.8*15.3;
        end

        if X(2)==1
            X_nn(2)=6.5;
            X_nn(3)=0.605;
            Inv_window=0;
        elseif X(2)==2
            X_nn(2)=3.67;
            X_nn(3)=0.77;
            Inv_window=106.05*16.81;
        elseif X(2)==3
            X_nn(2)=3.6;
            X_nn(3)=0.75;
            Inv_window=128.28*16.81;
        elseif X(2)==4
            X_nn(2)=3.46;
            X_nn(3)=0.41;
            Inv_window=169.45*16.81;
        elseif X(2)==5
            X_nn(2)=2.69;
            X_nn(3)=0.39;
            Inv_window=176.09*16.81;
        elseif X(2)==6
            X_nn(2)=2.56;
            X_nn(3)=0.77;
            Inv_window=219.4*16.81;
        elseif X(2)==7
            X_nn(2)=2.49;
            X_nn(3)=0.75;
            Inv_window=241.63*16.81;
        elseif X(2)==8
            X_nn(2)=2.36;
            X_nn(3)=0.41;
            Inv_window=282.8*16.81;
        elseif X(2)==9
            X_nn(2)=1.58;
            X_nn(3)=0.39;
            Inv_window=294.76*16.81;
```

```
end

if X(3)==1
    %%classe A
    SCOP=3.85;
    SEER=5.38;
    Inv_HVAC=3279;
elseif X(3)==2
    %classe A+
    SCOP=4.41;
    SEER=5.99;
    Inv_HVAC=4300;
elseif X(3)==3
    %classe A++
    SCOP=4.41;
    SEER=6.19;
    Inv_HVAC=4551;
end

if X(12)==1
    Inv_DHW=0;
    E_DHW=257.5398;
elseif X(12)==2
    Inv_DHW=392.9244;
    E_DHW=203.3209;
elseif X(12)==3
    Inv_DHW=475.5444;
    E_DHW=186.1733;
elseif X(12)==4
    Inv_DHW=2224.844;
    E_DHW=158.486;
end
if X(11)==1
    %%CFL
    Inv_Light=0;
    E_luzes=523.56*cE;
elseif X(11)==2
    Inv_Light=0.38*527.3125;
    E_luzes=523.56*0.6875*cE;
end
X_nn=X_nn';
X_nn=mapminmax('apply',X_nn,ps1);
out=net(X_nn); %%% OUTPUTS EVALUATED WITH THE ANN%%%
out_NN=mapminmax('reverse',out,ps2);
Ndiss=out_NN(1);
PMV_av=out_NN(2);
Qheat=out_NN(3);
Qcool=out_NN(4);
InvT=Inv_ins+Inv_window+Inv_HVAC+Inv_DHW+Inv_Light;
E_T=cE*((Qheat/SCOP)+(Qcool/SEER))+E_luzes+E_DHW;
if Ndiss < 0 %%ONLY POSITIVE Ndiss
    Y(2)=E_T;
    Y(1)=InvT;
elseif Ndiss>=0
    Y(2)=E_T*(Ndiss+1); %%%PENALTY%%%
    Y(1)=InvT*(Ndiss+1); %%%PENALTY%%%
end
end
```